Final Report 2000-34

PB2001-108017

Calibration Of An Earth Pressure Cell

Technical Report Documentation Page

1. Report No.	2.	3. Recipients Accession No.
MN/RC - 2000-34		

4. Title and Subtitle	5. Report Date
CALIBRATION OF AN EARTH PRESSURE CELL	September 2000
	6.

7. Author(s)	8. Performing Organization Report No.
Brent Theroux Joseph F. Labuz Andrew Drescher	

9. Performing Organization Name and Address	10. Project/Task/Work Unit No.
University of Minnesota – Dept. of Civil Engineering 500 Pillsbury Drive S.E. Minneapolis, MN 55455-0220	11. Contract (C) or Grant (G) No. c) 74708 wo) 61

12. Sponsoring Organization Name and Address	13. Type of Report and Period Covered
Minnesota Department of Transportation 395 John Ireland Boulevard Mail Stop 330 St. Paul, Minnesota 55155	Final Report 2000 14. Sponsoring Agency Code

15. Supplementary Notes

16. Abstract (Limit: 200 words)

In this study, researchers devised a scheme for calibration of earth pressure cells to observe their response to various loading configurations and to recommend a procedure for field installation. Transducers designed to provide an estimate of normal stress within a soil, earth pressure cells have provided readings that conflict with known loading conditions.

Initial calibration tests used hydraulic oil as the pressurizing medium in both hydrostatic and uniaxial pressure conditions, which mimic the manufacturers' procedure for pressure cell calibration. Researchers designed a new testing device to permit the application of uniaxial soil pressure to the earth pressure cells using various types of soil and load configurations.

As a result of calibration tests, a field installation procedure was developed and recommended. In the laboratory, a thin-walled steel cylinder with a geotextile bottom was filled with uniform silica sand of a known density, and the earth pressure cell was placed within the sand. The entire apparatus was carried into the field and installed in the desired locations. Once in place, the steel cylinder was pulled up out of the ground, leaving the cell and geotextile behind. Preliminary field data indicate that soil calibration and placement procedure provide reasonably accurate measurements.

17. Document Analysis/Descriptors		18. Availability Statement
earth pressure cell	in situ	No restrictions. Document available from:
soil	geotextile	National Technical Information Services, Springfield, Virginia 22161

19. Security Class (this report)	20. Security Class (this page)	21. No. of Pages	22. Price
Unclassified	Unclassified	114	

CALIBRATION OF AN EARTH PRESSURE CELL

Final Report

Prepared by

Brent Theroux
Joseph F. Labuz
Andrew Drescher

Department of Civil Engineering
University of Minnesota
500 Pillsbury Drive S.E.
Minneapolis, Minnesota 55455-0220

September 2000

Published by

Minnesota Department of Transportation
Office of Research Services
First Floor
395 John Ireland Boulevard, MS 330
St. Paul, MN 55155

TABLE OF CONTENTS

		Page
CHAPTER 1	INTRODUCTION	1
	The Earth Pressure Cell	2
	Motivation and Specific Application	6
	Kulite Earth Pressure Cell	7
CHAPTER 2	LITERATURE REVIEW	9
	Taylor's Indentation Analysis	9
	Monfore's Indentation Analysis	12
	Askegaard's Elasticity Analysis	16
	Experiments by Peattie and Sparrow	19
	Terzaghi's Trapdoor Analogy	22
	Trapdoor Experiments	24
	Extension of Related Work	26
CHAPTER 3	PRELIMINARY CALIBRATION	27
	Hydrostatic Fluid Calibration	28
	Uniaxial Fluid Calibration	30
	Radial Fluid Loading	31
	Temperature Effects	32
	Summary	33
CHAPTER 4	UNIAXIAL SOIL CALIBRATION	35
	Uniaxial Calibration Device	35
	Soil Loading Calibration	37
	Analysis	43
CHAPTER 5	UNIVERSAL CALIBRATION	51
	Universal Calibration Overview	55
	Universal Calibration – Dry Sand	56
	Universal Calibration – Clay	61
	Universal Calibration – Sand Pocket	63
CHAPTER 6	CONCLUSIONS	69
	Recommendations	71
	Future Research	72
REFERENCES		73
APPENDIX		

LIST OF FIGURES

Figure 1.1. Schematic of general earth pressure cell (EPC) application. 3

Figure 1.2. Hydraulic type embedment EPC. 4

Figure 1.3. Diaphragm type embedment EPC. 4

Figure 1.4. Typical EPC calibration curve. 5

Figure 1.5. Roadway cross-section at Mn/ROAD facility. 6

Figure 1.6. Kulite earth pressure cell. 7

Figure 2.1. Earth pressure cell embedded in soil. 9

Figure 2.2. Cross section through EPC and solid. 12

Figure 2.3. Stress distribution across mid-plane. 14

Figure 2.4. Effect of the ratio of cell thickness to diameter on cell error. 15

Figure 2.5. Effect of the ratio of elastic moduli on cell error. 16

Figure 2.6. Uniaxial stress change in matrix. 17

Figure 2.7. Triaxial stress change in matrix. 18

Figure 2.8. Inclusion stress versus cell height-diameter ratio. 19

Figure 2.9. Yielding trapdoor analogy, active case. 23

Figure 2.10. Limiting stress change versus soil cover. 26

Figure 3.1. Simple fluid calibration conditions. 28

Figure 3.2. Pressure setup for hydrostatic loading. 29

Figure 3.3. Uniaxial calibration device, configured for fluid loading. 30

Figure 3.4. Kulite EPC fluid calibration sensitivities. 32

Figure 3.5. Temperature influence on EPC output. 33

Figure 4.1. Uniaxial calibration device, configured for soil loading. 36

Figure 4.2. Calibration load/unload cycle. 38

Figure 4.3. One calibration test as a series of six load/unload cycles. 39

Figure 4.4. Soil calibration curves for different load areas. 41

Figure 4.5. Soil calibration curves for two types of silica sand at two column heights. 42

Figure 4.6. Sensitivity variation with soil column height. 43

Figure 4.7. Arching over a deflecting diaphragm. 45

Figure 4.8. EPC sensitivity relationship to soil height. 48

Figure 4.9. EPC sensitivity relationship to soil column diameter. 49

Figure 5.1. Universal calibration chamber. 52

Figure 5.2. Universal calibration bladder. 53

Figure 5.3. Universal calibration components. 54

Figure 5.4. Bladder response. 56

Figure 5.5. Static loading test (s14), conducted in Ottawa 20-30 sand. 58

Figure 5.6. Rapid loading test (d12), conducted in Ottawa 20-30 sand. 58

Figure 5.7. Static loading test (s19), conducted in Ottawa 20-30 sand after rapid loading. 59

Figure 5.8. Static loading (s32), conducted in "loose" Ottawa 20-30 sand. 60

Figure 5.9. Rapid loading test (d20), conducted in "loose" Ottawa 20-30. 61

Figure 5.10. Static loading test (s70), conducted in clay. 62

Figure 5.11. Rapid loading test (d44), conducted in clay. 62

Figure 5.12. Sand pocket container. 64

Figure 5.13. Static loading test (s95), conducted in pocket of Ottawa 20-30 sand. 65

Figure 5.14. Rapid loading test (d60), conducted in pocket of Ottawa 20-30 sand. 65

Figure 5.15. Static loading test (s118), conducted in pocket of Ottawa 20-30 sand with overlying class 6 gravel. 66

Figure 5.16. Rapid loading test (d116), conducted in pocket of Ottawa 20-30 sand with overlying class 6 gravel. 67

Figure A1. Test 1, cycle 1. A-3

Figure A2. Test 1, cycle 2. A-3

Figure A3. Test 1, cycle 3. A-4

Figure A4. Test 2, cycle 1. A-5

Figure A5. Test 2, cycle 2. A-5

Figure A6. Test 3, cycle 1. A-6

Figure A7. Test 3, cycle 2. A-6

Figure A8. Test 3, cycle 3. A-7

Figure A9. Test 3, cycle 4. A-7

Figure A10. Test 3, cycle 5. A-8

Figure A11. Test 3, cycle 6. A-8

Figure A12. Test 4, cycle 1. A-9

Figure A13. Test 4, cycle 2. A-9

Figure A14. Test 4, cycle 3. A-10

Figure A15. Test 4, cycle 4. A-10

Figure A16. Test 4, cycle 5. A-11

Figure A17. Test 5, cycle 1. A-12

Figure A18. Test 5, cycle 2. A-12

Figure A19. Test 5, cycle 3. A-13

Figure A20. Test 5, cycle 4. A-13

Figure A21. Test 5, cycle 5. A-14

Figure A22. Test 5, cycle 6. A-14

Figure A23. Test 6, cycle 1. A-15

Figure A24. Test 6, cycle 2. A-15

Figure A25. Test 6, cycle 3. A-16

Figure A26. Test 6, cycle 4. A-16

Figure A27. Test 6, cycle 5. A-17

Figure A28. Test 6, cycle 6. A-17

Figure A29. Test 7, cycle 1. A-18

Figure A30. Test 7, cycle 2. A-18

Figure A31. Test 7, cycle 3. A-19

Figure A32. Test 7, cycle 4. A-19

Figure A33. Test 7, cycle 5. A-20

Figure A34. Test 7, cycle 6. A-20

Figure A35. Test 7, cycle 7. A-21

Figure A36. Test 7, cycle 8. A-21

Figure A37. Test 7, cycle 9. A-22

Figure A38. Test 7, cycle 10. A-22

Figure A39. Test 7, cycle 11. A-23

Figure A40. Test 8, cycle 1. A-24

Figure A41. Test 8, cycle 2. A-24

Figure A42. Test 8, cycle 3. A-25

Figure A43. Test 8, cycle 4. A-25

Figure A44. Test 8, cycle 5. A-26

Figure A45. Test 8, cycle 6. A-26

Figure A46. Test 8, cycle 7. A-27

Figure A47. Test 8, cycle 8. A-27

Figure A48. Test 9, cycle 1. A-28

Figure A49. Test 9, cycle 2. A-28

Figure A50. Test 9, cycle 3. A-29

Figure A51. Test 10, cycle 1. A-30

Figure A52. Test 10, cycle 2. A-30

LIST OF TABLES

Table 3.1. Summary of Kulite EPC fluid calibrations. 30

Table 4.1. Summary of soil calibration sensitivities. 40

Table 4.2. Influence of load area on EPC sensitivity. 47

Table A1. EPC Uniaxial Calibration Tests A-2

EXECUTIVE SUMMARY

The objectives of this study were to devise a scheme for calibration of earth pressure cells, to observe their response to various loading configurations, and to recommend a procedure for field installation. Earth pressure cells, transducers designed to provide an estimate of normal stress within a soil, are used with apprehension in geotechnical engineering practice because of mixed results. Specifically, earth pressure cells have provided readings that are in conflict with known loading conditions.

Initial calibration tests employed hydraulic oil as the pressurizing medium in both hydrostatic and uniaxial pressure conditions, which mimic the manufacturers' procedure for pressure cell calibration. Sensitivities calculated from these tests matched the reported values of the respective manufacturers. A new testing device was designed to permit the application of uniaxial *soil* pressure to the earth pressure cells using various types of soil and load configurations. The response of the earth pressure cells was found to be different for soil pressure conditions than for fluid pressure conditions. Sensitivities computed from soil calibrations varied from those determined from fluid calibrations by 10-30%.

A universal calibration chamber 0.6 m in diameter and 0.5 m in height was designed to test the behavior of the cells in a controlled three-dimensional soil environment using sensitivities calculated from the soil pressure calibration tests. Finally, as a result of these universal calibration tests, a field installation procedure was developed and recommended: In the laboratory, a thin-walled steel cylinder with a geotextile bottom was filled with uniform silica sand with a known density and the earth pressure cell was placed within the sand. The entire apparatus (earth pressure cell, cylinder, and sand) was carried into the field and installed in the desired locations. Once in place, the steel cylinder was pulled up out of the ground, leaving the cell and geotextile behind. Preliminary field data indicate that the soil calibration and placement procedure provide reasonably accurate measurements.

CHAPTER 1
INTRODUCTION

The field of pavement engineering deals primarily with the interaction of structures with earthen materials, which include rocks and soils. Design and construction using these materials requires specific knowledge of their behavior and response to external forces. For example, pavement designs are often concerned with the magnitude and distribution of normal stress, either horizontal or vertical, within a pavement system. Because the distribution of vertical geostatic stress is linearly related to depth for soils of constant unit weight, the term earth pressure is used. Horizontal earth pressure can be related to vertical earth pressure by an arbitrary constant, the coefficient of earth pressure at rest.

Theoretical solutions exist for estimating stress distributions within an elastic solid. These solutions are based upon the framework of certain fundamental theories, such as isotropic elasticity. If particular assumptions are made, and if enough information is given, these solutions can be used to develop designs for practical problems.

While analytical and numerical solutions are useful tools, one cannot rely exclusively on theoretical relations for engineering work, as these solutions are inherently approximate explanations for real situations. They are based on simplified assumptions, which generally may not be representative of actual conditions. Therefore, existing theories for estimating earth pressure often need to be supplemented by field measurements. Field measurements can yield important clues concerning the actual condition of the site environment and can be used as a check against the theoretical models.

Nevertheless, measurement of earth pressure has been, and still remains, a difficult task. The in situ stress distributions are irrevocably changed to accommodate the introduction of a measuring device into the system for the purposes of estimating stresses. The in situ stress values, which were the aim of the measurements, are subsequently altered. This is generally referred to as an inclusion effect in earth pressure measurement.

The Earth Pressure Cell

In general, an earth pressure cell (EPC) is a device designed to provide an estimate of normal stress in soil (Fig. 1.1). Depending on the orientation of the cell, this can be an estimate of either vertical or horizontal stress. An EPC can be used in a range of geotechnical applications, from estimating lateral stresses on retaining walls to measuring vertical stresses beneath pavements. Most cells are cylindrical in shape, with their height-to-diameter ratios as small as possible, following recommendations by Taylor (1947). Hence, almost all cells appear disk-shaped, with one of the flat faces sensitive to changes in loading.

The practice of designing and manufacturing stress measurement devices revolves around the study of the interaction between the measuring device – the EPC – and the host material. Because of the aforementioned inclusion effect, it is desired that the EPC have as little impact on the in-situ stress distribution as possible. To this end, the cell's design is modified such that its calibrated output is approximate to the level of earth pressure that would exist if the cell were not present.

An EPC can be divided into two basic categories based on application: embedment and contact. Embedment cells are installed within a soil mass or fill to determine the distribution and magnitude of earth pressure (Filz and Brandon 1994). Contact cells are used for measuring earth pressures acting upon the boundaries of buried structures (Filz and Duncan 1993).

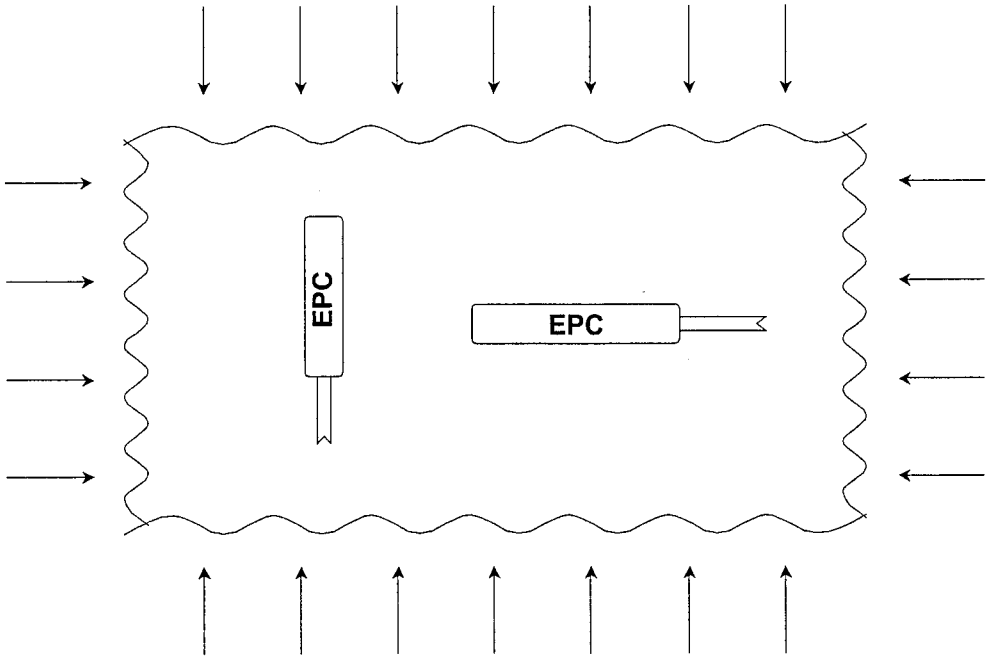

Figure 1.1. Schematic of general earth pressure cell (EPC) application. Depending on the desired orientation, EPCs provide estimates of vertical or horizontal stresses.

Embedment cells are of two types: hydraulic and diaphragm. Hydraulic cells were first used in Europe in the 1930's (Hvorslev 1976) and are quite simple in design. They are constructed by welding together two circular or rectangular plates around the periphery, creating an intervening cavity (Fig. 1.2), which is filled with liquid. A pressure transducer is connected to the cavity, and earth pressure acting on the plates is equilibrated by an equivalent amount of internal pressure in the cavity. It is essential in hydraulic cells for air to be completely removed from the cavity.

Whereas hydraulic cells are devices designed to match applied earth pressure with internal fluid pressure, diaphragm cells can be thought of as a structural member (some type of diaphragm) deflecting under loading. The amount of deflection is correlated to the level of earth pressure. As such, several designs have been proposed. One common diaphragm cell consists of a circular membrane, which is fully supported around the edge by a stiff ring (Fig. 1.3). The membrane, or diaphragm, deflects under loading. The stiff ring does not deflect, but instead anchors the membrane and acts as an inactive rim. This inactive rim isolates the active face of

the EPC, lessening the influence of stress concentration effects existing at the boundary (Dunnicliff 1988). Deflection is measured by a strain gage mounted on the interior surface of the membrane. Some cell types contain a small, fluid-filled chamber within the cell that acts to deflect the diaphragm. Depending on the manufacturer, diaphragm cells may have one or two independent active faces. The method used to estimate the normal stress acting upon the EPC typically involves strain gages mounted on the diaphragm providing output, in the form of an electrical signal, which is related to earth pressure.

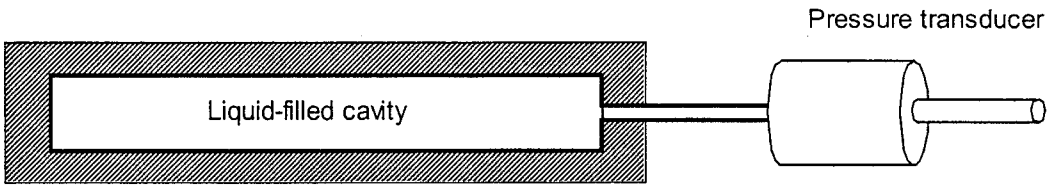

Figure 1.2. Hydraulic type embedment EPC.

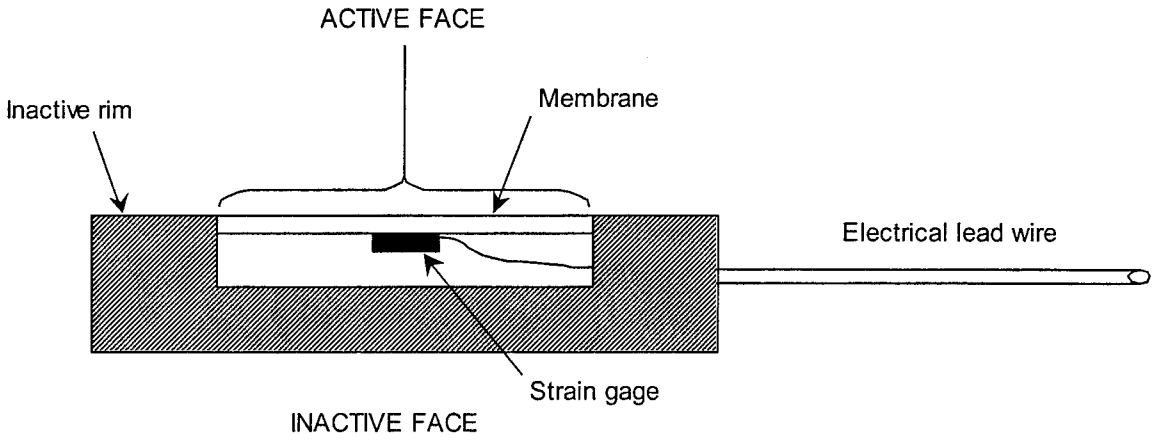

Figure 1.3. Diaphragm type embedment EPC.

The output from the EPC is related to earth pressure by applying the cell's sensitivity, S, defined as the calibration factor that converts the cell's electrical output from direct current voltage [vdc] to pressure [kPa]. It is usually determined from simple calibration tests by applying a known, fluid pressure to the EPC and recording the output. It is expected that the EPC output would be linearly proportional to the applied pressure. The data from such tests are plotted on a graph similar to Figure 1.4; the sensitivity is then the slope of the line [vdc/kPa].

The EPC sensitivity is supplied by the cell's manufacturer, with the calibration being performed with uniform fluid (air or water) pressure. However, earth pressure cells, as their name indicates, are not used to measure air or water pressure in geotechnical engineering applications. Distribution of normal stress within soil is not necessarily uniform across a given surface. Consequently, output from an EPC may be different under soil loading conditions than under corresponding fluid pressure application. In addition, depending upon the design of the cell, as the diaphragm deflects, an arching-type phenomenon may develop. Therefore, a primary goal of this study was to examine the differences, if any, between calibrations with fluid and calibrations with loading through soil. Accordingly, if significant disparities existed, the next task would be to decide which calibration technique proved more useful for field application.

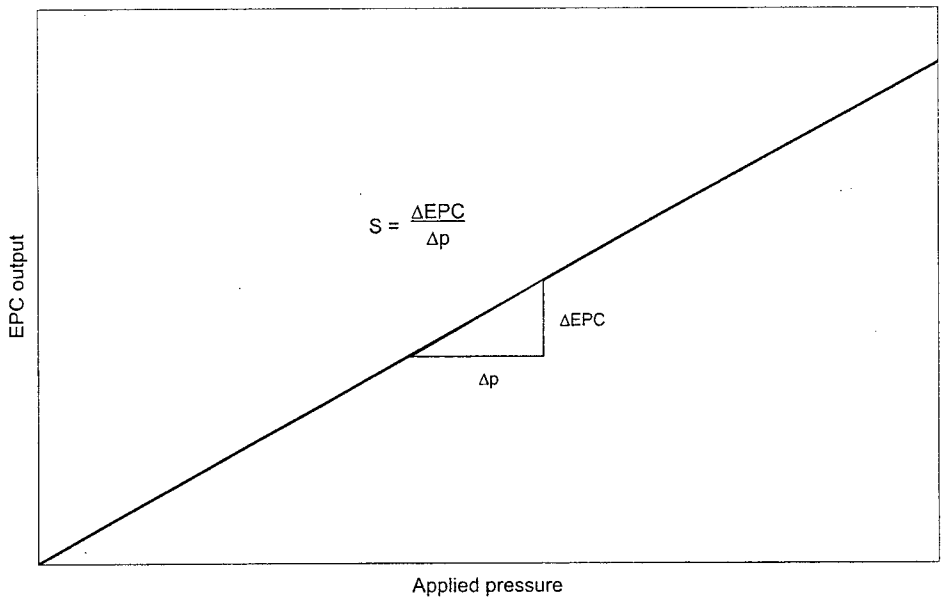

Figure 1.4. Typical EPC calibration curve. The recorded electrical output from the cell is plotted versus the known applied pressure.

Motivation and Specific Application

As stated earlier, EPC can be used in a variety of applications in pavement design. This research focused on the use of the cells to measure vertical stresses underneath paved roads (Fig. 1.5). The project's motivation and funding was provided by the Minnesota Department of Transportation (Mn/DOT). Mn/DOT has placed a group of EPCs at the Minnesota Road Research Project (Mn/ROAD), their roadway test facility in Otsego, Minnesota, in order to provide estimates of normal stresses in the underlying subgrade soil.

The aim of this project was to study the behavior and interaction of the EPC with soil, procure a suitable method of cell calibration, observe the cell's response to standard static and dynamic loadings within a controlled soil environment, and recommend a workable field installation procedure. Because of an inclusion effect, and where an EPC usually acts as a stress attractor, the cell tends to overestimate the magnitude of earth pressures in soils. However, arching can develop above an EPC and resistive shear stress can reduce the normal stress acting on the sensing face of the cell. In order to account for arching in the cell's registration, a new calibration method was devised. The performance of the EPC was then studied in a controlled soil environment.

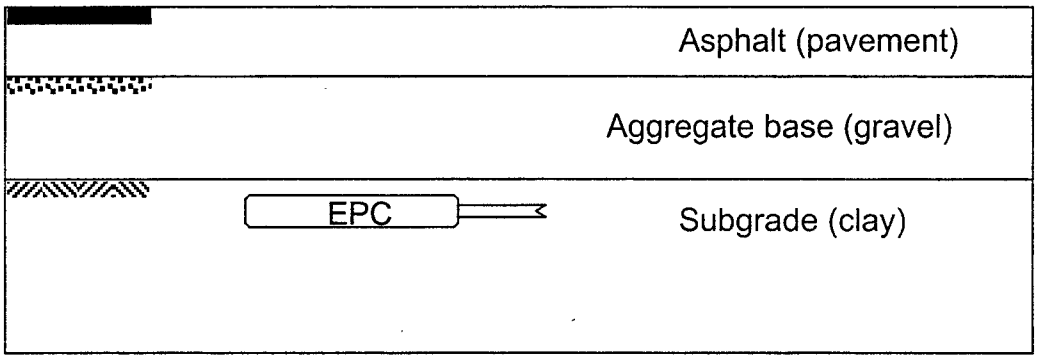

Figure 1.5. Roadway cross-section at Mn/ROAD facility. The earth pressure cells were intended to be placed within the clay subgrade, beneath the aggregate and overlying pavement. The cells would record changes in vertical stress resulting from traffic loads.

Kulite Earth Pressure Cell

The primary EPC used in this study was the Kulite soil pressure cell manufactured by Kulite Semiconductor Products, Inc. in Leonia, New Jersey. The Kulite earth pressure cell combines features of both the diaphragm and hydraulic cells (Fig. 1.6). The basic sensing element is a semi-conductor strain gage mounted on a diaphragm below a thin layer of hydraulic oil. A thin piece of steel isolates the oil from the outer annulus and reinforcing plate. The entire assembly is housed within a stiff steel casing. Loading applied to the sensing face is transmitted to the oil layer, which deflects the diaphragm. The strain gage element responds to the amount of deflection.

Part of the steel casing forms an inactive rim around the outer perimeter of the cell's sensing face. The central, active surface area on the sensing face is 1022 mm^2 (1.58 $in.^2$). The total area on the sensing face is 2331 mm^2 (3.61 $in.^2$), yielding an active/total surface area ratio of 0.44. This type of design is used to lessen the inclusion effect that results when introducing a different material within the host soil. However, an important aspect of the performance is also the displacement of the sensing face relative to the inactive rim, which may cause soil arching to occur over the cell. This behavior is critical in how the cell performs in the field.

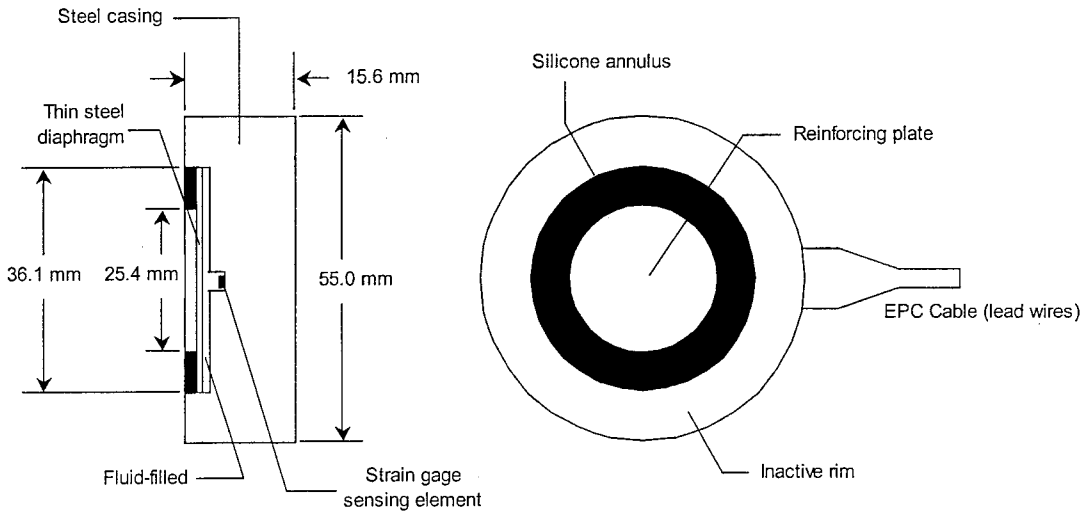

Figure 1.6. Kulite earth pressure cell.

CHAPTER 2
LITERATURE REVIEW

The quandary of placing an earth pressure cell within a soil mass influenced by a pre-existing stress field has been considered and well studied. Early solutions were based on the tenets of elasticity theory. The EPC was presented as a material inclusion within an elastic matrix. As such, stresses acting upon the cell were dependent on the elastic moduli of the inclusion and the surrounding matrix, and the assumed geometry (shape) of the inclusion. Later, studies were conducted that considered the interaction of particulate soil matter with a rigid structure. Terzaghi's soil arching theory provided the foundation for these solutions, with experimental support from McNulty (1965) and Mason (1965).

Taylor's Indentation Analysis

One of the first to consider the interaction between an EPC and soil was Taylor (1945). Taylor's method fell under the mantle of an indentation analogy. This approach (Fig. 2.1) consisted of estimating the difference between soil and cell deformations, or the indentation, and then computing the corresponding over- and under-registrations of the cell which would produce the same displacement (Hvorslev 1976).

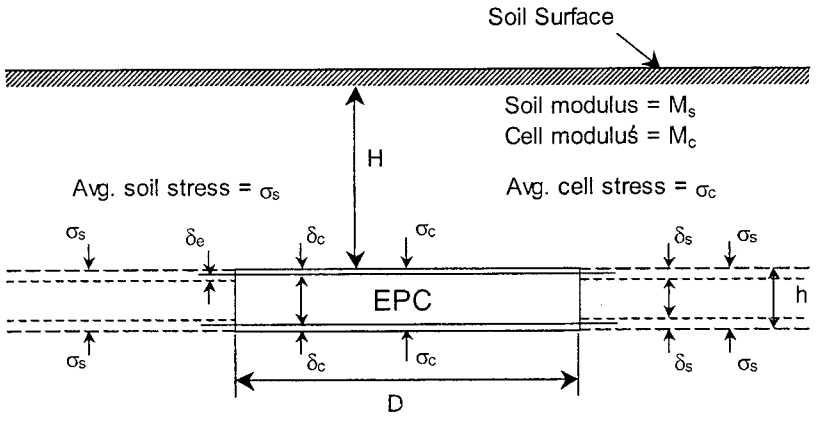

Figure 2.1. Earth pressure cell embedded in soil. (Taylor 1945, from Hvorslev 1976)

Taylor considered an EPC at a depth, H, below the free soil surface with diameter, D, and thickness, h. The cell and soil were subjected to a uniaxial stress change acting perpendicular to the face of the cell. Assuming symmetry of deformations of the cell and soil, the indentation of each side (face) of the cell is given by

$$\delta_e = \delta_s - \delta_c \tag{1}$$

where δ_s and δ_c are the deformations of the soil and cell respectively. In terms of the material parameters, δ_e may be expressed as

$$\delta_e = \frac{h}{2}\left(\frac{\sigma_s}{M_s} - \frac{\sigma_c}{M_c}\right) \tag{2}$$

where σ_s and σ_c are the average stresses and M_s and M_c are the Young's moduli of the soil and cell respectively. The difference, δ_e, is similar to the indentation of a circular plate or punch into an elastic solid under the load, σ_e, where

$$\sigma_e = \sigma_c - \sigma_s \tag{3}$$

δ_e is then given by

$$\delta_e = D\frac{\sigma_e}{N_s} \tag{4}$$

The parameter N_s is an indentation coefficient that is a function of the deformation characteristics of the soil. Manipulation of the equations yields the relation (Eqn. 5) for the cell-soil registration ratio, σ_c/σ_s. The coefficient K_s was defined as $K_s = N_s/M_s$.

$$\frac{\sigma_c}{\sigma_s} = \frac{\frac{D}{h/2} + \frac{N_s}{M_s}}{\frac{D}{h/2} + \frac{N_s}{M_c}} = \frac{\frac{D}{h/2} + K_s}{\frac{D}{h/2} + \frac{M_s}{M_c}K_s} \tag{5}$$

The coefficients N_s and K_s may be theoretically determined by employing the theories of Boussinesq, assuming that the soil acts as an elastic solid (Eqns. 6 and 7).

$$N_s = \frac{M_s}{(1-\nu^2)C} \tag{6}$$

$$K_s = \frac{N_s}{M_s} = \frac{1}{(1-\nu^2)C} \tag{7}$$

Where ν is the Poisson's ratio for the soil, and C is a shape factor. For an infinitely rigid circular plate at the soil surface, $C = \pi/4$. Taylor suggested that N_s was approximately equivalent to M_s, so that K_s approached unity. This assumption was also used by Peattie and Sparrow (1954). Hvorslev (1976) emphasized that the equations derived from the indentation analogy were theoretical and only rough approximations of the actual behavior.

Referring to Equation 3, the error ratio, σ_e/σ_s, that exists in the pressure cell with respect to the average stress in the soil is given by

$$\frac{\sigma_e}{\sigma_s} = \frac{\sigma_c}{\sigma_s} - 1 \tag{8}$$

In the form of Equation 5, with the indentation coefficients added, the error ratio becomes

$$\frac{\sigma_e}{\sigma_s} = K_s \frac{h/2}{D} \frac{1 - \dfrac{M_s}{M_c}}{1 + K_s \dfrac{h/2}{D} \dfrac{M_s}{M_c}} \tag{9}$$

For the case of an infinitely rigid pressure cell ($M_s/M_c = 0$), the limiting value of the error ratio is proportionally related to the cell geometry by

$$\frac{\sigma_e}{\sigma_s}(\lim) = K_s \frac{h/2}{D} \tag{10}$$

The above analysis assumes a uniaxial stress change within the soil applied perpendicular to the face of the cell. When lateral stresses are included as part of a triaxial stress change in the soil, the analysis is similar. However, the stress changes in the three principal directions and the influence of Poisson's ratio are incorporated into the solution. The stress registration ratio with respect to the principal z-direction is

$$\frac{\sigma_c}{\sigma_s} = \frac{\sigma_c}{\sigma_z} = \frac{\dfrac{D}{h/2} + K_s\left(1 - \nu \dfrac{\sigma_x + \sigma_y}{\sigma_z}\right)}{\dfrac{D}{h/2} + K_s \dfrac{M_s}{M_c}} \tag{11}$$

and similarly for the other x- and y- principal directions.

Monfore's Indentation Analysis

Unlike Taylor, Monfore (1950) considered a more rigorous approach within the framework of linear elasticity. He evaluated the theoretical situation of an EPC of Young's modulus, M_c, embedded in a solid of modulus, M_s. A cross-section of a cell within a solid is shown in Figure 2.2. A plane of symmetry, I, was drawn through the middle of the cell, lying parallel to its faces. The solid, representing a soil mass, was subjected to a loading of intensity, Q, acting on its boundary, perpendicular to plane I. If the cell were ideal, that is $M_c = M_s$, the stress distribution on plane I would be uniform and equal to the boundary loading, Q. However, for the case $M_c > M_s$, the stress across I is greater than Q within the cell and less than Q outside the cell.

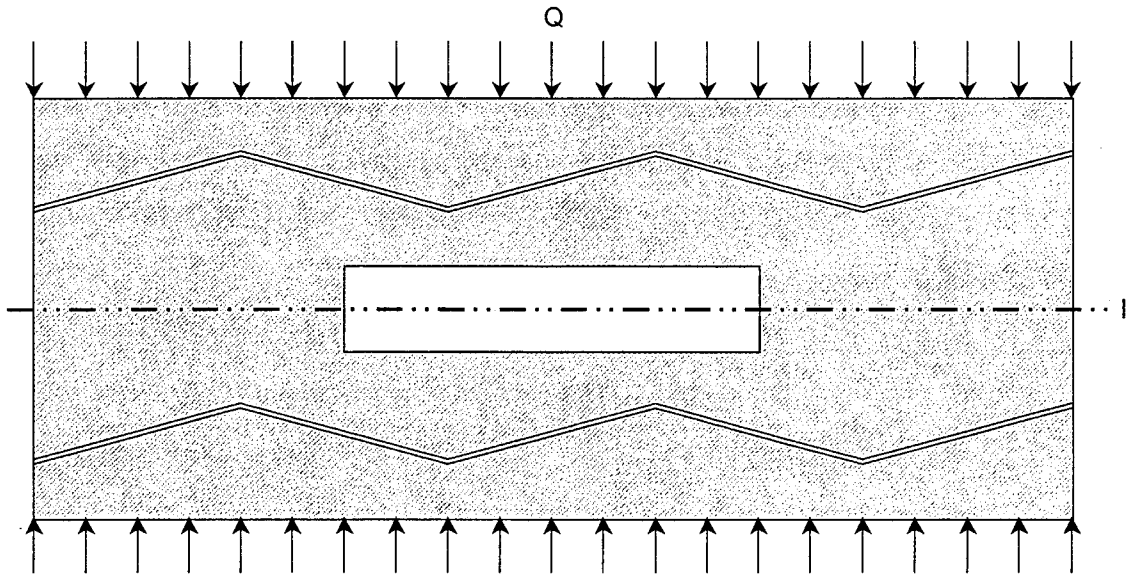

Figure 2.2. Cross section through EPC and solid. The solid is subjected to a boundary load intensity, Q, perpendicular to plane I. (Monfore 1950)

Monfore's analysis was concerned with achieving uniformity of displacement across plane I. He noted that deflections due to Q within the cell along I would not be equal to deflections outside the cell within the surrounding solid. Indeed, for the case of the stiff cell ($M_c > M_s$), deflections within the cell would be less than the respective deflections within the solid. In order to constrain deflections from both cell and solid to lie along I, a load distribution was

superimposed on Q. This load distribution would have the property of compressing the half cell downward to lie along the cut surface of plane I. Since the solid outside the half cell would displace more than the cell, a tensile loading was applied to pull the solid upward to lie along I.

The half cell and surrounding solid were modeled as a series of annular rings plus a central section, with the centers of each being coincident with the axial center of the cell. The central section and each annular ring were subjected to their own respective load intensity, q_i. Using the Boussinesq equations as presented by Timoshenko (1934), Monfore developed a system of equations for calculating the superimposed annular load intensities, q_i, that must be applied to each ring so that the deflections across plane I were uniform. The system of equations was derived from the general form:

For values of r outside a loaded area

$$\frac{w\pi M_s}{4(1-\nu^2)q} = r\left[\int_0^{\pi/2}\left(1-\frac{a^2}{r^2}\sin^2\theta\right)^{1/2}d\theta - \left(1-\frac{a^2}{r^2}\right)\int_0^{\pi/2}\frac{d\theta}{\left(1-\frac{a^2}{r^2}\sin^2\theta\right)^{1/2}}\right] \tag{12}$$

for values of r within a loaded area

$$\frac{w\pi M_s}{4(1-\nu^2)q} = a\int_0^{\pi/2}\left(1-\frac{r^2}{a^2}\sin^2\phi\right)^{1/2}d\phi \tag{13}$$

where q is the load intensity, w is the deflection of the loaded surface, a is the radius of the loaded area, and ν is Poisson's ratio of the solid.

Using the above equations, Monfore developed a series of relations for the deflections of each segment, i, as functions of each loading intensity, q_i. By employing Hooke's law for expressing the deflections, w_i, in terms of M_c, M_s, ν, H, and Q, a system of equations for the I unknown q_i's resulted.

Monfore expressed his solution graphically for different cases. Figure 2.3 shows the variation in field stress across plane I as a percentage of the boundary loading, Q, for a particular case of cell geometry and material constants. As seen in the figure, the vertical stress in the cell is greater than the far field stress, with significant increases near the cell boundaries. Likewise, the stress in the solid near the cell boundaries decreases sharply.

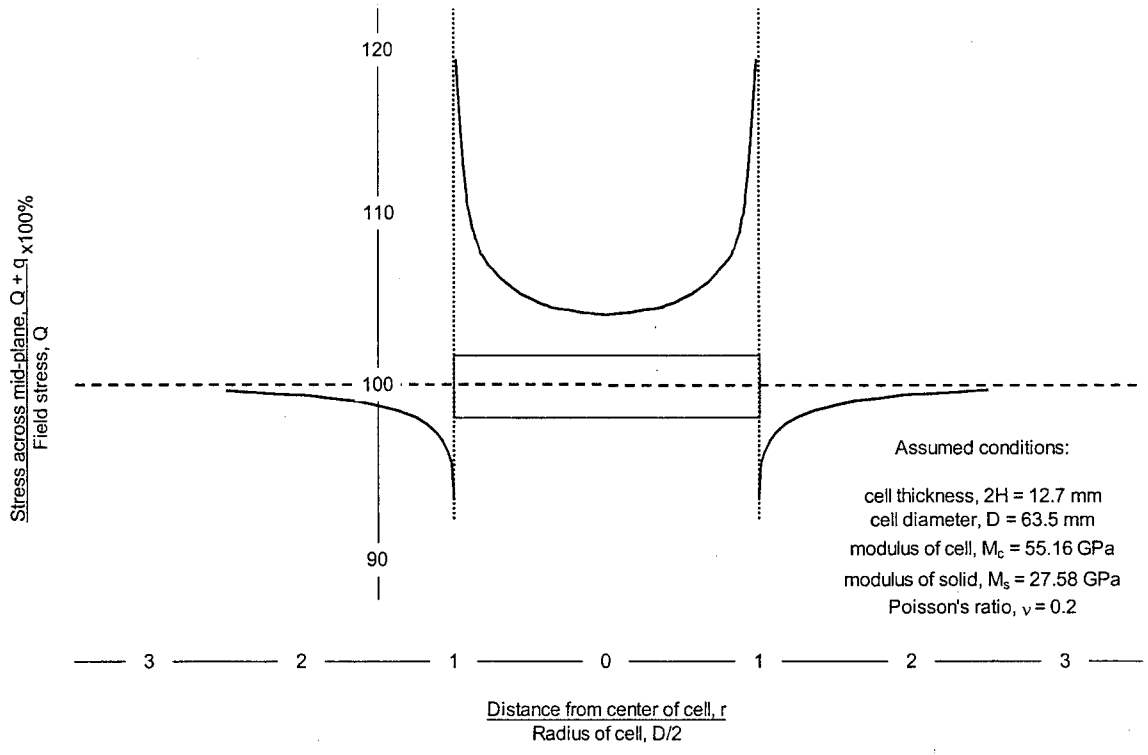

Figure 2.3. Stress distribution across mid-plane. (Monfore 1950)

Cell error was defined as the difference between the cell-indicated stress ($Q + q_{cell}$ in Fig. 2.3) and the far-field stress (Q in Fig. 2.3). The normalized cell error is q_{cell}/Q x 100%. It can be deduced from Figure 2.3 that a cell face sensitive to stress over a central area only, and not over its entire face, will have a lower cell error. Similarly, a cell that measures stress across its total area will have a higher cell error. Moreover, the thickness-to-diameter ratio of a cell is proportional to the cell error (Fig. 2.4). The degree of proportionality varies depending on whether the cell is sensitive over a central area or across the entire face (Fig. 2.4).

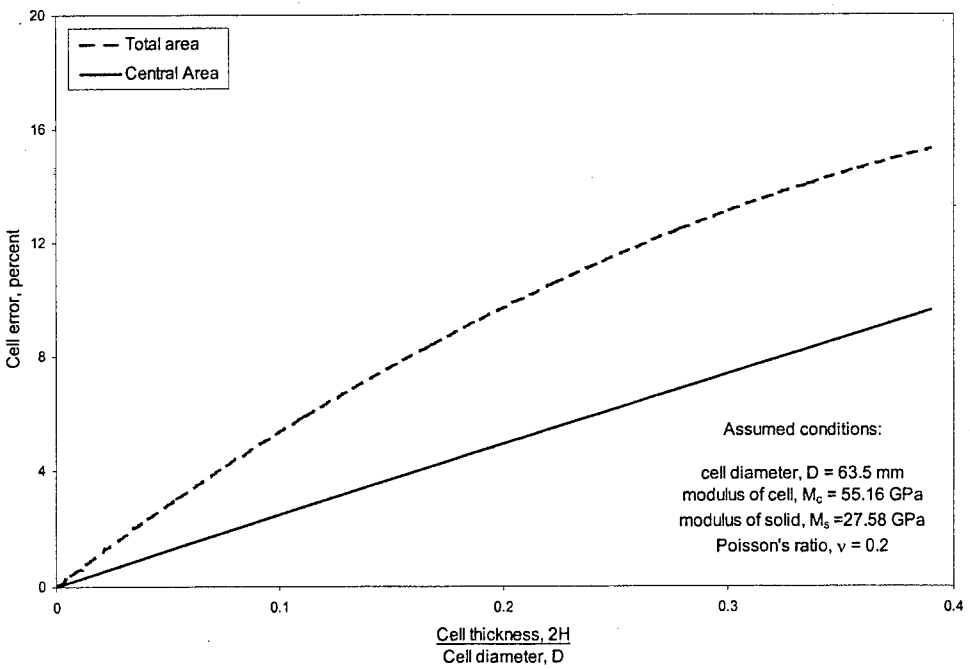

Figure 2.4. Effect of the ratio of cell thickness to diameter on cell error. For cells sensitive over a central area, the error is approximately linearly related to the cell thickness-diameter ratio. (Monfore 1950)

The effect of modulus variation on cell error is shown in Figure 2.5. When the modulus of the cell is larger than the soil, the error will be positive and the stress in the cell will be larger than the far field stress. Conversely, when the modulus of the solid is larger, the error will be negative and the stress in the cell will be smaller than the far field stress. It is interesting to note that the errors are smaller in absolute value when the cell modulus is larger than when the solid modulus is reciprocally higher. Also, when the ratio of $M_c/M_s > 1$ and given by a constant, A, the error is smaller in absolute value compared to the situation when $M_s/M_c = A$.

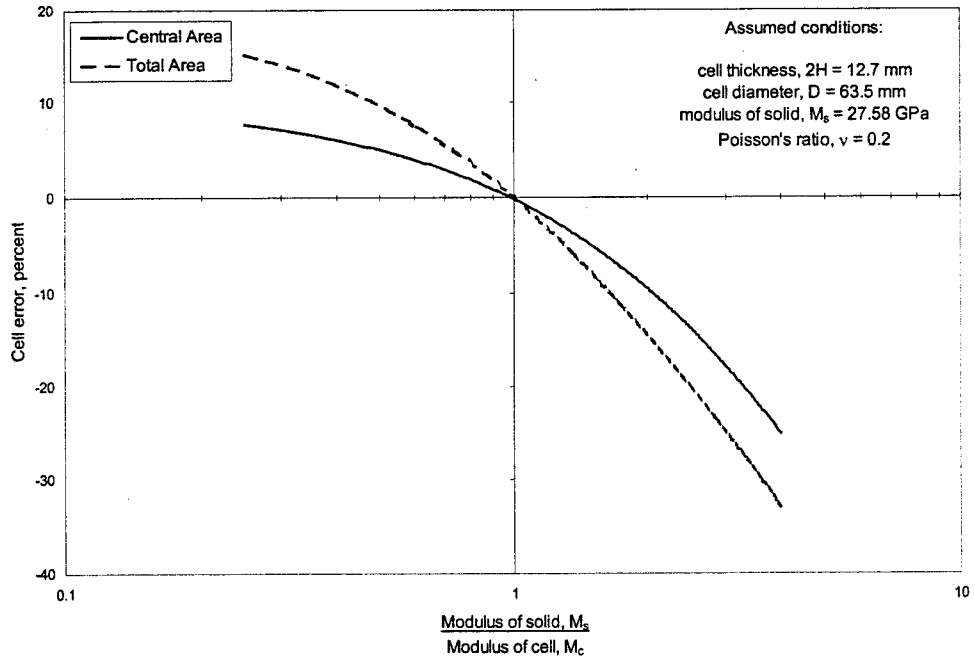

Figure 2.5. Effect of the ratio of elastic moduli on cell error. (Monfore 1950)

Askegaard's Elasticity Analysis

Askegaard (1963) studied the stress interaction effects between an elastic matrix and an ellipsoidal inclusion embedded within the matrix. The study followed the classical work of Eshelby (1957). Askegaard obtained equations for stresses in a rigid ellipsoidal inclusion and for pressures in a liquid-filled ellipsoidal cavity. He based his solutions on free-field stress conditions.

Askegaard assumed the inclusion to be rigid or fluid-like. The material in the surrounding matrix (i.e. soil) was assumed to be isotropic and fully elastic. Both normal and tangential forces were also assumed to be transferred between the inclusion and the matrix without slipping. The ellipsoid was defined to have height, h, and diameter, D, and the height-diameter ratio was defined as $\alpha = h/D$.

The Askegaard solution for a rigid ellipsoidal inclusion is graphically summarized in Figures 2.6 – 2.7. Figure 2.6 shows the stress ratio due to a uniaxial stress change in the elastic matrix as a function of the Poisson's ratio of the matrix. The solution shows a series of curves pertaining to different values of inclusion geometry, α. The stress ratio is given by σ_c^A/σ_s^A, where the subscripts "c" and "s" refer to stresses within the inclusion and matrix, respectively, in the vertical z-direction. The superscript "A" indicates the stresses were due to a uniaxial stress change in the matrix ($\sigma_z = \sigma_s^A$, $\sigma_x = \sigma_y = 0$). Figure 2.7 similarly shows the relationships between the stress ratio and matrix Poisson's ratio due to a triaxial, "T," stress change ($\sigma_x = \sigma_y = \sigma_z = \sigma_s^T$), as a series of inclusion geometry values, α. The triaxial stress ratio, however, is given by σ_c^T/σ_c^A, the ratio of inclusion stresses in the z-direction due to a triaxial and uniaxial stress change in the matrix.

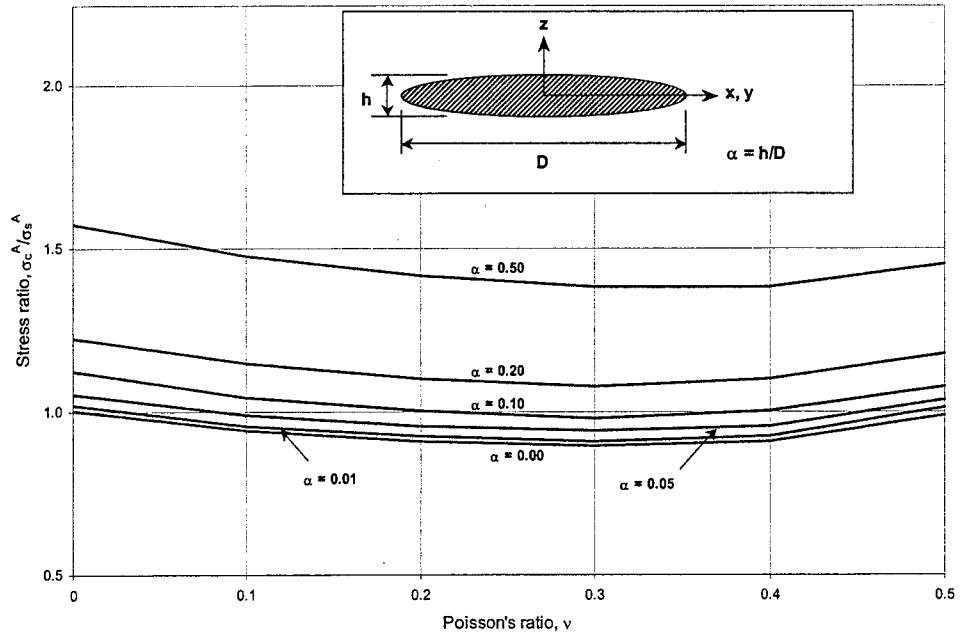

Figure 2.6. Uniaxial stress change in matrix. (Askegaard 1963, from Hvorslev 1976)

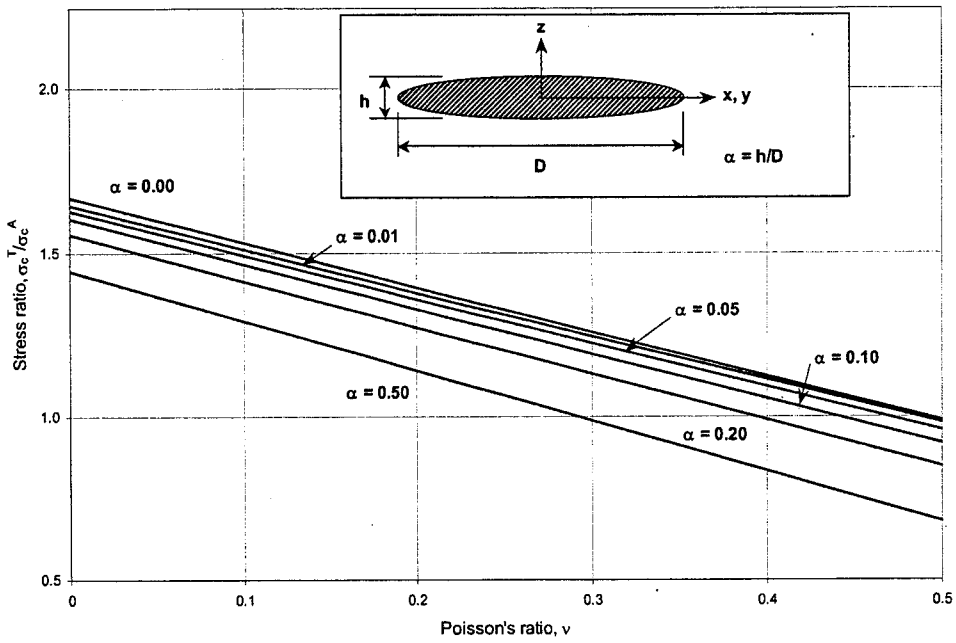

Figure 2.7. Triaxial stress change in matrix. (Askegaard 1963, from Hvorslev 1976)

Conversely, the stress ratio, σ_c/σ_s, and the error ratio, σ_e/σ_s, where $\sigma_e = \sigma_c - \sigma_s$, are plotted in Figure 2.8 as a function of the height-diameter ratio, α, for three values of the matrix Poisson's ratio, ν. As illustrated in Figure 2.8, σ_e was approximately linear with respect to α, the height-diameter ratio.

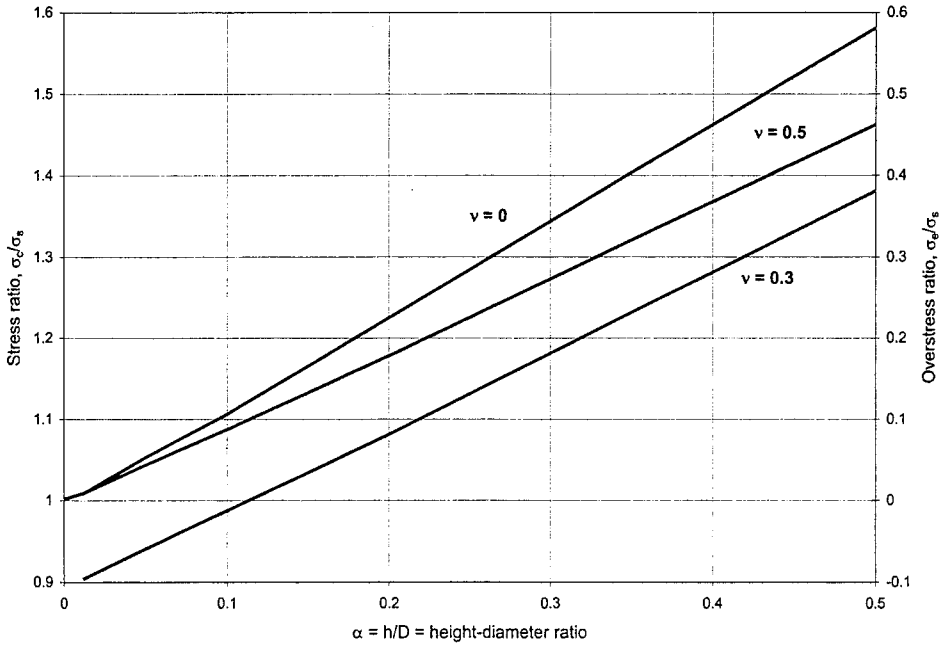

Figure 2.8. Inclusion stress versus cell height-diameter ratio. (Askegaard 1963, from Hvorslev 1976)

In his review of Askegaard's model, Hvorslev (1976) noted that the matrix Poisson's ratio has a small, but not negligible, influence on the stress ratio for a uniaxial stress change in the matrix. Medium values of ν have the highest impact on the stress ratio, whereas this impact is minimized for values of $\nu = 0$ and $\nu = 0.5$. Also noted is the effect of geometry on the inclusion model. As illustrated in Figure 2.7, when α is small, axial stresses in the inclusion increase with an increase in the lateral stresses in the matrix. However, for larger values of α and ν, axial stresses in the inclusion may decrease. The registration error involved with determining inclusion stresses (defined above as the overstress ratio) was linearly proportional to the geometry, α, which agrees with a simplified analysis by Hvorslev (1976) based on Taylor's earlier work and Peattie and Sparrow (1954).

Experiments by Peattie and Sparrow

Experiments were conducted by Peattie and Sparrow (1954) to investigate the dependence of various design parameters and soil types on the behavior of earth pressure cells.

Cells of differing height-diameter ratios, modular ratios (M_c/M_s), and sensitive-area-to-total-area ratios were constructed and tested in a soil chamber. Loose and dense sand, as well as clay at multiple water contents, were used. The chamber was filled with soil, the cell was placed in the middle of the chamber, and a uniform load was applied to the surface of the soil at the top of the chamber.

In order to determine earth pressures acting on the cell within the chamber and thus evaluate the response of the cells, the following solution, derived from Taylor (1947) and similar to Equation 5, was used:

$$\frac{\sigma_e}{\sigma_s} = C_A \frac{H}{D} \tag{14}$$

with C_A being the cell action factor, defined by

$$C_A = \left[\frac{K\left(1 - \frac{M_s}{M_C}\right)}{1 + \frac{H}{D}\frac{M_s}{M_C}K} \right] \tag{15}$$

where $\sigma_e = \sigma_c - \sigma_s$ is the pressure recorded by the cell, σ_s is the field pressure existing at the plane of the cell in its absence, M_s is the Young's modulus of the soil, M_c is the Young's modulus of the cell, K is a constant value defined by soil properties, H is half the height of the cell, and D is the diameter of the cell. Assuming that σ_c, the pressure recorded by the cell, was given by $\sigma_c = \sigma_s + \sigma_e$, the following equation was used to calculate pressure on the cell, where σ_o was the pressure applied to the soil surface:

$$\frac{\sigma_c}{\sigma_o} = \left(C_A \frac{H}{D} + 1 \right) \frac{\sigma_s}{\sigma_o} \tag{16}$$

However, since σ_c/σ_o varied with pressure, the pressure reading from the thinnest cell, σ_{c1}, was substituted for σ_o. So the relation for calculating pressure on the cell became

$$\frac{\sigma_c}{\sigma_{c1}} = \left(C_A \frac{H}{D} + 1 \right) \frac{\sigma_s}{\sigma_{c1}} \tag{17}$$

Results from the experiments by Peattie and Sparrow investigated the variation of cell errors with H/D, the effect of applied pressure, the effect of the ratio of sensitive area to total

area of the cell, the value of the modular ratio, and the effect of the time for which the load was allowed to act. The cell error was seen to be directly proportional to the height-diameter ratio, H/D, for all soil types tested; loose sand unit weight = 15.9 kN/m^3 (101 lb/ft^3), dense sand dry unit weight = 16.3 kN/m^3 (104 lb/ft^3), clay unit weights = 18.4, 17.3, and 17.4 kN/m^3 (117, 110, and 111 lb/ft^3). As the ratio increased, so too did the cell error. The cell action factor, C_A, was found not to be constant for cells of equivalent H/D ratios tested in different soil types.

The effect of the applied pressure on cell registration (p_c/p_{c1} vs p_0) was examined for various cases of H/D. There was no variation in C_A for tests in loose and dense sand. In dense sand, C_A changed only when the diameter of the sensitive area was greater than 38.1 mm (1.5 in). For tests in clay, C_A became more dependent on pressure as the water content was decreased. However, as the pressure increased, this dependence decreased.

The effect of the ratio of sensing area to total area of the cell was studied. The percentage of normal stress above the field stress (value of normal stress in the absence of the cell) was mapped across the face of the cell. The pressure near the center of the cell was observed to be higher than the field value, in accordance with the Monfore's (1950) prediction. It was seen, for all soil types, that high pressures developed at the cell edges. This trend was also in agreement with the solution by Monfore. However, in tests with loose and dense sand, the pressure at the edge of the cell approached a limiting value. The dense sand, in fact, showed the pressure to increase to a maximum value near the edge of the cell and then decrease slightly. To minimize errors, it was advised that the edges of the cell not be sensitive to pressure. For cells 76.2 mm (3.0 in) in diameter, a sensitive area with a 38.1 mm (1.5 in) diameter was suggested as optimum.

The value of the modular ratio, M_c/M_s, and its effect on cell error was studied. It was found that the cell error was independent of the value of M_c/M_s when the ratio was greater than 10. It was concluded that cells should have a modulus such that M_c/M_s is larger than 10, because the error, though at a maximum, is then independent of the ratio. When the ratio is at unity, the error is minimized, but will be greatly affected by small changes in M_s.

The effect of the time for which the load was allowed to act was also explored. All tests conducted in sand, both loose and dense, were observed to be independent of time. The driest of the clays tested, water content = 13.5%, also exhibited time independence. For wetter clay, water content = 16%, C_A varied, but for sensitive area diameters of 38.1 mm and 50.8 mm (1.5 in. and 2 in.) C_A was time independent.

The conclusions reached by Peattie and Sparrow were that (1) the cell error was directly proportional to H/D, (2) cell error was dependent on the relative size of the sensing area, and (3) cell error was not large when due to changes in the modular ratio. Indeed, the error was independent of the modular ratio when its value was greater than 10. For design purposes, H/D should be kept as small as possible. Design recommendations for the ratio of sensing area to total area of the cell were given: for pressure-averaging (fluid filled) cells, a ratio of less than 0.25 was recommended; for cells employing pressure responsive diaphragms, a ratio of less than 0.45 was recommended.

Terzaghi's Trapdoor Analogy

Terzaghi (1943) considered the problem posed by an unsupported strip of a rigid boundary yielding under the weight of overlying soil. The soil forces acting on the strip were then regarded as analogous to those forces resulting from the displacement of the sensitive face of an EPC under loading. This situation was termed a "trapdoor analogy" by Hvorslev (1976).

When the trapdoor yields away from the soil mass, the soil above the strip will displace downward. The relative movement of the yielding soil to the adjoining stationary part is opposed by a shearing resistance due to friction along particle contacts between the zones (Fig. 2.9). The stresses that are generated tend to decrease the active pressure acting on the trapdoor. The decrease of stress from the yielding support strip to the adjacent soil is commonly referred to as an arching effect, since the soil is considered to effectively arch over the yielding trapdoor (Terzaghi 1943).

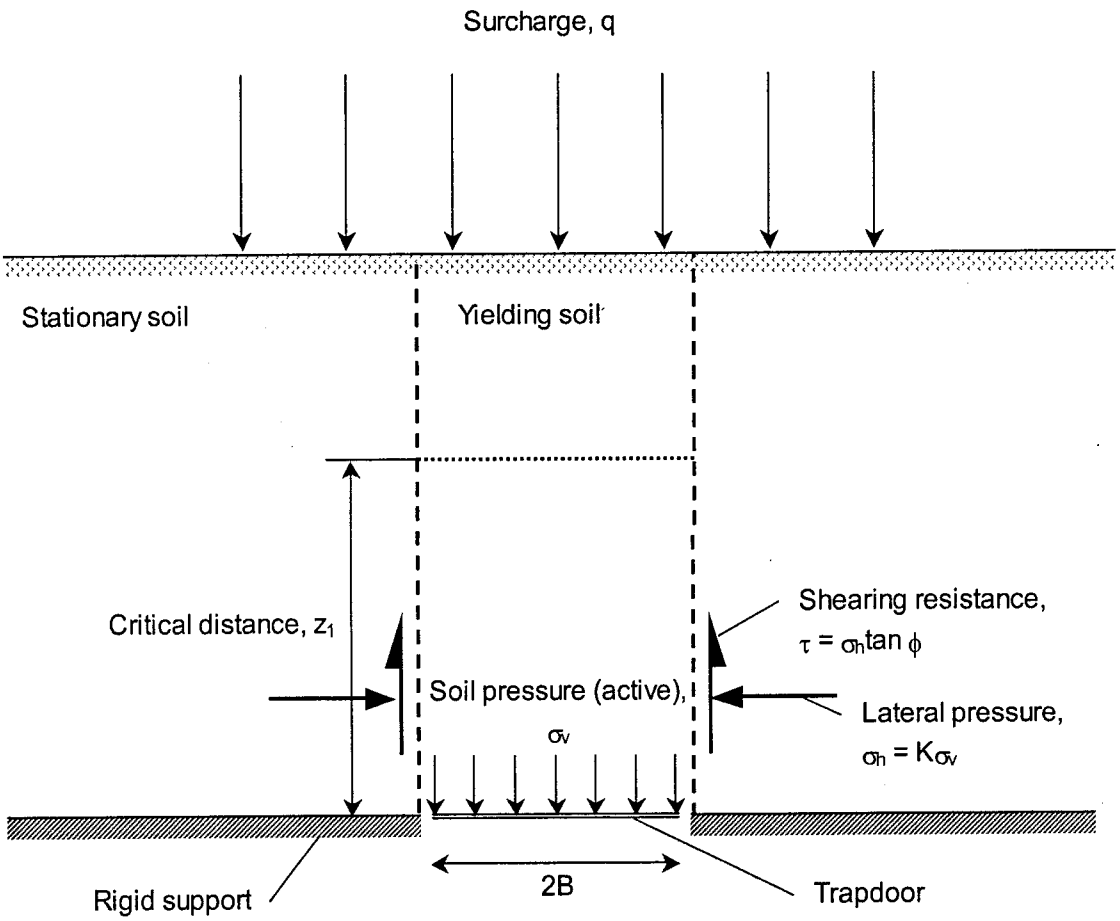

Figure 2.9. Yielding trapdoor analogy, active case. (Terzaghi 1943)

The shearing interface between the moving and stationary soils was idealized as a vertical, planar surface. The boundaries of the shearing interface extended from the edges of the trapdoor upward to a critical distance, z_1. Beyond the distance, z_1, the soil would not be affected by arching, but soil above the zone of arching would contribute to the overall surcharge acting on the yielding soil mass. For sandy soils, the active pressure, σ_v, acting on the trapdoor was given by

$$\sigma_v = qe^{-K \tan \phi \left(z/B\right)} \tag{18}$$

where q is the surcharge above the arching zone, K is the coefficient of earth pressure at rest, z is the distance above the trapdoor within the arching zone ($z < z_1$), and B is the half-width of the

trapdoor. According to Terzaghi, the critical distance, z_1, above the yielding strip beyond which arching does not occur, was between 4B and 6B for active pressure conditions.

Trapdoor Experiments

A series of experiments with circular trapdoors were carried out by McNulty (1965) at the Waterways Experiments Station. The tests involved circular doors of two diameters installed at the bottom of a test bin, and two types of medium grained sand placed at two different densities. The depth of sand was varied, but never exceeded twice the diameter of the trapdoor being tested. The pressure on the trapdoor and its displacement were recorded. Nearly linear relations between pressure and displacement were observed for displacements less than 0.0002 times the diameter of the door. McNulty noted that such small movements may change the pressure on the door by as much as 50 percent. In a theoretical treatment of the test data, for the case where the trapdoor yields downward and away from the sand (active case), the results agree fairly well with Terzaghi (1943) when Equation 18 is transformed from a strip-type to a circular door of radius, R:

$$\sigma_v = qe^{-2K\tan\phi\left(z/R\right)} \tag{19}$$

The circular trapdoor experiments were thought to be excellent models for the action of EPC placed flush with rigid boundaries.

A theory for the determination of the approximate axial stress on a cell in a free stress field was proposed by Mason (1965). It was assumed that soil deformations and stresses at distances greater than z_1 were not influenced by the cell, similar to Terzaghi (1943). Mason's theory considered only the average stresses within a soil cylinder above and below the cell. The stress, σ_s, was taken to be either the uniform stress in the free soil or the uniform load acting at the critical distances. The relation between the stress on the cell, σ_c, and the field stress, σ_s, was the same as that for a trapdoor (Eqn. 19). The relation between σ_c and σ_s at the critical distance z_1 was given by:

$$z_1 = \frac{R}{2K\tan\phi}\ln\left(\frac{\sigma_c}{\sigma_s}\right) \tag{20}$$

Also presented were equations for the differential settlement around the cell due to soil and for relating the stress ratio (σ_c/σ_s) and the modular ratio (M_s/M_c), (active pressure case):

$$\frac{M_c}{M_s} = \frac{\left(\frac{B}{R}\right)\left(\frac{\sigma_c}{\sigma_s}\right)2K\tan\phi}{\ln\left(\frac{\sigma_s}{\sigma_c}\right)-1+\left(\frac{\sigma_c}{\sigma_s}\right)+\left(\frac{B}{R}\right)2K\tan\phi} \tag{21}$$

The above equations were compared to test data produced from a cell embedded in a free soil stress field (Fig. 2.10). The solid lines represent theoretical relations and the dashed lines indicate experimental data. Both showed a decrease in active stresses with increasing depth below the free soil surface until a critical distance was reached. Thereafter, the stress ratio (σ_c/σ_s) was constant with additional increases in depth.

The experiments by Mason and Associates were of the same form as McNulty (1965) in terms of measuring load and deflection, but the cell was embedded in a free soil stress field instead of a trapdoor at a rigid boundary. Both experiments showed good agreement with theory (Eqns. 20-21) for small deformations. This depended in large part on the values of the soil parameters used in the theoretical equations.

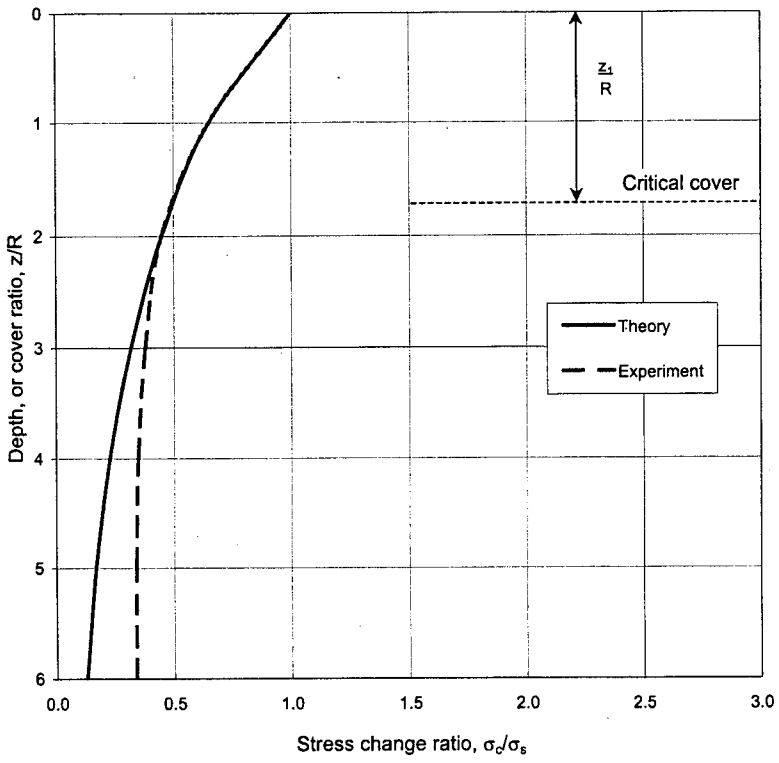

Figure 2.10 (Mason 1965, from Hvorslev 1976). Limiting stress change versus soil cover.

Extension of Related Work

Recent EPC calibration work was conducted by Van Deusen (1992) and also by Selig (1995). Both calibrated an EPC under fluid (air) pressure and studied its performance within a chamber of soil subjected to a surface loading. Neither Van Deusen or Selig conducted experiments that isolated the sensing face of the cell in order to measure the effect soil arching had on the EPC output. Because of an inclusion effect, where an EPC usually acts as a stress attractor, the cell tends to overestimate the magnitude of earth pressures within soils. However, as shown by Terzaghi (1943), arching can develop above an EPC and resistive shear stress can reduce the normal stress acting on the sensing face of the cell.

CHAPTER 3
PRELIMINARY CALIBRATION

An EPC, as previously stated in Chapter 1, is calibrated by applying a known, uniform pressure to the sensing face of the cell. The electrical output from the cell is recorded and plotted versus pressure. The relation between pressure and cell output should be linear, with the slope of the line yielding the EPC sensitivity [vdc/kPa]. Manufacturers typically use fluid pressure when calibrating their cells. However, an EPC is used primarily to measure normal stresses within a soil mass. Therefore sensitivities obtained from fluid calibrations may not be suitable for practical applications. A more appropriate calibration method may be to load the EPC through soil to account for possible non-uniform loading and arching effects.

Preliminary study of EPC calibration methods involved analyzing the response of the cell under simple fluid loading calibrations (Fig. 3.1), verifying the EPC sensitivity value as provided by the manufacturer, and observing any possible changes in EPC output as a result of temperature variation. Fluid calibrations were performed under three basic conditions: all-around hydrostatic loading, uniaxial loading on the active face, and radial loading around the perimeter of the EPC. A calibration sensitivity was calculated for each loading condition. They were compared with each other and with the manufacturer's value. A separate set of experiments was conducted where the EPC output (with no external load) was monitored with changes in temperature.

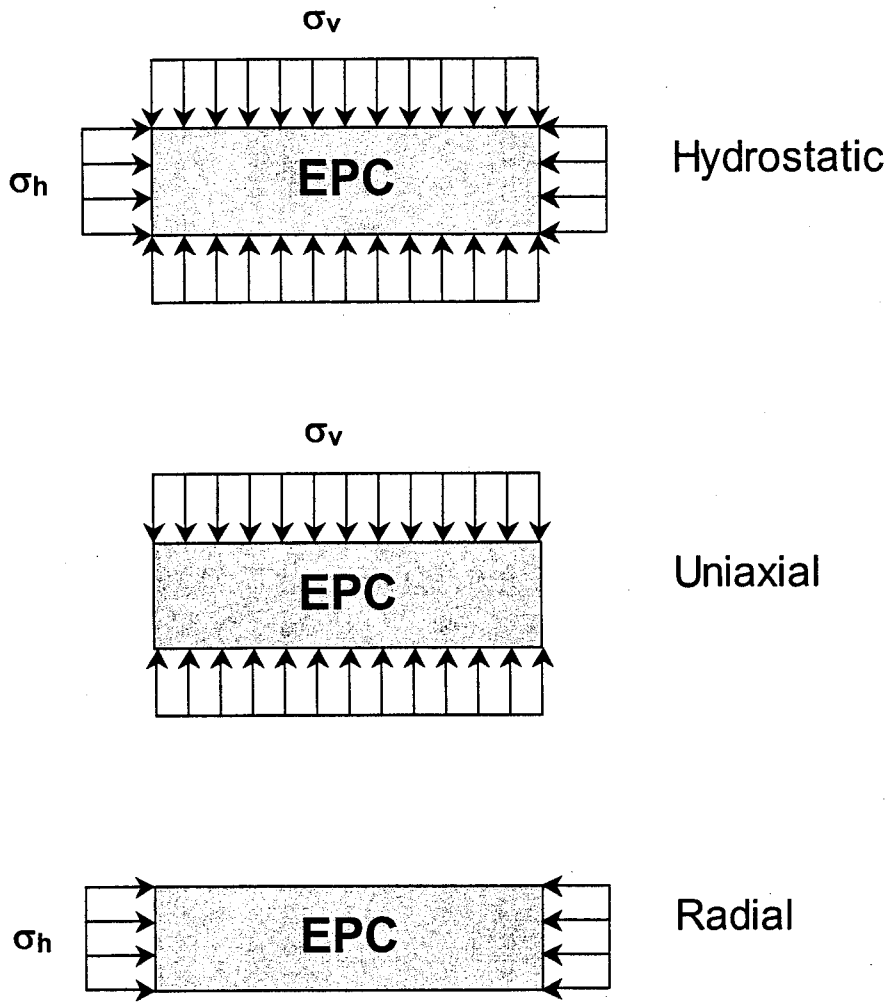

Figure 3.1. Simple fluid calibration conditions: hydrostatic pressure (top), acting on all sides; uniaxial (middle), acting on the active face only; radial (bottom), acting around the perimeter.

Hydrostatic Fluid Calibration

The EPC was tested under simple hydrostatic pressure conditions. The cell was placed inside a pressure vessel (Fig. 3.2). Hydraulic oil was injected into the vessel and used as the pressurizing medium. The test was controlled by an external hydraulic pressure application system, with a manually operated hand pump. The pressure within the hydraulic system was monitored by a pressure transducer and multimeter.

A series of hydrostatic calibration tests were conducted. The tests involved pressurizing fluid in the vessel and monitoring the response of the EPC upon both loading and unloading. Pressures ranged up to a maximum of 689.5 kPa (100 psi). EPC output readings were manually recorded at 137.9 kPa (20 psi) increments. The EPC readings were plotted against the applied hydraulic pressure on a calibration curve. A trend line was drawn through the data and fixed through the origin. The sensitivity of the cell was determined from the slope of the line. The sensitivity results from the hydrostatic calibration tests agreed well with the manufacturer's value (Table 3.1).

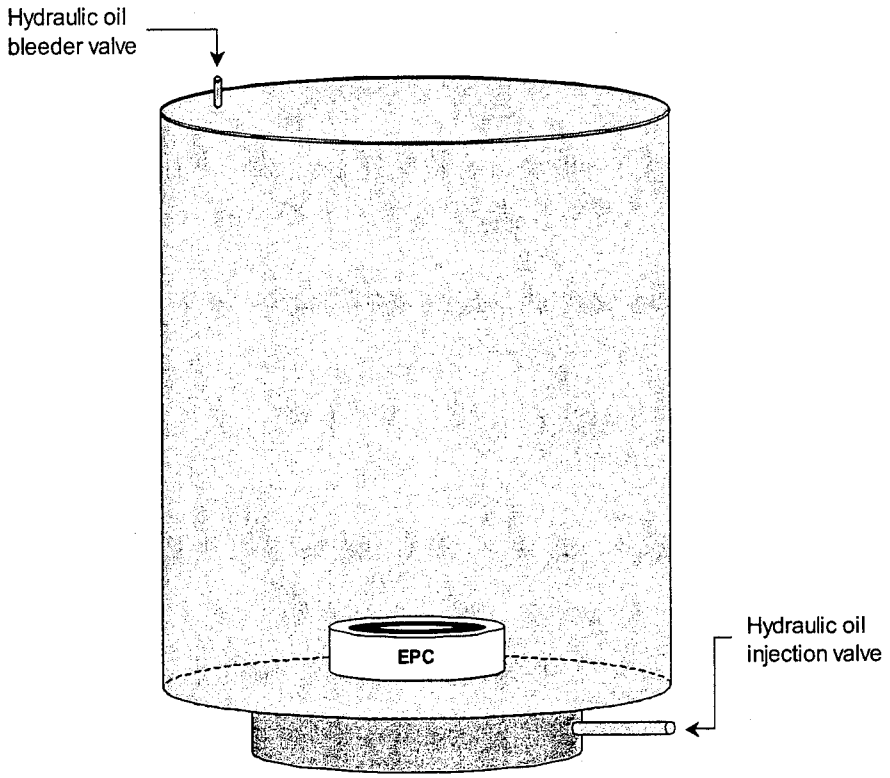

Figure 3.2. Pressure setup for hydrostatic loading.

Table 3.1. Summary of Kulite EPC fluid calibrations.

Loading type	Sensitivity (vdc/kPa)	Sensitivity (vdc/psi)
Kulite manufacturer	0.0208	0.1435
Hydrostatic	0.0211 (+1.4%)	0.1454 (+1.3%)
Uniaxial	0.0209 (+0.5%)	0.1438 (+0.2%)
Radial (In-plane)	0.0000 (n/a)	0.0000 (n/a)

Uniaxial Fluid Calibration

In order to allow the direct application of a uniaxial load upon the active face of the EPC, a uniaxial calibration device was designed and constructed. The primary function of the device was to permit the uniaxial loading of the EPC through fluid or an isolated soil column. A detailed description of the device and its design and an explanation on how it operates are given in Chapter 4. For fluid calibration purposes, the device permitted the application of fluid to the active face of the EPC (Fig. 3.3).

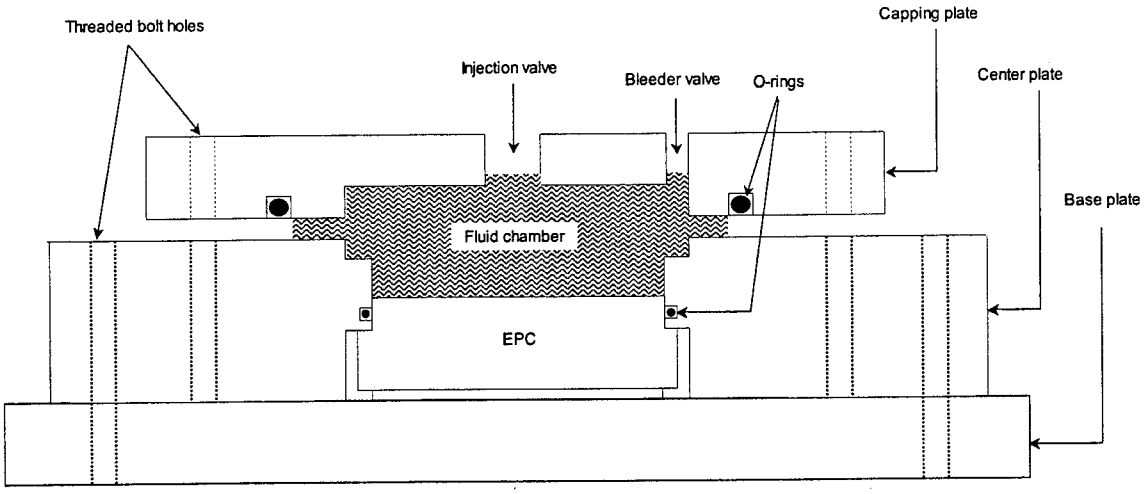

Figure 3.3. Uniaxial calibration device, configured for fluid loading.

Several uniaxial fluid calibration tests were performed on the cell, with hydraulic oil used to pressurize the active face of the cell. During each test, the response of the cell to loading and

unloading was monitored. Output from the EPC was manually recorded at 68.95 kPa (10 psi) intervals during both loading and unloading. The EPC readings were plotted against the applied uniaxial fluid pressure on a calibration curve. A line was drawn through the data and the origin. The sensitivity of the cell was determined from the slope of this line. The sensitivity results from the uniaxial fluid calibration tests showed good agreement with the value from the manufacturer (Table 3.1), with the percent difference given in parentheses.

Radial Fluid Loading

The aim of the in-plane loading study was to determine if pressure applied radially to the rim of the EPC was detectable. The earth pressure cell was placed in the uniaxial calibration device in the same manner as for a uniaxial fluid calibration. However, the quick-release fitting was removed and replaced with a hydraulic plug, thus completely isolating the active face of the EPC from external hydraulic oil pressure. The entire apparatus, device and EPC, was placed inside the pressure vessel that was used during the hydrostatic loading tests. The test was conducted the same as a hydrostatic calibration. However, since the active face of the EPC was sealed and isolated from any fluid contact, loading took place around the sides of the cell. Cell readings were manually recorded at 68.95 kPa (10 psi) loading and unloading increments.

The EPC output recorded from the radial loading test was found to be negligible when compared to the other fluid calibration tests (Table 3.1). A graphical summary of the fluid calibration sensitivities from all three loading conditions is presented in Figure 3.4. The uniaxial and hydrostatic sensitivities were virtually identical, illustrating the negligible influence of pressure acting on the rigid sides of the EPC.

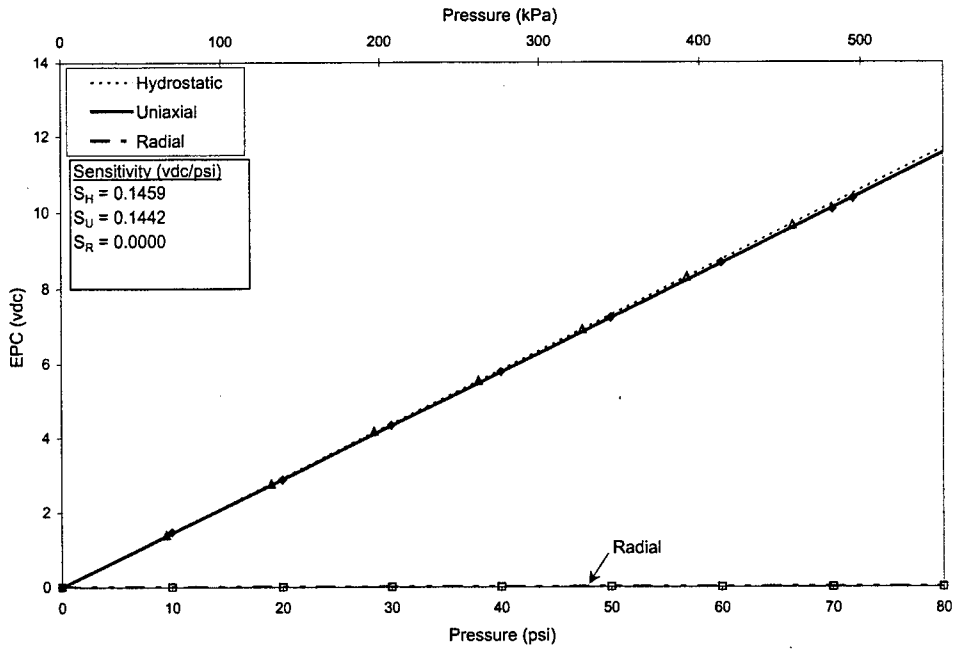

Figure 3.4. Kulite EPC fluid calibration sensitivities. The response of the EPC under hydrostatic loading was equivalent to its response under uniaxial loading.

Temperature Effects

Because of the wide range of temperature extremes experienced during Minnesota's seasons, the possible consequences of temperature variation on EPC output were also explored. Temperatures in Minnesota can range from over 37.8°C (100°F) to well under –17.8°C (0°F).

The EPC was placed in an environmental chamber. The cell was cooled from 24°C (75°F) to -9°C (15°F) in 3°C (5°F) decrements. Approximately fifteen minutes were allowed during each decrement for the EPC to equilibrate with the new temperature. No loading or pressure of any kind was applied to the active face of the cell during the test. EPC output was monitored through the test and readings were manually recorded at the end of each step, just before the temperature decreased to its next level.

The output from the cell was plotted versus temperature (Fig. 3.5). The fluid calibration sensitivity was used to convert the variation in EPC output from volts [vdc] to the corresponding

variation in pressure [kPa]. However, this pressure variation is only the *apparent* change since no pressure was applied to the EPC during the test. Any recorded change in output from the EPC was due exclusively to changes in temperature.

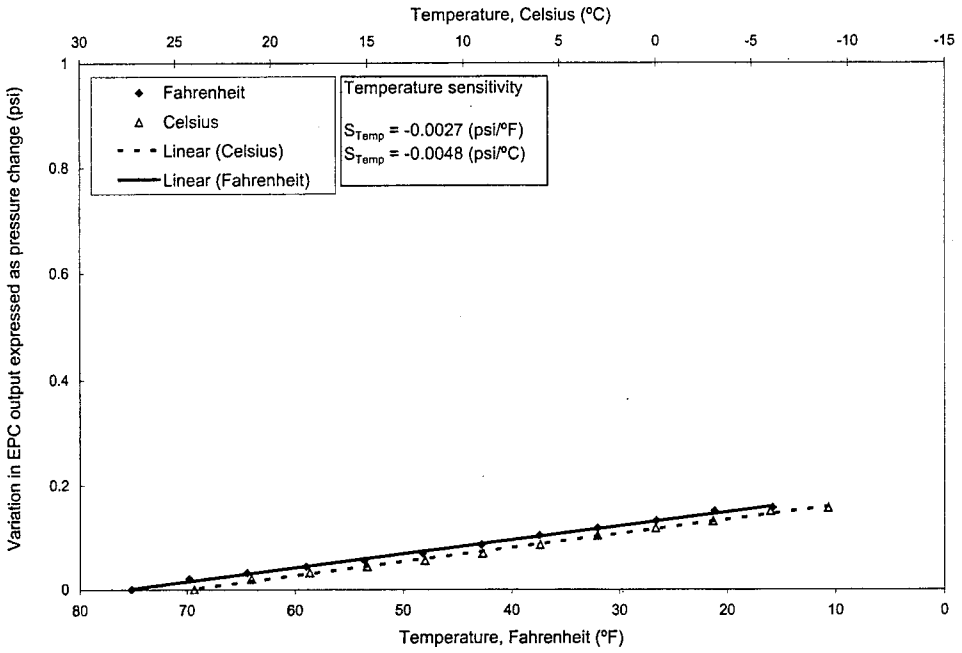

Figure 3.5. Temperature influence on EPC output.

As illustrated in Figure 3.5, the EPC interpreted a decrease in surrounding temperature as an increase in pressure. However, this apparent increase was minute, only 1.34 kPa (0.2 psi) over a range of nearly 35° C (65° F).

Summary

EPC manufacturers usually employ fluid pressure, typically air, for their calibrations. Through fluid calibration, the response of the EPC was observed to be consistent with the information provided by the manufacturer. The cell registered loading only when pressure was applied to its active face. Likewise, no loading was registered by the cell when fluid pressure

was radially applied to its sides. It responded the same to hydrostatic loading as it did to uniaxial loading, and the results of both loadings were the same as the results from the manufacturer.

However, when in actual use, an EPC is placed within soils of various types. It is likely that an EPC will not respond the same when exposed to soil pressure as for fluid pressure. Therefore, it would seem appropriate for an EPC to be calibrated in a manner that involved loading through soil.

CHAPTER 4
UNIAXIAL SOIL CALIBRATION

An EPC is typically calibrated by utilizing fluid pressure to determine a sensitivity, which can then be used to transform a cell's recorded electrical output into a pertinent estimate of earth pressure. It is implicitly assumed from such a calibration procedure that the response of the EPC under uniform fluid pressure would be equivalent to the earth pressure experienced under field conditions. However, that assumption does not acknowledge the potential for arching to occur in the soil.

In this chapter, a new method of calibration is proposed, whereby an EPC will be evaluated by applying pressure on a soil column. A device was designed to allow loading to the sensitive face of the EPC through soil. From these calibrations, a sensitivity will be calculated. It is expected that this *soil* sensitivity will be more appropriate for practical use than the *fluid* sensitivity, S_f, of the previous chapter, which was computed from application of uniform pressure.

Uniaxial Calibration Device

In order to conduct uniaxial calibration tests on an individual EPC, a special loading apparatus was devised. A schematic cross-section of the device is shown in Figure 4.1. The apparatus was designed to allow uniaxial loading on only the sensitive face. The EPC was placed in a cavity at the center of a steel plate. A radial groove containing a rubber O-ring surrounded and sealed the cavity. The O-ring provided a radial seal to the sides of the EPC and held it securely in place. A plastic sleeve was inserted into the center plate, in the space above the EPC. Soil was poured into the cylindrical space within the plastic sleeve and above the active face of the EPC.

Another steel plate formed the cap of the apparatus and was attached to the first steel plate, above the EPC active face, by six bolts. A small cavity was constructed in the inner portion of the plate to house the hydraulic oil that would generate pressure during a calibration test. A quick-release hose fitting and a bleeder plug were threaded on the top of the capping plate. The quick-release fitting was connected, through a rubber hose, to a hydraulic oil supply. A hand pump injected oil from its container, through the hose, and into the inner cavity of the capping plate. An axial O-ring sealed the boundary between the capping plate and center plate. The bleeder plug allowed for air to be extracted from the system during oil injection (see also design sketch in the Appendix).

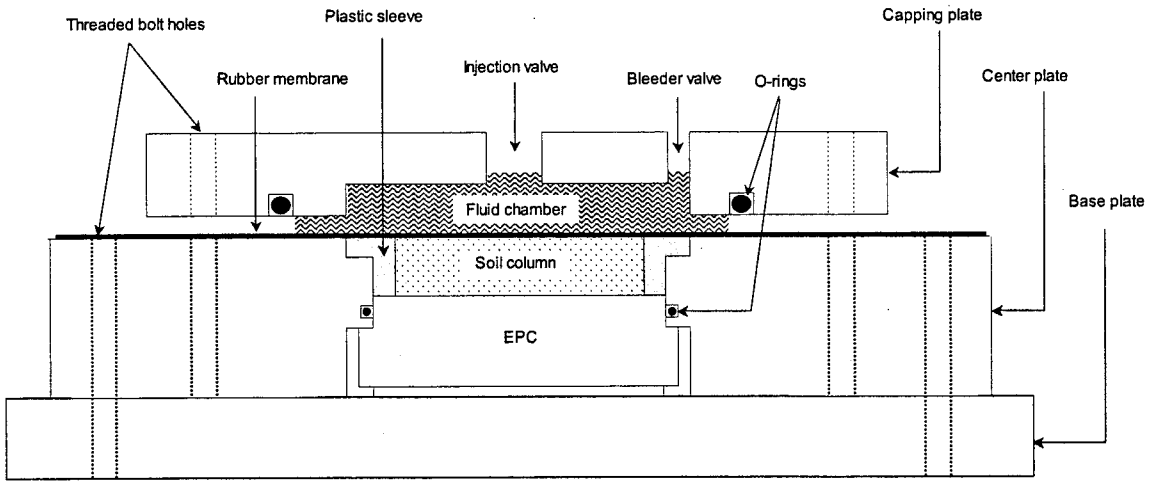

Figure 4.1. Uniaxial calibration device, configured for soil loading.

The uniaxial calibration device was used to observe the EPC response to simple loading conditions through soil. Loading of the EPC was initiated as fluid pressure (hydraulic oil) was applied to a rubber membrane, which was inserted between the capping and center plates of the device. The rubber membrane isolated the oil from a soil column, which was in contact with the cell's sensing face. Fluid pressure applied to the membrane was subsequently applied to the surface of the soil column, and transferred through the column to the face of the EPC. The plastic sleeves that housed the soil column was composed of a low-friction material. Because the sleeve could be removed from the device, the height and diameter of the sleeve could be varied.

Soil Loading Calibration

Two dry sands, Ottawa 20-30 and 50-70, were used for the soil pressure calibration tests. Ottawa 20-30 silica sand is a uniform sand with grains passing a #20 sieve and retained on a #30 sieve (grain size ~ 0.73 mm). Ottawa 50-70 is also a uniform sand with grains passing a #50 sieve and retained on a #70 sieve (grain size ~ 0.25 mm).

Plastic sleeves were machined in varying combinations of heights at 12.7 and 25.4 mm (0.5 and 1 in.) and diameters of 25.4, 38.1, and 50.8 mm (1, 1.5, and 2 in.). The largest diameter sleeve (50.8 mm) allowed for loading over the entire face of the EPC. The unit weight of the sand in the column was kept constant at 16.3 kN/m^3 (104 lb/ft^3) during all tests (voids ratio of 0.59).

The EPC was tested in the uniaxial calibration device under various loading configurations. The fluid pressure applied to the soil column was increased in 69 kPa (10 psi) increments to maximum values of either 480 or 550 kPa (70 or 80 psi). From the maximum value, the EPC was unloaded by decreasing the fluid pressure in 69 kPa (10 psi) steps back to zero gage pressure. EPC data were taken by manually recording the output voltage reading from the cell at each load step. Readings were recorded once the fluid pressure had stabilized, typically in thirty seconds. Several load/unload pressure cycles were performed for each calibration test. One pressure cycle was comprised of a single set of loading and unloading steps.

The fluid pressure applied to the soil column was plotted on the horizontal axis, and the electrical output from the EPC was plotted on the vertical axis. A calibration curve showing a typical load/unload cycle is given in Figure 4.2. The response of the cell to an increase in soil pressure was linear. Upon unloading, hysteresis was observed. It is hypothesized that the sand grains locked together and temporarily retained a portion of the previous load level. The effect vanished upon complete unloading. This behavior was observed in all tests, for all cycles.

A typical calibration test, with the series of load/unload cycles is shown Figure 4.3. The output values for consecutive cycles have been artificially increased by one volt from the previous cycle to aid in viewing the figure. For example, although the true output level for Cycle 2 at zero pressure was 0.0 vdc, the figure shows an output reading of 1.0 vdc for zero pressure so that one can distinguish the trend of Cycle 2 from the other load/unload cycles. This was done for all six cycles. As seen from the figure, all cycles exhibited hysteresis upon unloading.

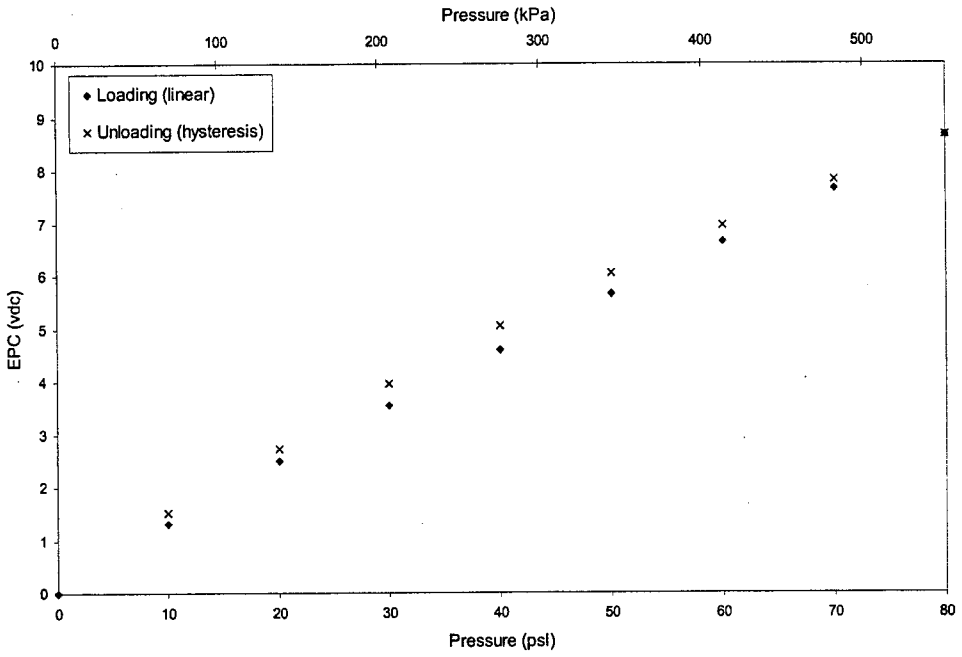

Figure 4.2. Calibration load/unload cycle.

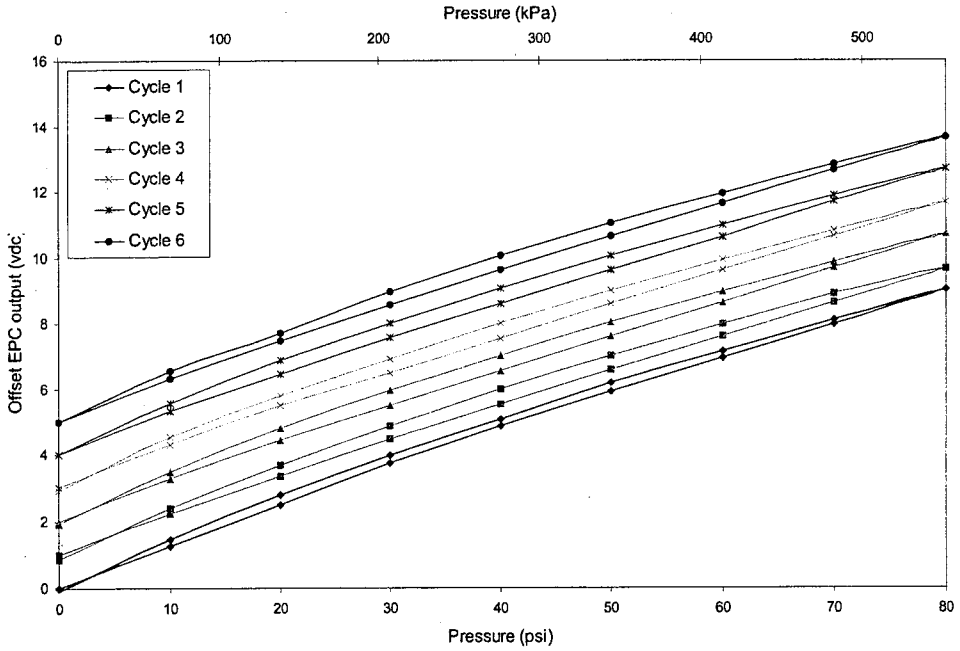

Figure 4.3. One calibration test as a series of six load/unload cycles.

To determine a calibration sensitivity, only the loading part of the calibration curve was used. A linear trendline was fitted through this portion and the slope was calculated. The slope was then taken as the sensitivity of the EPC.

The results of the soil calibration tests are summarized in Table 4.1. Sensitivities are given in units of volts of EPC output per kPa of applied pressure [vdc/kPa]. The fluid sensitivity computed from the fluid calibration tests is also given for comparison purposes. The EPC yielded a smaller change in output when loaded with soil than with fluid. In other words, the sensitivity values calculated from the soil calibration tests were lower than the sensitivity determined from fluid calibration. This would indicate that the EPC responded differently under soil loading than under fluid pressure. That is, for equivalent values of pressure applied through fluid and soil, the EPC yielded differing levels of output. This result suggests that arching developed. An average soil sensitivity was calculated to be 0.017 vdc/kPa (0.118 vdc/psi) while the value provided by the manufacturer was given as 0.021 vdc/kPa (0.144 vdc/psi), a difference of 20% (Table 4.1).

The effect of load area is presented in Figure 4.4. Calibration sensitivities relating to the different soil column diameters are plotted. All tests were conducted with Ottawa 20-30 sand. The fluid sensitivity is also given as a solid line for comparison.

Table 4.1. Summary of soil calibration sensitivities.

Soil	Height		Sensitivity	
	(mm)	(in)	(vdc/kPa)	(vdc/psi)
fluid	0	0.0	0.021	0.146
2030	12.7	0.5	0.018	0.123
2030	12.7	0.5	0.018	0.122
2030	12.7	0.5	0.016	0.112
2030	12.7	0.5	0.018	0.126
2030	12.7	0.5	0.020	0.137
2030	12.7	0.5	0.019	0.132
2030	25.4	1.0	0.014	0.097
2030	25.4	1.0	0.015	0.101
5070	12.7	0.5	0.018	0.123
5070	12.7	0.5	0.018	0.122
5070	25.4	1.0	0.015	0.106
5070	25.4	1.0	0.017	0.118
	Mean		0.017	0.118
	Standard Deviation		0.002	0.012

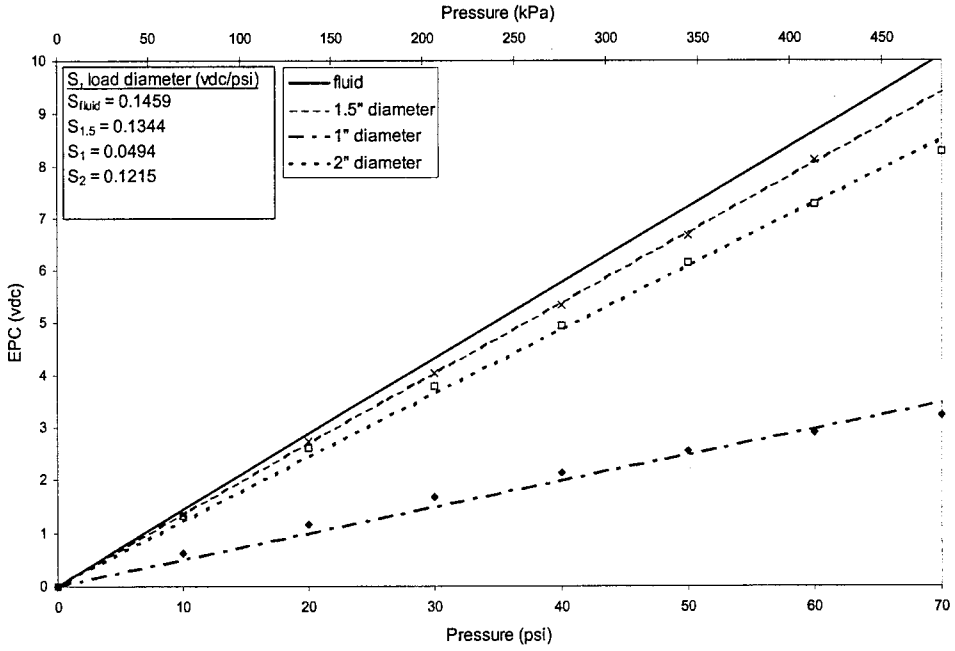

Figure 4.4. Soil calibration curves for different load areas.

The sensitivities computed from the two larger soil diameters were nearly the same, although the sensitivity from the 38.1 mm (1.5 in.) diameter was higher than that from the 50.8 mm (2 in.) diameter. This was believed to be due to an arching effect developing within the 50.8 mm (2 in.) soil column as a result of loading taking place over the entire cell face, which includes the rigid, inactive rim (Fig. 4.5). Soil loading through the 38.1 mm (1.5 in.) column did not include this rim and the arching effect was lessened (friction was reduced along the plastic sleeve). Thus, the resulting sensitivity was higher.

Calibration sensitivities pertaining to the two soil types at two different heights (Ottawa 20-30 and 50-70 sand) are presented graphically in Figure 4.5. The curves shown are typical for their respective calibration condition. The fluid sensitivity is again given for comparison purposes. All soil sensitivities were less than the fluid sensitivity; that is, the cell output was reduced for the same value of applied pressure. The sensitivity for a column height of 12.7 mm (0.5 in.) was nearly the same for both soil types. As the height was increased, the soil sensitivity decreased.

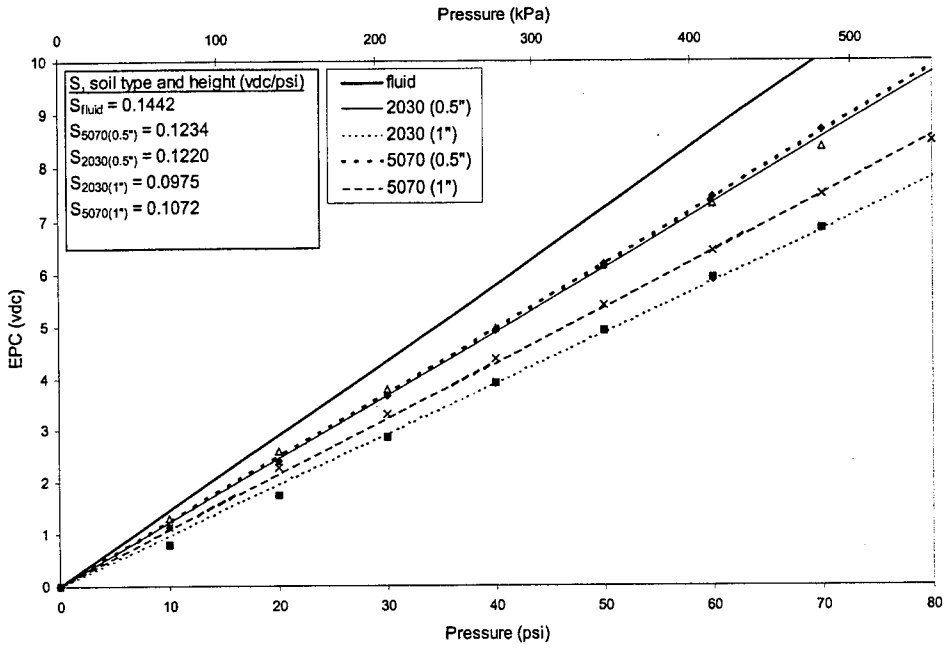

Figure 4.5. Soil calibration curves for two types of silica sand at two column heights.

While the soil sensitivity was not seen to differ significantly between the two soil types (calibration values from both soils fell within ±10% of each other), the EPC sensitivity was observed to decrease when the soil height was increased (Fig. 4.6). The trend between the soil sensitivity and soil height appeared to converge to a limiting value. As the soil height increased, the EPC approached what could be considered a far-field soil sensitivity. As the height of the soil column, H, increases, no additional decrease in the sensitivity should be expected as the critical distance where no further arching can develop was reached. Nevertheless, this trend was inconclusive since only two soil heights were tested. A sensitivity line was drawn at 0.017 vdc/kPa (0.118 vdc/psi). This was the average value from Table 4.1a and will subsequently be taken as the EPC soil sensitivity.

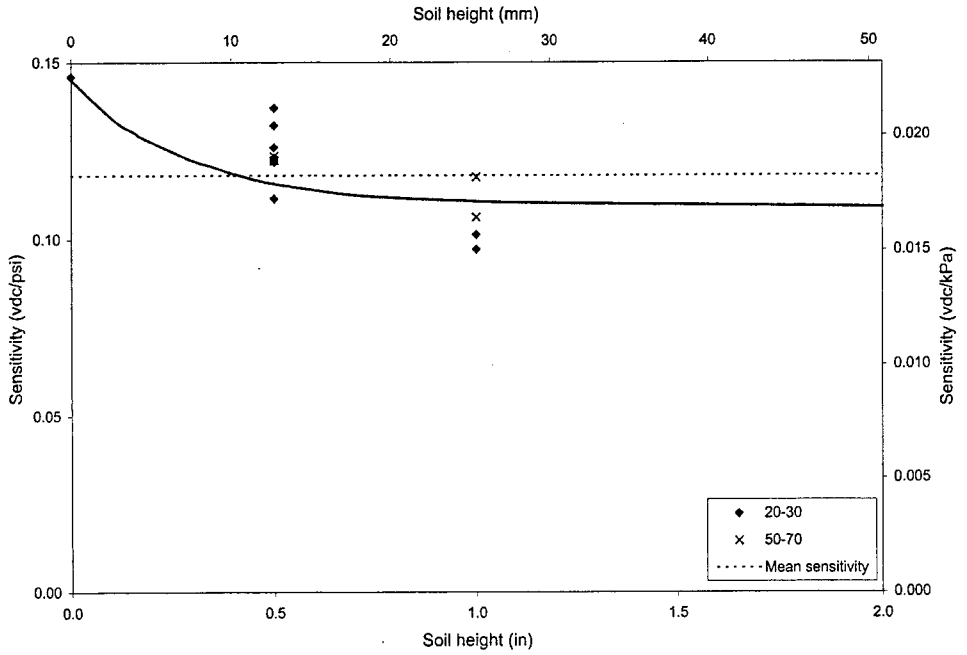

Figure 4.6. Sensitivity variation with soil column height.

Analysis

Effect of the Sensing Area

The response of an earth pressure cell to the applied pressure is governed by force equilibrium:

$$pA_i = q_i A_{EPC} \tag{22}$$

where p = uniform pressure, A_i = loading area, and q = loading on the EPC, A_{EPC} = EPC sensing area. The EPC sensitivity, S_i, for loading over an area, A_i, is given by

$$S_i = \frac{V_i}{p} \tag{23}$$

and V_i is the voltage output from the cell. Solving Equation 23 for the uniform pressure, p, and substituting it into Equation 22 yields

$$\frac{V_i}{S_i} A_i = q_i A_{EPC} \tag{24}$$

or rearranging

$$\frac{V_i}{q_i} = \frac{A_{EPC}}{A_i} S_i = C \tag{25}$$

The ratio, V_i/q_i, is a unique property of every cell and it remains constant for all loading areas on the earth pressure cell under uniform loading conditions. The sensitivities calculated from two different load areas, A_1 and A_2, which are subjected to the same uniform pressure, p, are related by

$$\frac{A_{EPC}}{A_1} S_1 = \frac{A_{EPC}}{A_2} S_2 \tag{26}$$

The above relation reduces to a ratio of the sensitivities to the squares of the respective loading diameters, D_1 and D_2 (Eqn. 27).

$$\frac{S_2}{S_1} = \frac{A_2}{A_1} = \frac{D_2^{\,2}}{D_1^{\,2}} \tag{27}$$

Equation 27 holds for the ideal case of uniform loading applied across any area on the EPC. It is not valid when loading the cell through a soil column because shear stresses invariably develop that reduce the effective loading over the face of the cell.

Effect of Arching

Figure 4.7 illustrates the free body diagram of the soil column during calibration. The applied uniform fluid pressure, p, acted on the top of the soil column of height, H. As a result of the applied pressure and the deflection of the cell diaphragm, frictional resistance developed within the soil column, which gave rise to opposing shear stresses. The result was an arching effect in the soil column that effectively reduced the load acting on the face of the EPC.

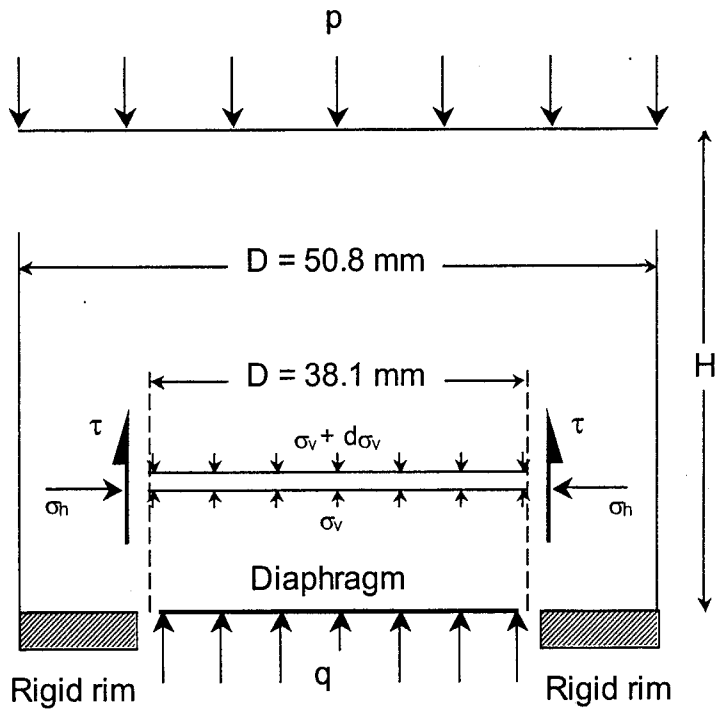

Figure 4.7. Arching over a deflecting diaphragm.

Depending upon the diameter of the applied pressure, the shearing resistance developed either along the interface of the sand and the plastic sleeve, or between particle contacts along an idealized vertical boundary extending from the inner edge of the rigid rim. The shearing resistance, τ, is a function of the horizontal stress, σ_h, in the soil column and the friction angle of the shear boundary, ϕ, which corresponded to either the sand or the sand/plastic sleeve interface. The horizontal stress can be related to the vertical stress by the coefficient $K_0 = \sigma_h/\sigma_v$. The shearing resistance can then be given by

$$\tau = \sigma_v K_0 \tan\phi \tag{28}$$

Equilibrium in the vertical z-direction for a soil section of thickness, dz, can be written as

$$\sigma_v \frac{\pi D_i^2}{4} - (\sigma_v + d\sigma_v)\frac{\pi D_i^2}{4} + \pi D_i dz\,\tau = 0 \tag{29}$$

where D_i is diameter of the soil column, and σ_v and $\sigma_v + d\sigma_v$ are the vertical stresses acting above and below the soil section. Equation 32 can be rearranged as

$$\frac{d\sigma_v}{\sigma_v} = \frac{4\lambda}{D_i} dz \tag{30}$$

where $\lambda = K_0 \tan \phi$. Integrating the above equation yields

$$\sigma_v = A \exp\left(4\lambda \frac{z}{D_i}\right) \tag{31}$$

The constant A can be determined by applying the boundary condition at the top of the column. When z = H, the height of the soil column, σ_v = p, the fluid pressure. This yields

$$\sigma_v = p \exp\left(4\lambda \frac{z-H}{D_i}\right) \tag{32}$$

Also, at z = 0, at the bottom of the soil column, σ_v = p', the effective loading through the soil on to the cell. Therefore, the ratio of the fluid pressure, p, and the effective loading on the cell, p', is given by

$$p' = p \exp\left(-4\lambda \frac{H}{D_i}\right) \tag{33}$$

The effective loading, p', is the resultant pressure acting through the soil on the face of the EPC. It reflects the influence of the shear stress existing in the soil above the cell. Once the effective loading is found, the corresponding reactive loading, q present in the cell can be determined. From equilibrium at the soil-EPC interface, the loading q is found in the same fashion as in Equation 22.

$$p' A_i = q A_{EPC} \tag{34}$$

Substituting Equation 33 into the above relation and writing the areas in terms of the diameters, D_i and D_{EPC}, gives

$$p \exp\left(-4\lambda \frac{H}{D_i}\right) \frac{\pi D_i^2}{4} = q \frac{\pi D_{EPC}^2}{4} \tag{35}$$

Upon rearranging, Equation 35 becomes

$$\frac{p}{q} = \frac{D_{EPC}^2}{D_i^2} \exp\left(4\lambda \frac{H}{D_i}\right) \tag{36}$$

For the case of the 38.1 mm diameter soil column, the diameter of the sleeve was approximately equal to that of the diaphragm and the inner edge of the rim ($D_i = D_{EPC}$ = 38.1 mm). Therefore, the shearing resistance, τ, is dependent on the friction angle of the soil-plastic

sleeve interface. Since the friction angle along the soil-sleeve interface is less than the internal friction of the soil, arching was reduced and the sensitivity value was larger (Table 4.2).

The sensitivity from the smallest diameter showed a significant decrease (Table 4.2). This was due simply to the fluid loading being applied over a much smaller area. The fluid pressure, p, exerted a force across a small soil column area, A_i, and the sensitivity value was small. For the largest soil column (D = 50.8 mm, 2 in.), frictional resistance to the applied fluid pressure developed along an idealized vertical boundary at the inner edge of the rigid rim (D_i = 38.1 mm, 1.5 in.) because of the deflection of the diaphragm on the sensing face of the EPC. The sensitivity value was therefore smaller than that from the 38.1 mm diameter soil column.

Table 4.2. Influence of load area on EPC sensitivity.

Soil	Diameter		Sensitivity	
	(mm)	(in.)	(vdc/kPa)	(vdc/psi)
2030	25.4	1.0	0.007	0.048
2030	25.4	1.0	0.007	0.049
2030	25.4	1.0	0.007	0.049
2030	38.1	1.5	0.019	0.132
2030	38.1	1.5	0.019	0.134
2030	50.8	2.0	0.017*	0.118*

* Mean sensitivity values from Table 4.1.

The loading ratio, p/q, from Equation 36 can be expressed as a ratio of sensitivities for fluid and soil loading. The fluid pressure, p, is equivalent to the voltage output from a fluid calibration test divided by the fluid sensitivity, S_f. The reactive loading, q, is equivalent to the voltage output from a soil calibration test divided by the fluid sensitivity. The ratio p/q then becomes a ratio of the voltage levels, which is equivalent to the ratio of the fluid sensitivity to the soil sensitivity, S_f/S_i:

$$\frac{p}{q} = \frac{V_f / S_f}{V_i / S_f} = \frac{V_f}{V_i} \Rightarrow \frac{S_f}{S_i} = \frac{D_{EPC}^{\ 2}}{D_i^{\ 2}} \exp\left(4\lambda \frac{H}{D_i}\right) \tag{37}$$

The exponential term indicates the level of shear resistance present in the soil column, where $\lambda = K_o \tan \phi$; K_o being the ratio of horizontal to vertical stress, and ϕ being the friction angle along the shear resistance interface. Figure 4.8 plots the two states of soil friction between the sensitivities and the soil column height for the two different soils. The slopes of the two lines represent the values of the exponential term in Equation 37, $4\lambda(H/D_i)$, for the two conditions. From the two slopes in the figure, $\lambda = 0.1405$ and 0.0942. Assuming $K_o = 0.25$ for 1D compression, the friction angle is estimated to be 20 – 30°.

Figure 4.9 shows a similar plot of the states of shear resistance present at the soil-plastic sleeve interface. The log of the sensitivity ratio is plotted versus the height-to-diameter ratio for two different diameters at a constant height. From the figure, $\lambda = 0.1335$ and 0.0596. Assuming $K_o = 0.25$ for 1D compression, the friction angle of the soil-plastic sleeve interface is estimated to be 15 – 30°.

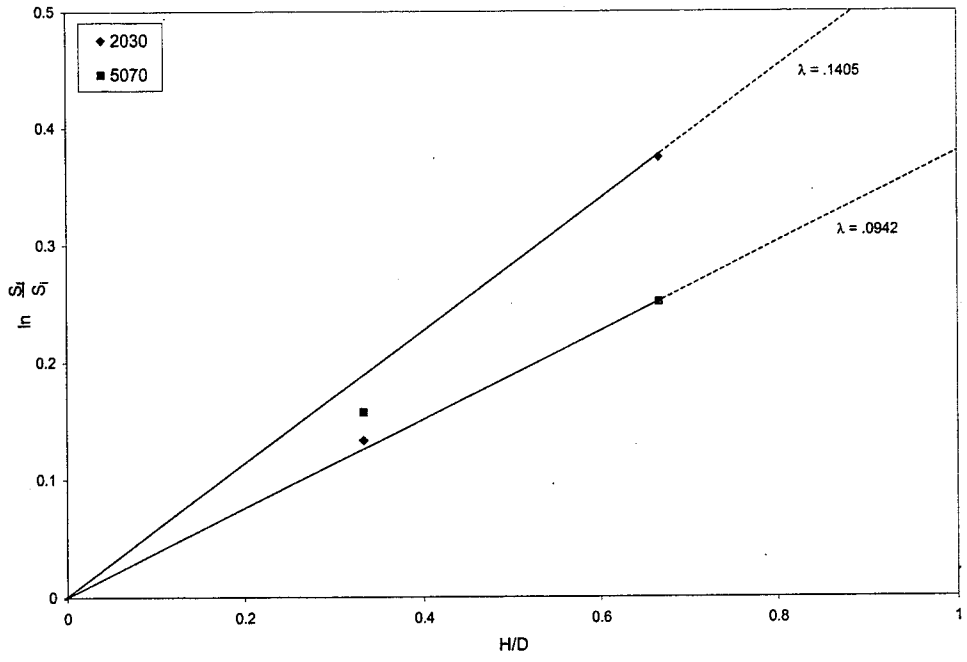

Figure 4.8. EPC sensitivity relationship to soil height.

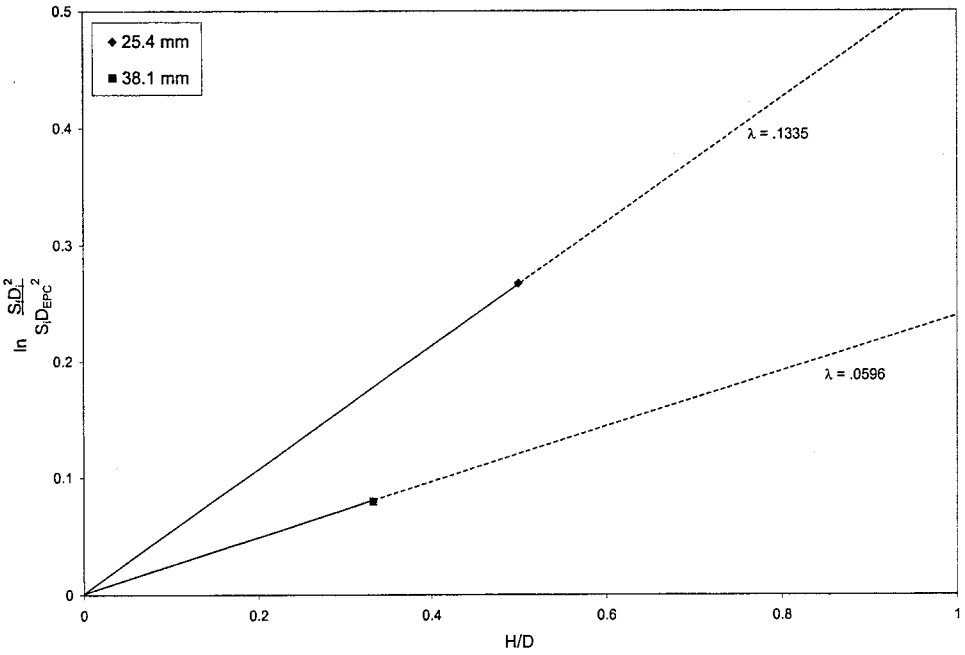

Figure 4.9. EPC sensitivity relationship to soil column diameter.

CHAPTER 5
UNIVERSAL CALIBRATION

A universal calibration chamber was devised to test the EPC in a three dimensional soil environment subjected to an axial load. For convenience, a 55-gallon drum was used to construct the chamber (Fig. 5.1). The inside diameter, D, of the drum was 572 mm (22.5 in.), and the height, H, was cut down to 584 mm (23.0 in.). Sand was filled into the bottom third of the drum. A fluid-filled rubber bladder was placed on top of the soil. A second layer of soil was filled into the middle third of the drum. The EPC was placed in the center of the chamber within the middle layer. A second fluid-filled rubber bladder was placed on top of the middle layer. Finally, a third layer of soil was poured on top of the second rubber bladder. The top soil layer acted as a buffer between the load frame and the upper rubber bladder.

The purpose of the rubber bladders was to develop a boundary condition of uniform pressure across the top and bottom of the middle layer. In addition, any difference in pressure between the upper and lower bladders was used to evaluate frictional effects along the inside walls of the drum. The frictional effects were observed to be minimal; the pressure in the lower bladder was only slightly smaller than in the upper bladder.

The fluid-filled rubber bladders were used to measure vertical pressure at two locations within the chamber (Figs. 5.2 and 5.3). The bladders were pancake-shaped and sized to fit flush with the inner diameter of the drum. Diametrally opposing holes 19.1 mm (0.75 in.) in diameter were drilled into the drum at positions of one-third and two-thirds the overall height. The outlet valves from the bladders protruded from the drum at those locations. Pressure transducers connected to the outlets provided electrical signals from the bladders. The response of the bladders to loading matched well with the expected stresses calculated by dividing the load by the circular area of the drum.

A 13 kN (3000 lb) capacity load cell with a sensitivity of 1.3 kN/vdc (300 lb/vdc) measured the applied force. A series of four steel plates with diameters equal to 76.2, 229, 381, and 533 mm (3, 9, 15, and 21 in.) were used to transfer the force from the load frame actuator to

the soil-filled chamber. The plates were stacked with the largest one of diameter 53.3 cm (21 in.) resting on the surface of the top soil layer and then stacked sequentially upwards in order of decreasing diameter. All four plates were 12.7 mm (0.5 in.) thick. The stacking provided a distribution of stress that was approximately given by the force divided by the drum diameter, which matched within 2% of the fluid pressure measured from the bladders (Fig. 5.4).

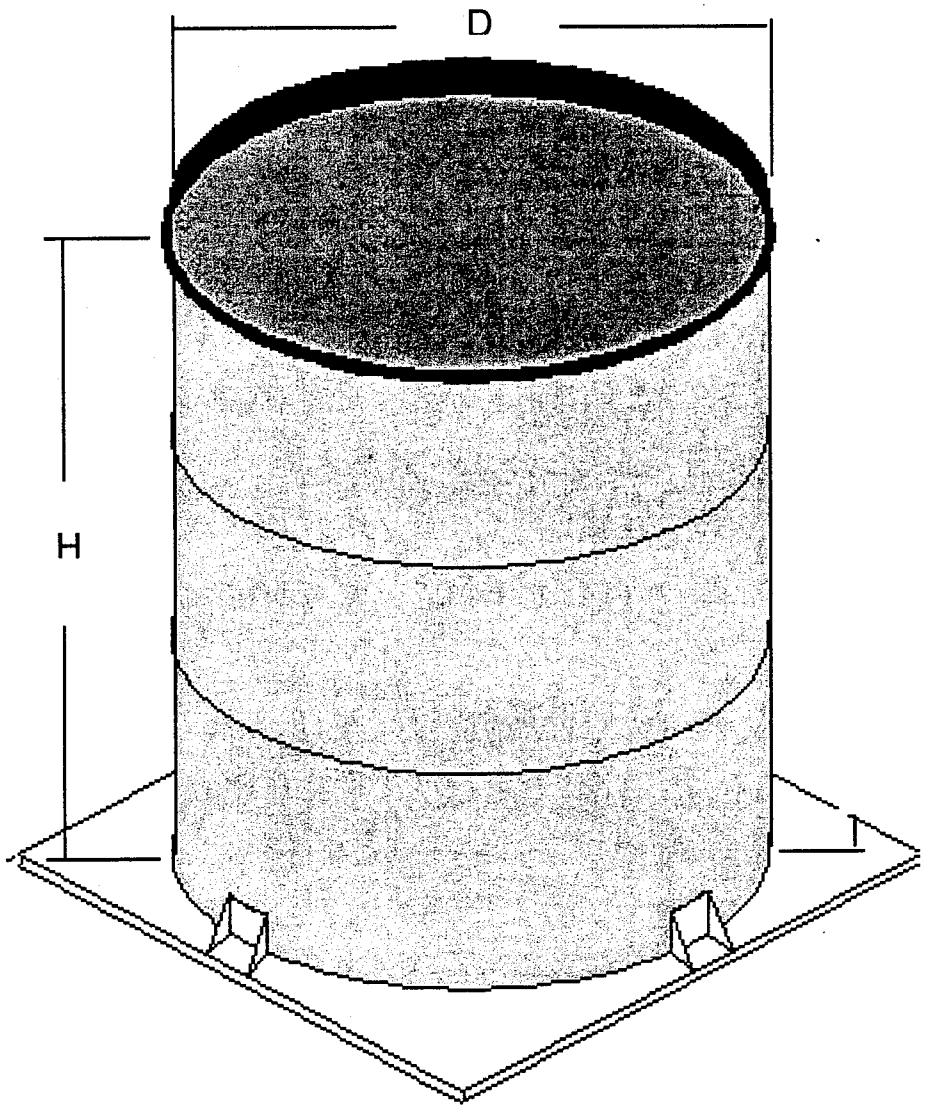

Figure 5.1. Universal calibration chamber.

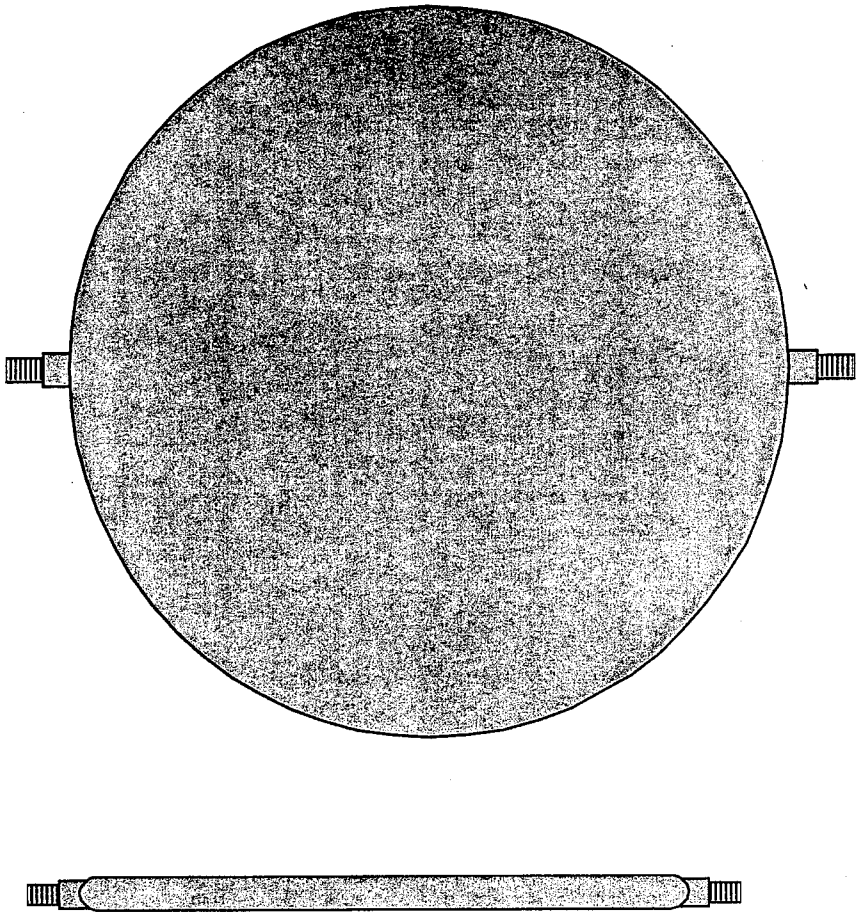

Figure 5.2. Universal calibration bladder. The bladders were custom-designed by Perma-Type Rubber, Inc., Plainville, Connecticut.

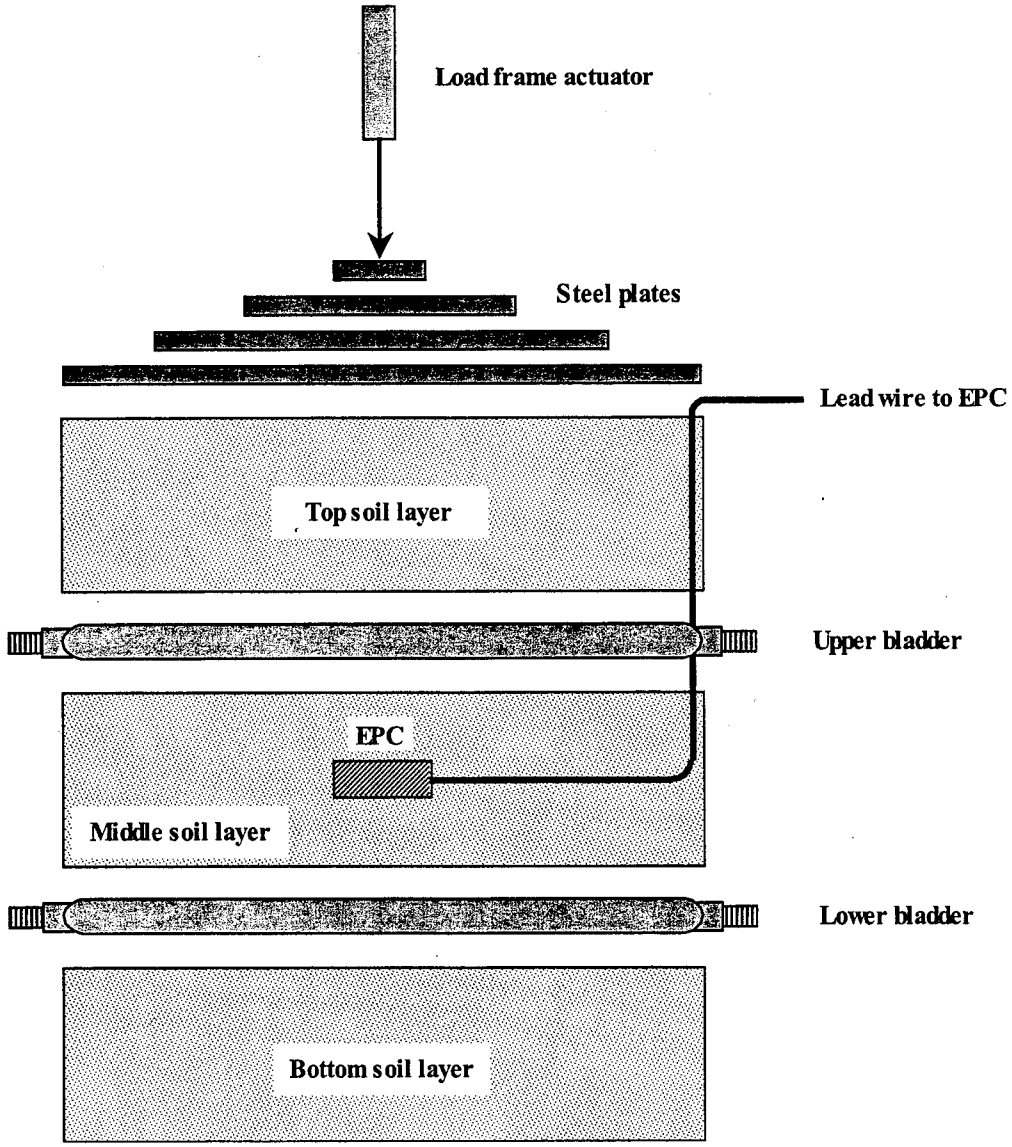

Figure 5.3. Universal calibration components. The above schematic represents the configuration of steel plates, bladders, soil, and EPC within the universal calibration chamber.

Universal Calibration Overview

The universal calibration tests were conducted at the Mn/DOT Materials and Road Research facility in Maplewood, Minnesota. An Interlaken (Minneapolis, MN) load frame was used to generate the force needed to load the EPC. The load frame was a part of a closed-loop/servo-hydraulic system that was controlled by a desktop PC.

Two types of tests were conducted: static and rapid loading. The peak load generated for both test types was 13.3 kN (3000 lb), which translated to approximately 55.5 kPa (8 psi) over a 572 mm (22.5 in.) diameter circular area. Static loading tests consisted of constant load and unload rates of 44.48 N/s and 88.96 N/s (10 lb/s and 20 lb/s). Rapid loading tests consisted of a 0.1 second load pulse applied cyclically to the chamber. The pulse was haver-sine in shape and took 0.05 s to load, 0.05 s to unload; a sleep time of 0.9 s was used before the next pulse was applied. One rapid loading test consisted of twenty cycles.

The electrical output from the EPC was collected by an independent data acquisition unit. Data from the load frame's load cell, and from the bladder's transducer, were gathered by a desktop PC. A temporal delay, on the order of four milliseconds, existed between the arrival of the EPC output and the load cell and bladder transducer data. This delay was observed in all plots of rapid loading test data.

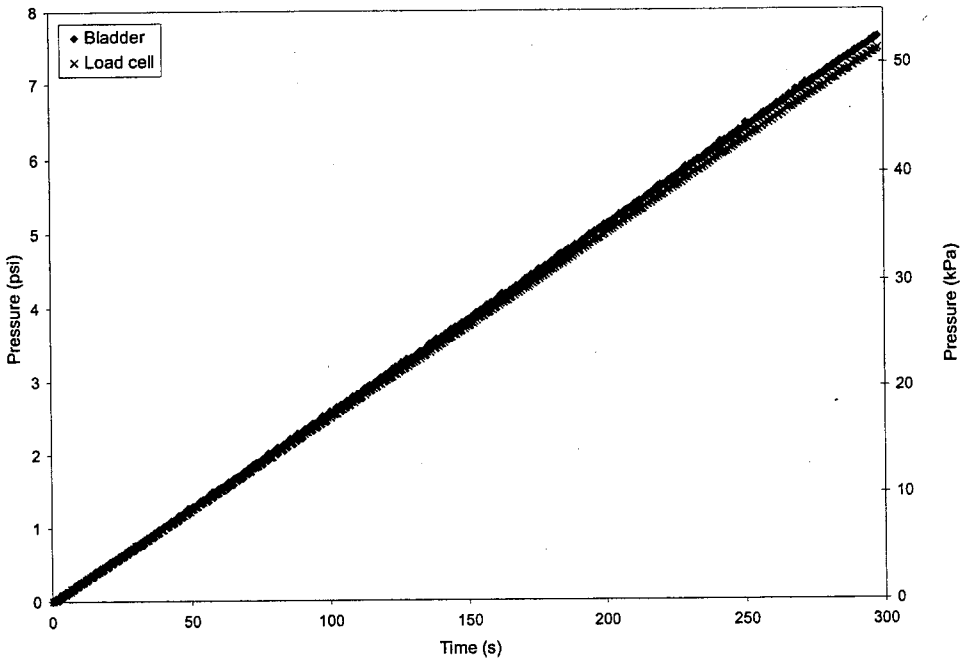

Figure 5.4. Bladder response. The pressure measured in the bladder matches the force (divided by the area of the chamber) recorded by the load cell; the two curves are virtually indistinguishable from one another.

Universal Calibration – Dry Sand

The first series of universal calibration tests were performed with the EPC placed in the middle layer, which was comprised entirely of dry, uniform sand. Ottawa 20-30 sand was the primary material used, although some tests were conducted with Ottawa 50-70 sand. For most tests the unit weight of the sand was kept as close as possible to the unit weight used in previous uniaxial calibration tests, which was 16.3 kN/m^3 (104 lb/ft^3). Other tests were performed where the dry sand was placed in a loose state; the sand was poured into the barrel so as to be as loose as possible. The EPC was tested under both static and rapid loadings. Tests were conducted with the EPC's sensing area facing both up and down.

Data from the EPC and the bladders were plotted on universal calibration curves (for example, Fig. 5.5). The curves displayed the "pressure versus time" responses of the bladder and the cell. Two curves illustrating measured EPC pressures were shown. One curve represented

cell pressures calculated using the fluid sensitivity; the other curve indicated cell pressures calculated from the soil sensitivity.

Universal calibration curves were developed from tests conducted within dry sand. Figures 5.5 – 5.7 are representative of tests where the unit weight of the sand was 16 kN/m^3, roughly the same value used for the soil calibrations. Under static loading (Fig. 5.5), with respect to its fluid sensitivity, the cell registered a value of earth pressure that was less than the fluid pressure recorded by the bladder. For these conditions, the EPC's average registration ratio, R, was 0.8. Thus the cell under-registered the applied earth pressure. However, when the soil sensitivity was applied to the EPC data, the cell produced earth pressures that were consistent with the fluid pressure values observed in the bladder. Hence the soil sensitivity produced a registration ratio close to unity ($R \approx 1$).

Figure 5.6 represents tests conducted under rapid loading conditions. It was observed that under rapid loading the fluid pressure in the bladder did not consistently match the average axial stress calculated by dividing the applied load by the area, as was the case for static loading. It is believed that this effect was due to the poor response of the pressure transducer to the high frequency of the load/unload pulse and not to any time dependent soil properties or inertial effects. For comparison purposes, the average stress (axial load/area) was plotted on the universal calibration curve with the EPC data. With respect to its fluid sensitivity, the cell under-registered the applied earth pressure ($R = 0.6$). However, when the soil sensitivity was applied to the EPC data, the cell yielded a registration ratio closer to unity ($R = 0.9$).

Static loading tests were conducted upon completion of the rapid loading tests (Fig. 5.7). As before, the cell's fluid sensitivity under-registered the applied earth pressure ($R = 0.7$) whereas applying its soil sensitivity resulted in an earth pressure that again closely matched the fluid pressure in the bladder ($R \approx 1$).

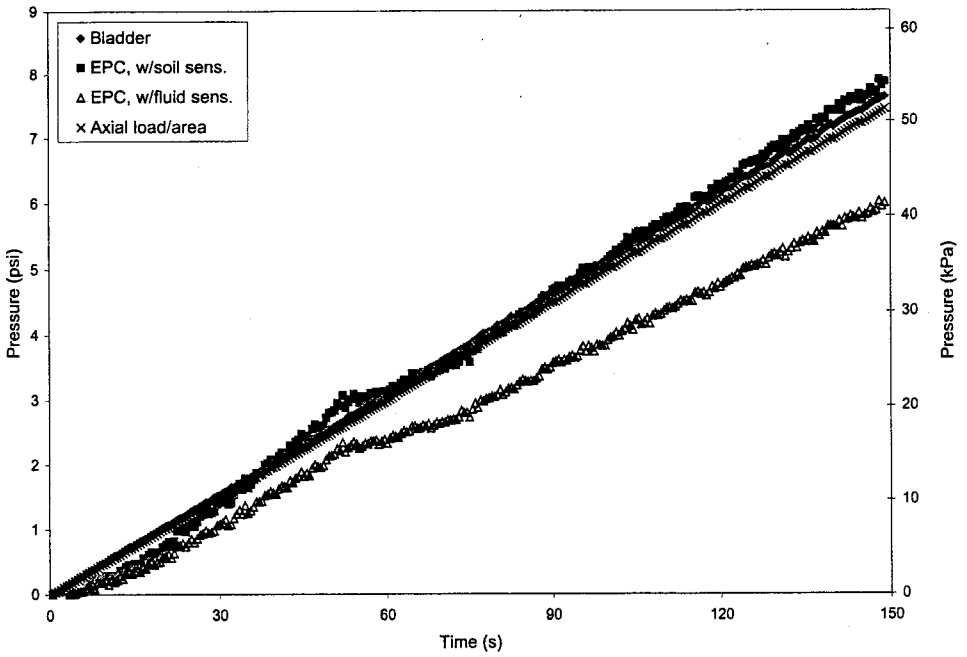

Figure 5.5. Universal calibration curve, static loading test (s14), conducted in Ottawa 20-30 sand.

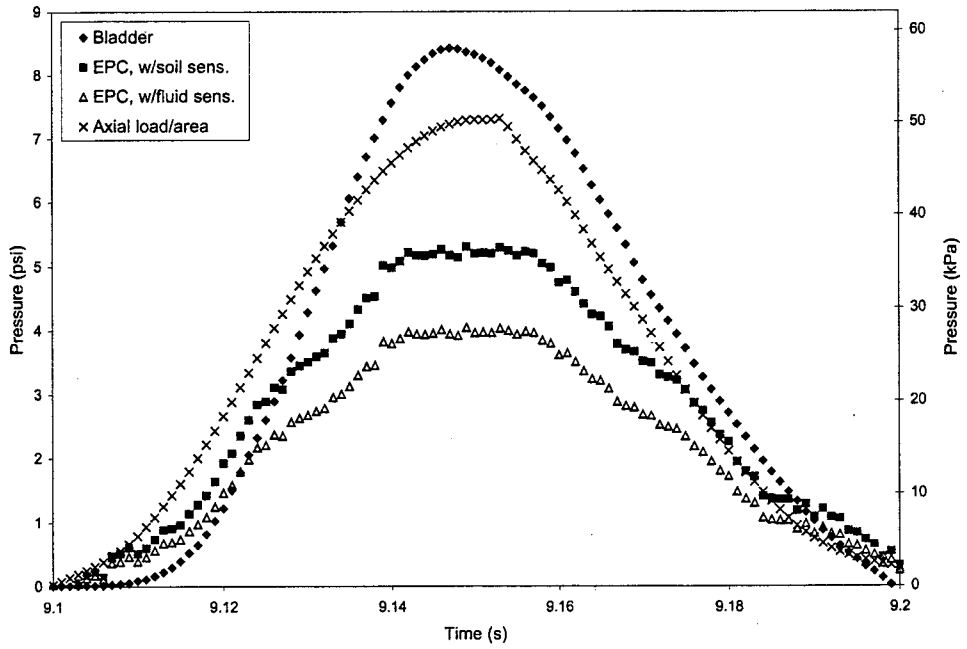

Figure 5.6. Universal calibration curve, rapid loading test (d12), conducted in Ottawa 20-30 sand.

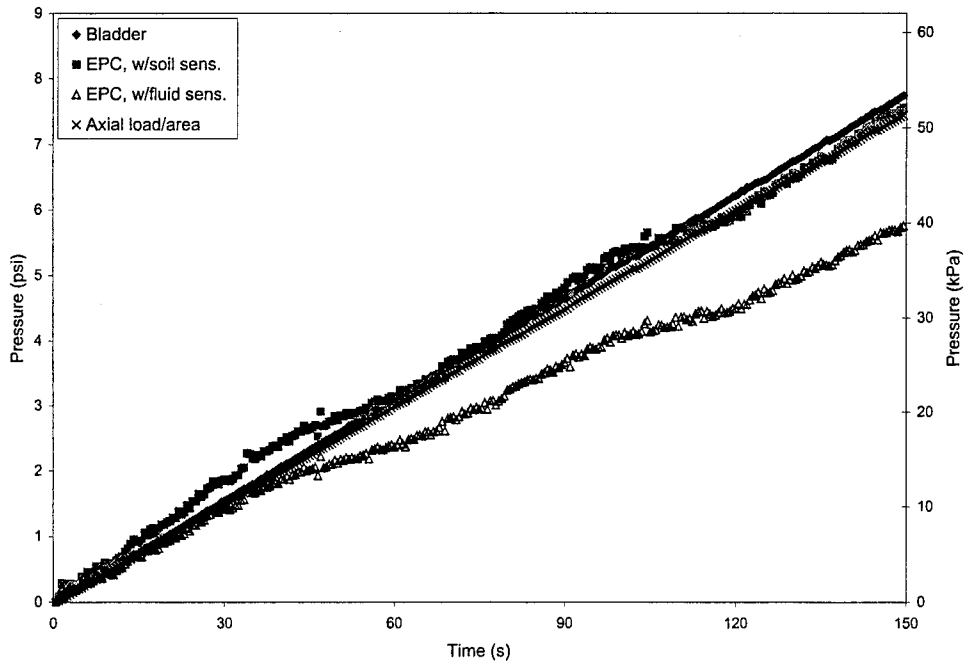

Figure 5.7. Universal calibration curve, static loading test (s19), conducted in Ottawa 20-30 sand after rapid loading.

Figures 5.8 and 5.9 represent universal calibration tests conducted in dry sand that was placed at a relatively lower density of 13.5 kN/m^3 (86.1 lb/ft^3). The EPC was seen to respond much differently. Universal calibration curves determined from tests performed with loose sand show the observed earth pressures measured by the cell to be much greater than the pressure recorded in the bladder. Thus the cell over-registered the earth pressure with respect to its fluid sensitivity. Registration ratios ranged from R = 1.4 to 1.9. Accordingly, the soil sensitivity, being a number with a smaller value than the fluid sensitivity, over-registered the earth pressure by an even larger amount. This response would tend to support the inclusion effect solutions of Taylor (1947), Monfore (1950), and others where a more rigid inclusion takes on a greater stress than the surrounding material. If the EPC is approximated as a rigid ellipsoid (after Askegaard 1963), with geometry, α = 0.3, it would have a stress registration ratio, R, between roughly 1.2 and 1.4 for a range of Poisson's ratios between 0 and 0.5. Similarly, Monfore predicted an over-registration of the normal stress across the face of the earth pressure cell. The degree of over-registration depended on the dimensions of the cell and the ratio of the Young's modulus between the cell and the soil.

However, within a denser soil, the EPC under-registers the applied normal stress when considering fluid sensitivities. This would appear to contradict Askegaard's result. While the soil is stiffer, it is still not as stiff as the earth pressure cell. An explanation is that arching in the granular soil above the cell accounts for this decrease in earth pressure. During uniaxial calibration, the EPC was calibrated such that the effect of arching was taken into account when calculating the soil sensitivity. So then the cell registers reasonable values of earth pressures with dense sand because arching has been accounted for and the dense sand is sufficiently stiff to yield registration ratios close to unity (the inclusion effect is minimal). In tests with loose sand, the Young's modulus of the soil is low, and the cell's extremely high stiffness dominates its response with respect to arching.

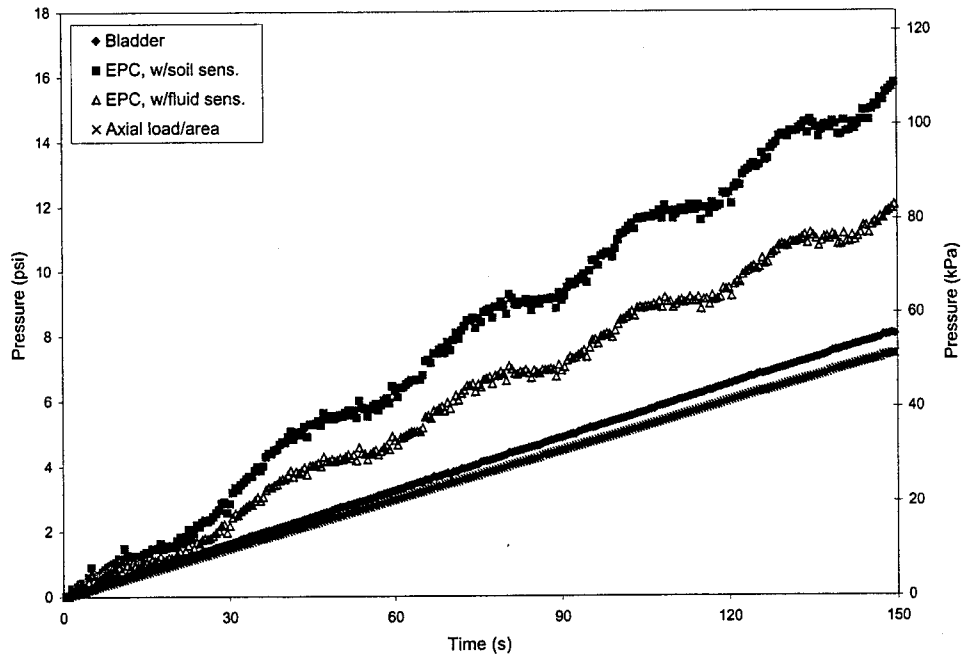

Figure 5.8. Universal calibration curve, static loading (s32), conducted in "loose" Ottawa 20-30 sand.

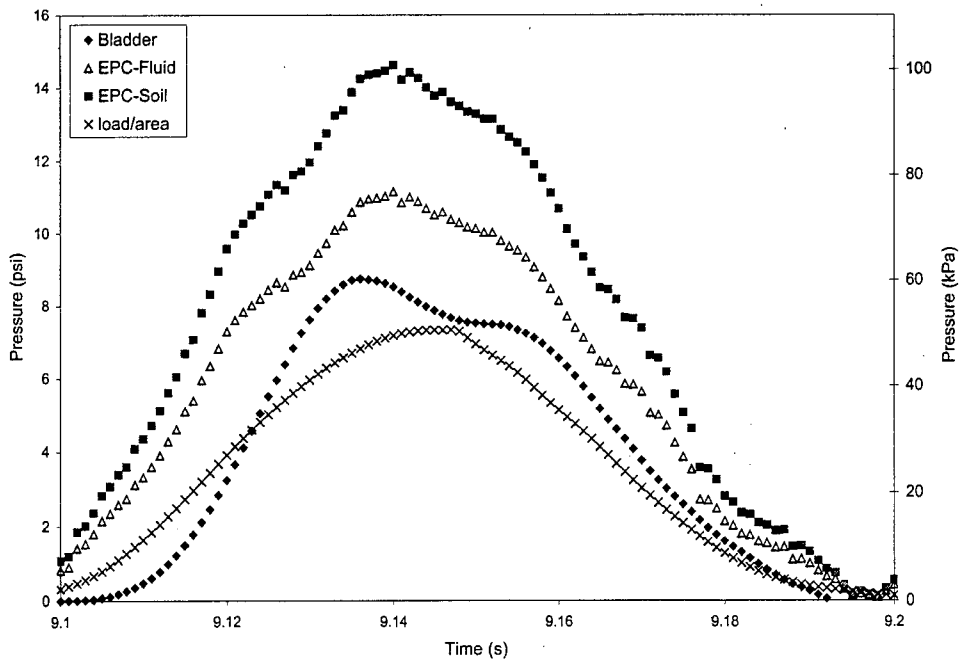

Figure 5.9. Universal calibration curve, rapid loading test (d20), conducted in "loose" Ottawa 20-30.

Universal Calibration – Clay

Universal calibration tests were conducted with the middle layer of the chamber comprised of clay. The response of the EPC, when placed within the clay layer, revealed highly scattered data (Figs. 5.10 and 5.11). Analysis on universal calibration curves was not practical because the load and unload trends were difficult to discern in both static and rapid loading tests.

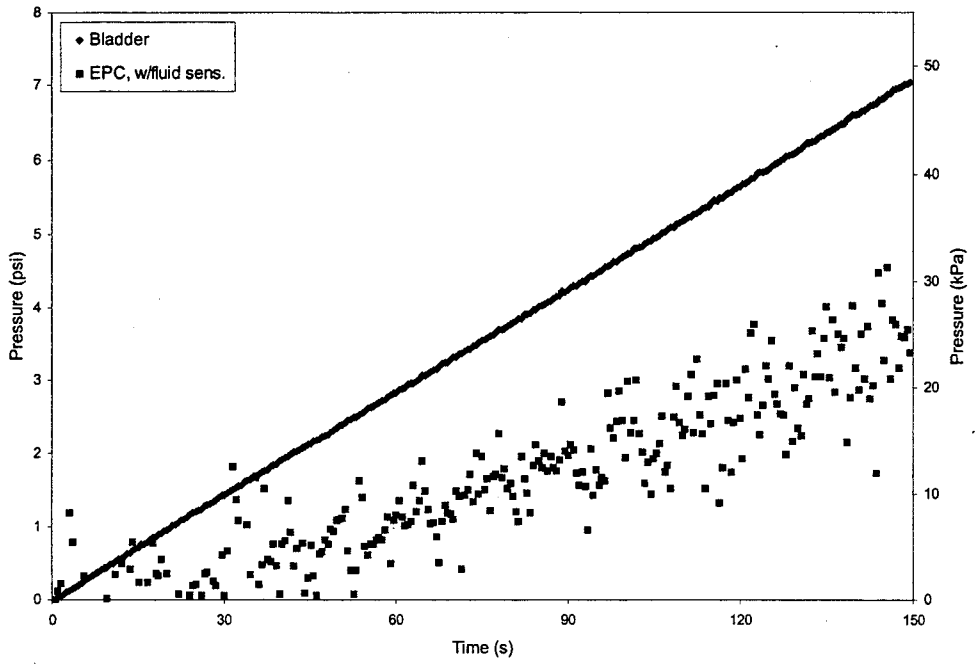

Figure 5.10. Universal calibration curve, static loading test (s70), conducted in clay.

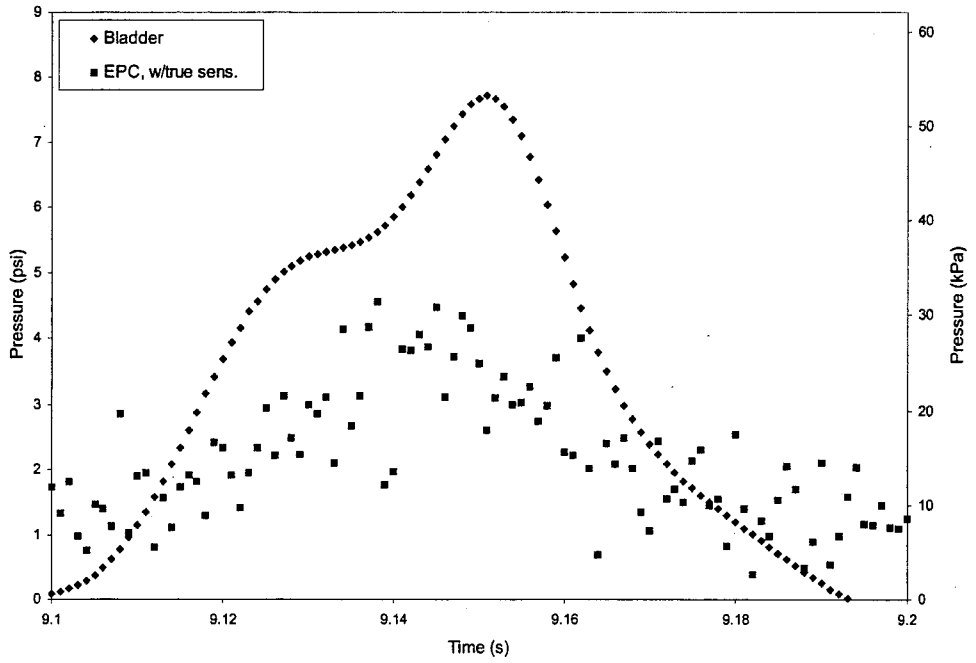

Figure 5.11. Universal calibration curve, rapid loading test (d44), conducted in clay.

Universal Calibration – Sand Pocket

In order to improve resolution of the EPC data within clay, a configuration was devised where the cell was placed within a pocket of dry sand. Loading would thus be transferred through the sand and applied to the cell. The sand's density was equal to the uniaxial calibration value of 16 kN/m^3 (104 lb/ft^3). The expectation was that the EPC, if installed properly in clay, would respond in much the same manner within the sand pocket as it had when placed exclusively in dry sand.

Preparation of the sand pocket and placement of the EPC within it was carried out in a special container prior to installing the entire arrangement within the clay. The soil pocket container (Fig. 5.12) consisted of a thin-walled steel cylinder of diameter 152 mm (6 in.), height 127 mm (5 in.) and a piece of geotextile, which acted as the bottom of the cylinder. The container was filled with Ottawa 20-30 silica sand at the uniaxial calibration density of 16 kN/m^3 (104 lb/ft^3). The EPC was carefully placed at a known position within the sand. A slot cut into the side of the cylinder and lined with a piece of slitted rubber, allowed the lead wire from the EPC to extend outside the steel cylinder. The piece of geotextile was folded over one end of the cylinder and clamped firmly around the outside of the cylinder with a hose clamp.

A hole with the approximate dimensions of the sand pocket container was excavated in the clay. The depth of the hole was 102 mm (4 in.), or 25.4 mm (1 in.) smaller than the container height, and the hole diameter was 17.8 cm (7 in), or 25.4 mm (1 in) larger than the container diameter. The container was placed in the hole. The hose clamp was removed from the outside of the steel cylinder. Extra sand was poured into the gap between the edge of the hole and the side of the cylinder to a height that was even with the sand inside the container. The last step was to carefully pull the steel cylinder out from the pocket of dry sand. The unclamped geotextile was left buried. The cylinder's rubber slit allowed the EPC lead wire to remain in place so as not to disturb the orientation of the cell.

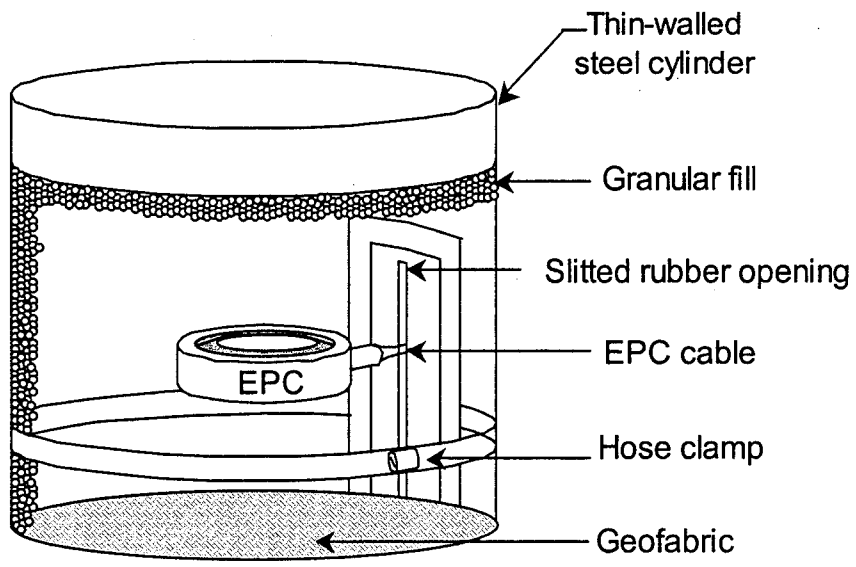

Figure 5.12. Sand pocket container.

The EPC demonstrated excellent response to both static and rapid loading within the sand pocket. Results of universal calibration tests with the EPC-sand pocket configuration are given in Figures 5.13 and 5.14. The EPC output was very similar to results from tests conducted with uniform, dry sand. As before, when the soil sensitivity was applied, the cell output agreed well with respect to the pressure measured in the bladder.

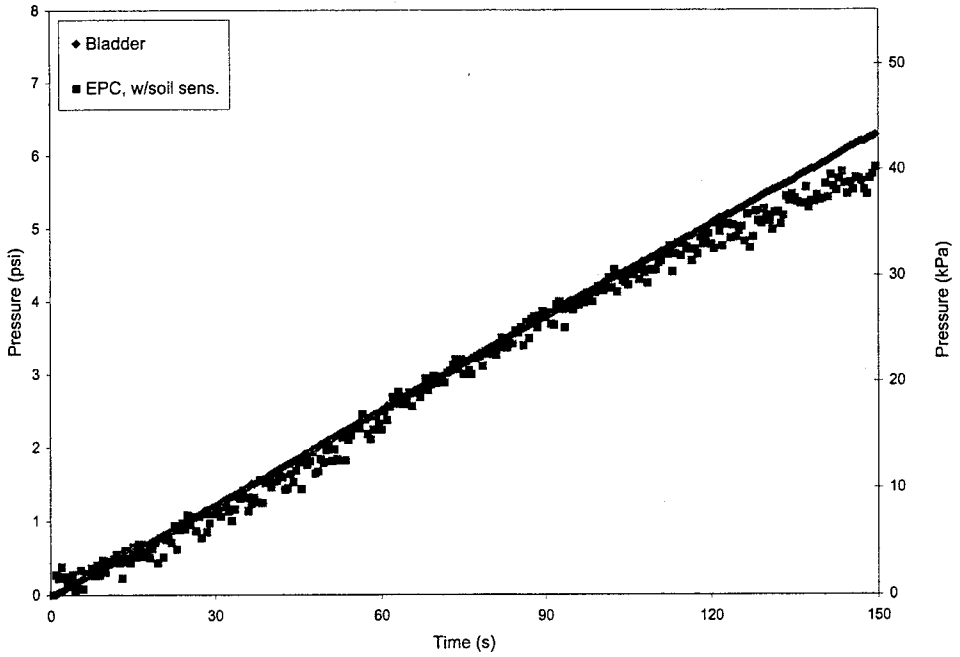

Figure 5.13. Universal calibration curve, static loading test (s95), conducted in pocket of Ottawa 20-30 sand.

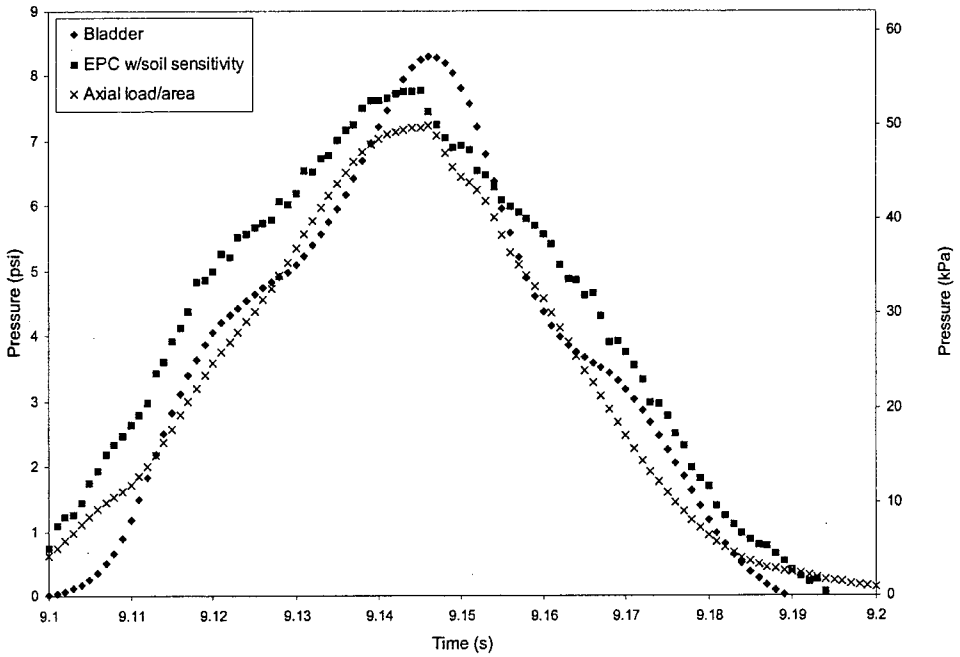

Figure 5.14. Universal calibration curve, rapid loading test (d60), conducted in pocket of Ottawa 20-30 sand.

Sand pocket universal calibration tests were also conducted where class 6 gravel was placed in the top soil layer. Class 6 gravel is a coarse-grained material that is used in practice as

an aggregate base overlying the subgrade soil underneath paved roads. The gravel was placed above the upper bladder. The EPC and sand pocket were installed as before. A circular piece of geotextile was placed between the gravel and the top of the upper bladder to help protect the bladder. The response of the EPC was excellent to both static and rapid loading through the gravel (Figs. 5.15 and 5.16).

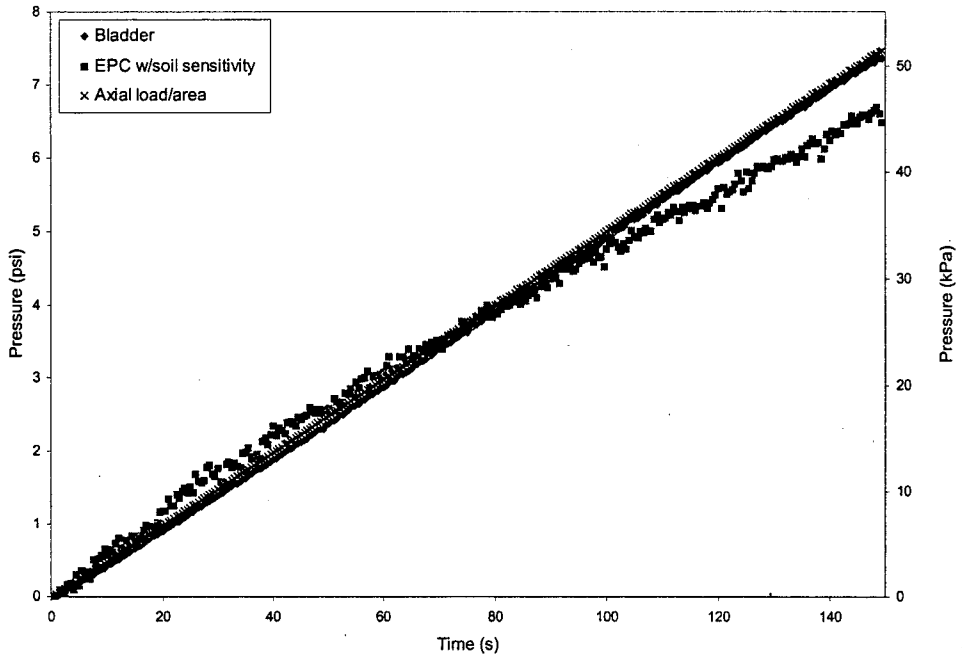

Figure 5.15. Universal calibration curve, static loading test (s118), conducted in pocket of Ottawa 20-30 sand with overlying class 6 gravel.

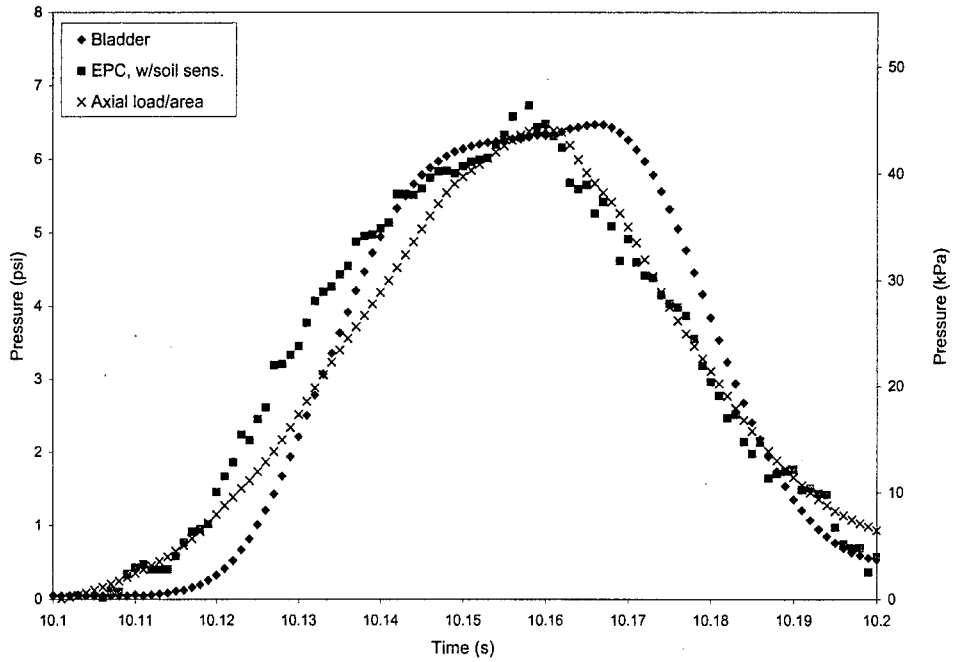

Figure 5.16. Universal calibration curve, rapid loading test (d116), conducted in pocket of Ottawa 20-30 sand with overlying class 6 gravel.

CHAPTER 6
CONCLUSIONS

The aim of this research was to study the interaction between an EPC and soil, develop a simple laboratory calibration method, and propose a suitable field installation procedure. A uniaxial calibration device was designed to permit the application of loading through a soil column to the sensitive face of an EPC. Calibration tests were conducted under a variety of loading conditions that included loading from both fluid and soil pressure. It was observed that the EPC output was influenced by an arching effect across the face of the cell. This was evidenced by a comparison of sensitivities. It was found that calibrations under uniform fluid pressure conditions produced a sensitivity that matched the cell manufacturer's value. However, sensitivities derived from soil pressure tests were significantly, and consistently, lower, on the order of 20%.

Arching occurred when soil pressure was applied over the entire diameter of the EPC. The outer rim of the cell acted as a rigid support while the central diaphragm deflected. Frictional forces developed over the rim and lessened the effective load applied to the diaphragm. A lower sensitivity than the fluid sensitivity resulted. When the diameter of the soil column was reduced to the inner diameter of the outer rim, no rigid support was available to allow arching to develop. Hence, the pressure acting on the diaphragm of the cell was not reduced and a sensitivity higher than the value for the larger soil column resulted. Thus, the area of the cell over which loading took place was important as it influenced the amount of arching allowed to develop over the EPC.

Loading during soil calibrations was applied to the entire area of the cell face in order to monitor its response and calculate a sensitivity relevant to field conditions. Soil calibrations were performed using two types of uniform silica sand (Ottawa 20-30, Ottawa 50-70) at two soil column heights (12.7 mm or 0.5 in., 25.4 mm or 1 in.). The sensitivities from each calibration configuration were compared. Sensitivities calculated from tests with the coarser Ottawa 20-30 sand were, in general, just slightly lower than similar tests with the finer Ottawa 50-70 sand. The soil calibration sensitivity decreased and exhibited a trend toward a limiting value as the soil

column height was increased. This limiting value was taken to correspond to far-field loading conditions and was termed the cell's soil sensitivity.

Universal calibration tests were performed to observe the response of the EPC to static and rapid loading inside a soil chamber. Fluid-filled rubber bladders were used to assure a uniform pressure distribution and to monitor the vertical stress that was applied to the cell. Static loading tests involved a constant load and unload rate being applied to the soil. Rapid loading tests consisted of a cycle of twenty load/unload pulses being applied to the soil. The cell was tested in silica sand (Ottawa 20-30) and clay. The EPC responded well to the applied loads when placed in silica sand, but the data were highly scattered for tests in clay.

When the cell's soil sensitivity was used, its data yielded good agreement with the measured fluid pressures in the bladder. However, EPC output was sensitive to changes in soil density. When the cell was placed within soil at a lower density, its output over-registered the bladder pressure. When the soil was sufficiently dense, its output decreased and sometimes even under-registered the bladder pressure.

In order to test the EPC in clay and achieve good resolution of data, an installation involving a sand pocket was devised. The sand pocket consisted of a measured amount of silica sand (Ottawa 20-30) filled into a hole of known volume that was cut into the clay; hence the density of the sand was also known. The EPC was placed within the pocket. Universal calibration tests were conducted with the EPC with good results; it responded in the same way it had when placed exclusively in sand. Since the density of the sand in the pocket was known, the soil sensitivity provided a reasonable measurement of the vertical pressure acting on the cell.

Recommendations

The following general procedure is recommended for field installation and overall EPC application. The earth pressure cell should be calibrated in the lab with the uniaxial calibration device using soil pressure. The cell should be loaded to its capacity at such a rate so that 8 – 10 data points are collected. For the case of the Kulite cell, which has a capacity of 483 kPa (70 psi), a calibration from 0 to 483 kPa in 69 kPa (10 psi) increments is appropriate. Silica sand (20-30) at a column height of 25.4 mm (1 in.) is suitable for calibration purposes (20-30 is recommended over 50-70 as it is easier to work with). Once the cell has been calibrated and its soil sensitivity has been determined, it should be installed in the ground within a sand pocket. Whatever sand type was used for cell calibration should then also be used to fill the sand pocket. It is suggested that the unit weight of the sand pocket be the same as, or as close as possible to, the value used in calibration. In this report, 16.3 kN/m^3 (0.104 lb/ft^3) was used. At least 50 – 80 mm (or 2 – 3 in) of sand cover should be above the face of the cell and at least 25 mm (1 in.) of sand underneath. The EPC should be properly oriented for accurate earth pressure measurement.

The diameter of the sand pocket should be about three times the diameter of the EPC. A hole in the soil should be created for the installation of the sand pocket. If the condition of the subgrade soil permits, the hole should be dug to the required dimensions and the EPC and sand placed within it. Otherwise, if the subgrade is too stiff to allow ease of hole construction, the sand pocket should be prepared within a steel cylinder as described in Chapter 5 prior to placement in the hole. Then the cylinder should be unclamped, extra sand poured into the space between the cylinder and the side of the hole, and the cylinder carefully removed from the sand pocket leaving the EPC in place.

Future Research

A similar investigation should be conducted on earth pressure cells of differing types. The effect, or lack thereof, of arching over cells with fully active faces (no rigid rims) should be studied. For such cells, the distribution of pressure across the cell face would be important in determining how the cell responds. For the Kulite EPC with an inactive, rigid rim and central deflecting diaphragm, the effect of soil density was qualitatively documented, but not quantitatively studied. Future experiments should aim to monitor EPC response within soils of various, known densities. The competing effects of a stiff inclusion within a softer material and soil arching occurring over the face of a cell should be investigated further. Also of interest would be the simultaneous response of multiple earth pressure cells in various configurations. The spacing at which cells begin to interact with each other would be of practical significance.

REFERENCES

1. Askegaard, V. (1963), "Measurement of Pressure in Solids by Means of Pressure Cells," Structural Research Laboratory, Technical University of Denmark, Bulletin No. 17, Copenhagen.

2. Craig, R. F. (1974), Soil Mechanics, Chapman and Hall, New York.

3. Dunnicliff, John, (1988), Geotechnical Instrumentation For Monitoring Field Performance, John Wiley & Sons, Inc., New York, pp. 165-183.

4. Eshelby, J. D. (1957), "The Determination of the Elastic Field of an Ellipsoidal Inclusion, and Related Problems," Proceedings, Royal Society, London, Series A, Vol 241, pp 376-396.

5. Filz, G.M. and Brandon, T.L. (1994), "Static and Dynamic Measurements Using Embedded Earth Pressure Cells," Transportation Research Record, 1432, 86-95.

6. Filz, G.M. and Duncan, J.M. (1993), "Pressure Cell Drift," Geotechnical Testing Journal, ASTM, Vol. 16, No. 4, 432-441.

7. Hvorslev (1976), "The Changeable Interaction Between Soils and Pressure Cells; Tests and Reviews at the Waterways Experiment Station," Technical Report S-76-7, U.S. Army Engineer Waterways Experiment Station, Soils and Pavements Laboratory, Vicksburg, Mississippi.

8. Mason, H. G. (1965), "Effects of Structural Compressibility on Active and Passive Arching in Soil-Structure Interaction," Defense Atomic Support Agency, DASA 1718, URS 645-8.

9. McNulty, J. W. (1965), "An Experiment Study of Arching in Sand," Technical Report No. 1-674, U.S. Army Engineer Waterways Experiment Station, CE, Vicksburg, Mississippi.

10. Monfore, G. E. (1950), "An Analysis of the Stress Distribution in and near Stress Gauges Embedded in Elastic Soils," Structural Laboratory Report No. SP 26, U.S. Bureau of Reclamation, Denver, Colorado.

11. Peattie, K. R., and Sparrow, R. W. (1954), "The Fundamental Action of Earth Pressure Cells," Journal of the Mechanics and Physics of Solids, Pergamon Press Ltd., London, Vol. 2, pp. 141 – 155.

12. Selig, E. T. (1964), "A Review of Stress and Strain Measurement in Soil," Proceedings, Symposium on Soil-Structure Interaction, Tucson, Arizona, pp. 172 – 186.

13. Taylor, D. W. (1945), "Review of Pressure Distribution Theories and Earth Pressure Cell Investigations," Chapter 2 in report to the U.S. Army Engineer Waterways Experiment Station of November 1945.

14. Terzaghi, K. (1943), Theoretical Soil Mechanics, Wiley, New York, pp. 66-76.

15. Timoshenko, S. (1934), Theory of Elasticity, McGraw-Hill Book Company, Inc., New York.

16. Van Deusen, D. A. (1992), "A Review of Instrumenation Technology for the Minnesota Road Research Project," Report No. FHWA/MN/RC – 92/10, Minnesota Department of Transportation, St. Paul, Minnesota.

17. Weller, W. A., Jr., and Kulhawy, F. H. (1982), "Factors Affecting Stress Cell Measurements in Soil," Journal of the Geotechnical Engineering Division, American Society of Civil Engineers, Vol. 108, No. GT12, Dec., pp. 1529 – 1548.

APPENDIX

RESULTS FROM UNIAXIAL SOIL CALIBRATION

Table A1. EPC Uniaxial Calibration Tests.

Soil column height (mm)	Test #	EPC sensitivities per cycle (vdc/kPa)										
		1	2	3	4	5	6	7	8	9	10	11
Ottawa 20-30												
12.7	1	0.018	0.018	0.018								
12.7	2	0.018	0.018									
12.7	3	0.017	0.016	0.016	0.016	0.016	0.016					
25.4	4	0.014	0.014	0.014	0.014	0.014						
Ottawa 50-70												
12.7	5	0.018	0.018	0.018	0.018	0.018	0.018					
12.7	6	0.018	0.018	0.018	0.018	0.018	0.018					
25.4	7	0.016	0.015	0.015	0.015	0.015	0.015	0.015	0.016	0.016	0.016	0.016
25.4	8	0.018	0.017	0.017	0.017	0.017	0.017	0.017	0.017			

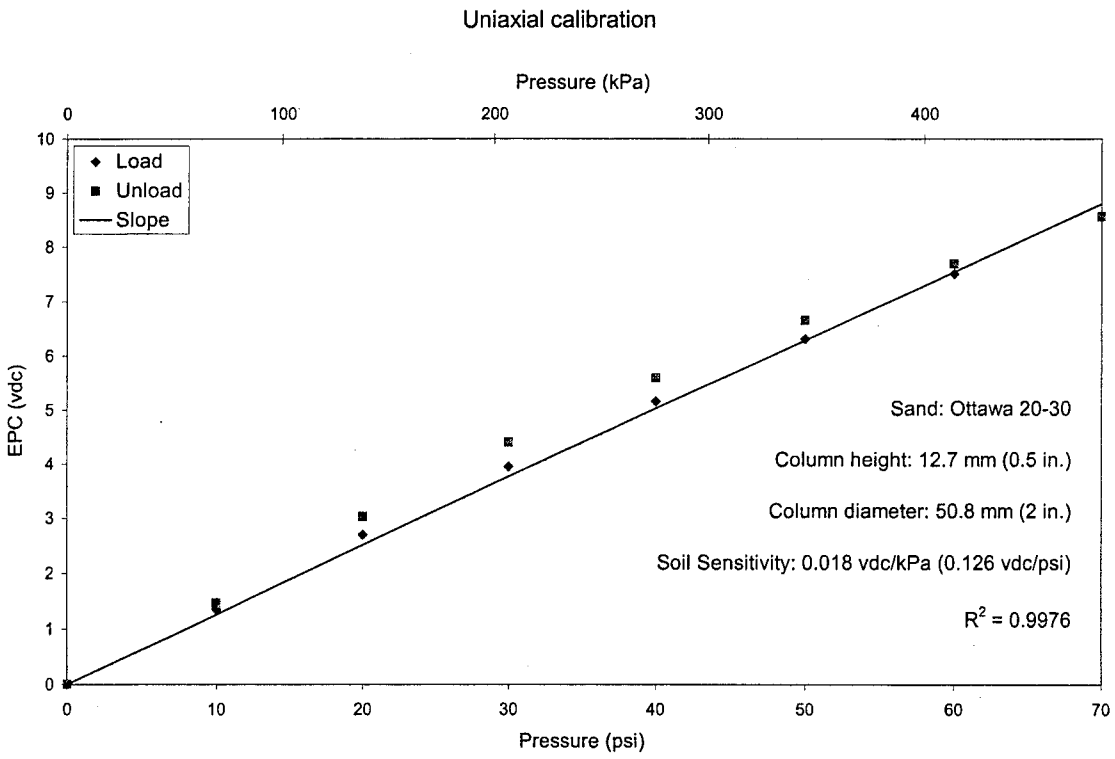

Figure A1. Test 1, cycle 1.

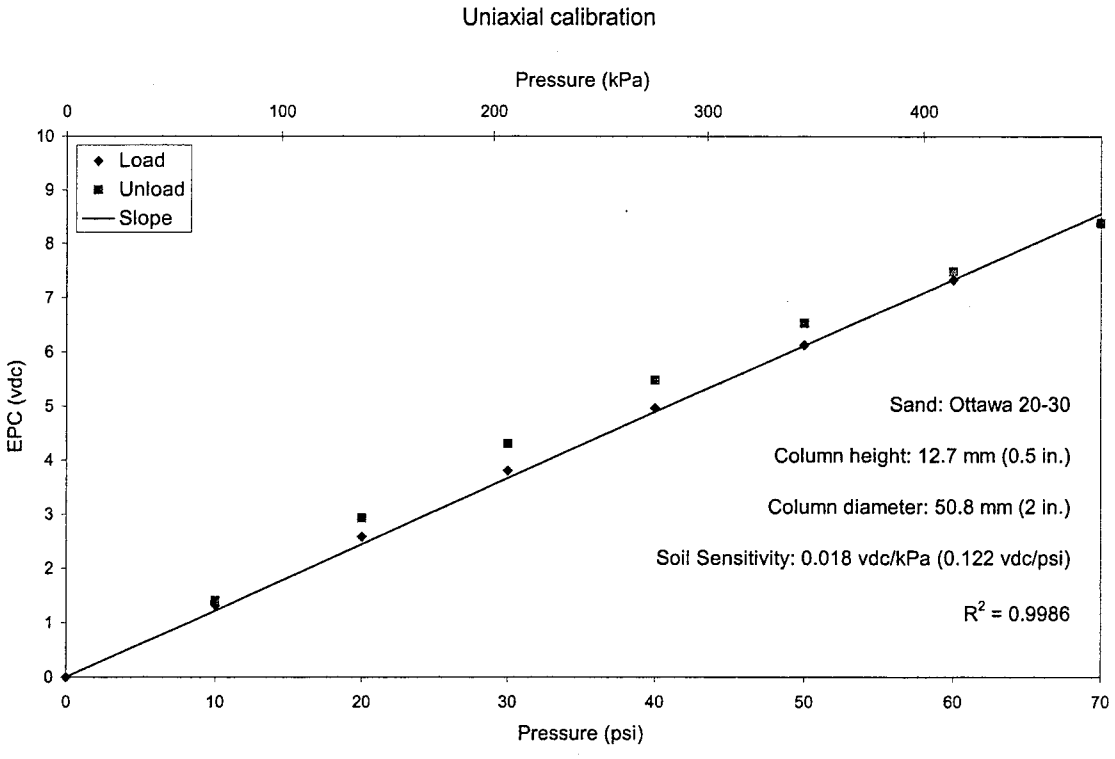

Figure A2. Test 1, cycle 2.

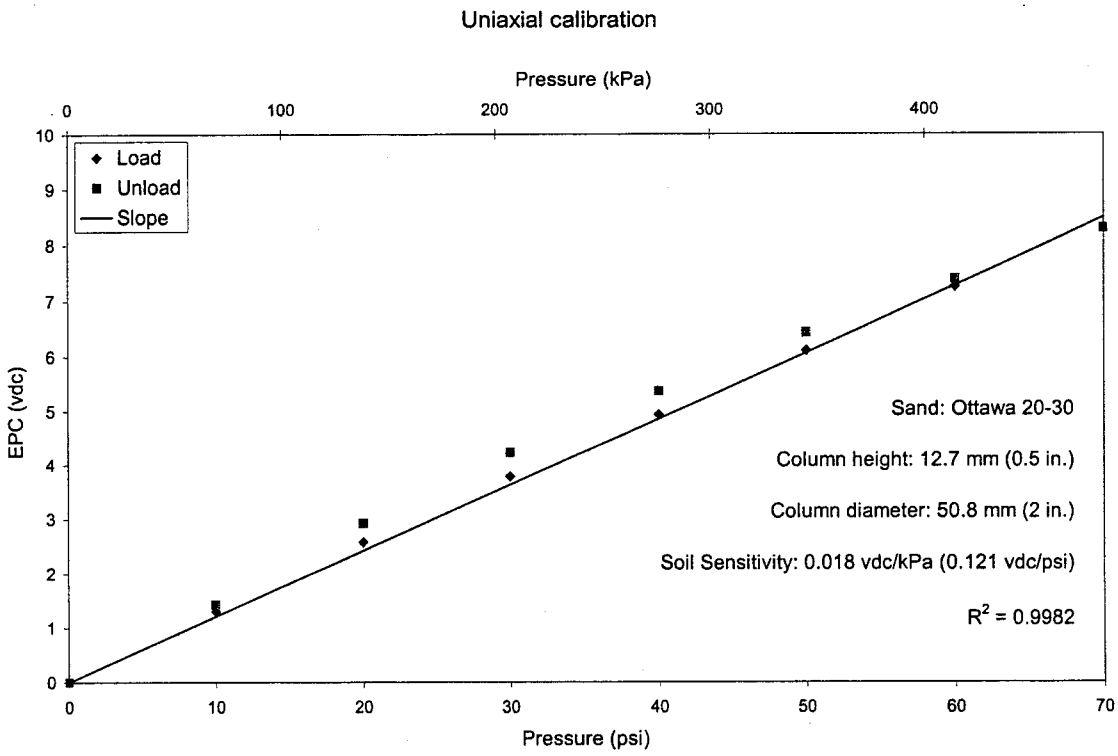

Figure A3. Test 1, cycle 3.

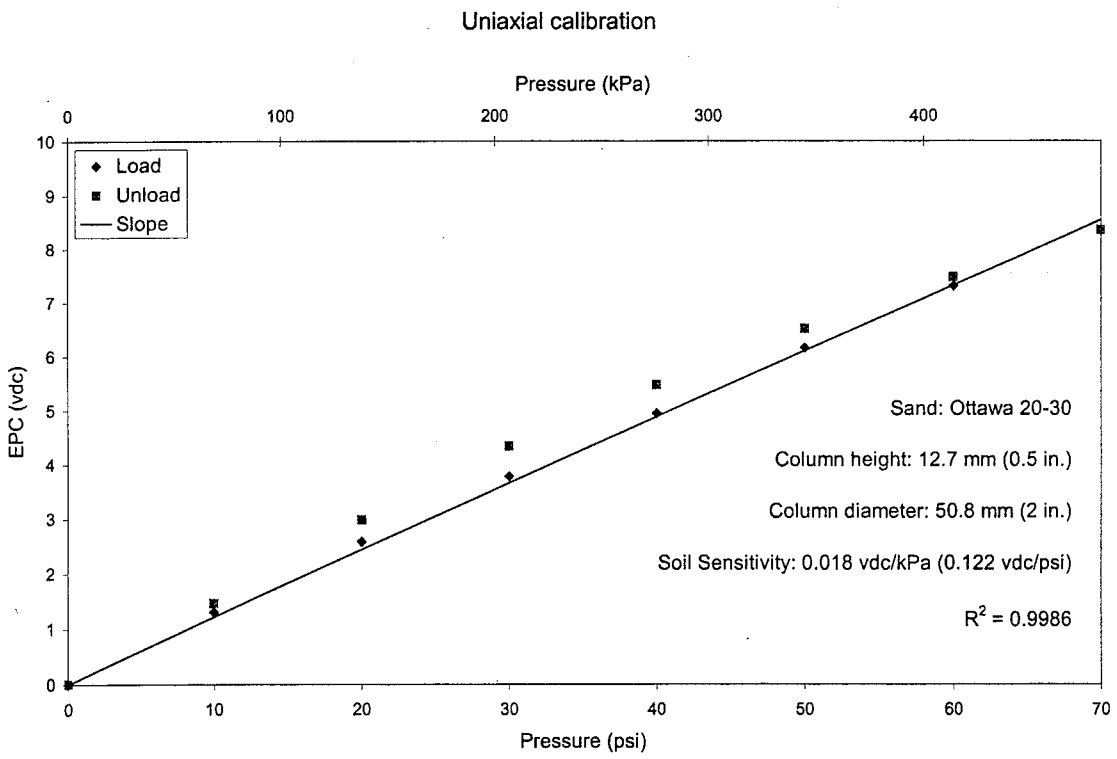

Figure A4. Test 2, cycle 1.

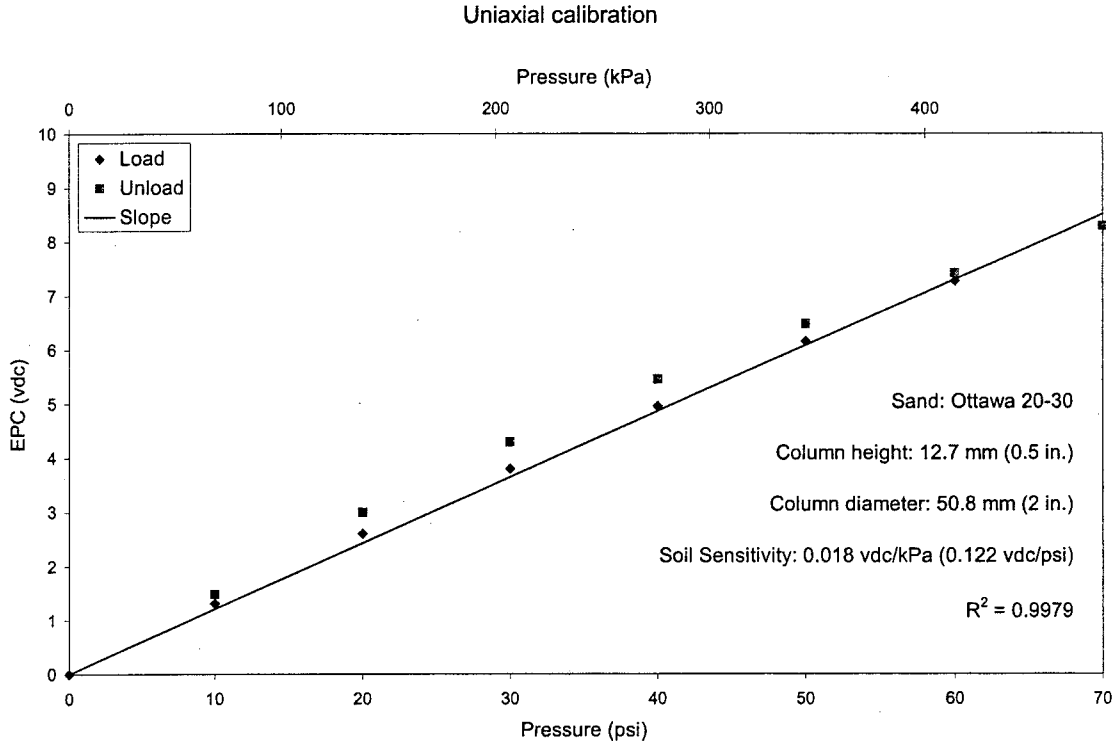

Figure A5. Test 2, cycle 2.

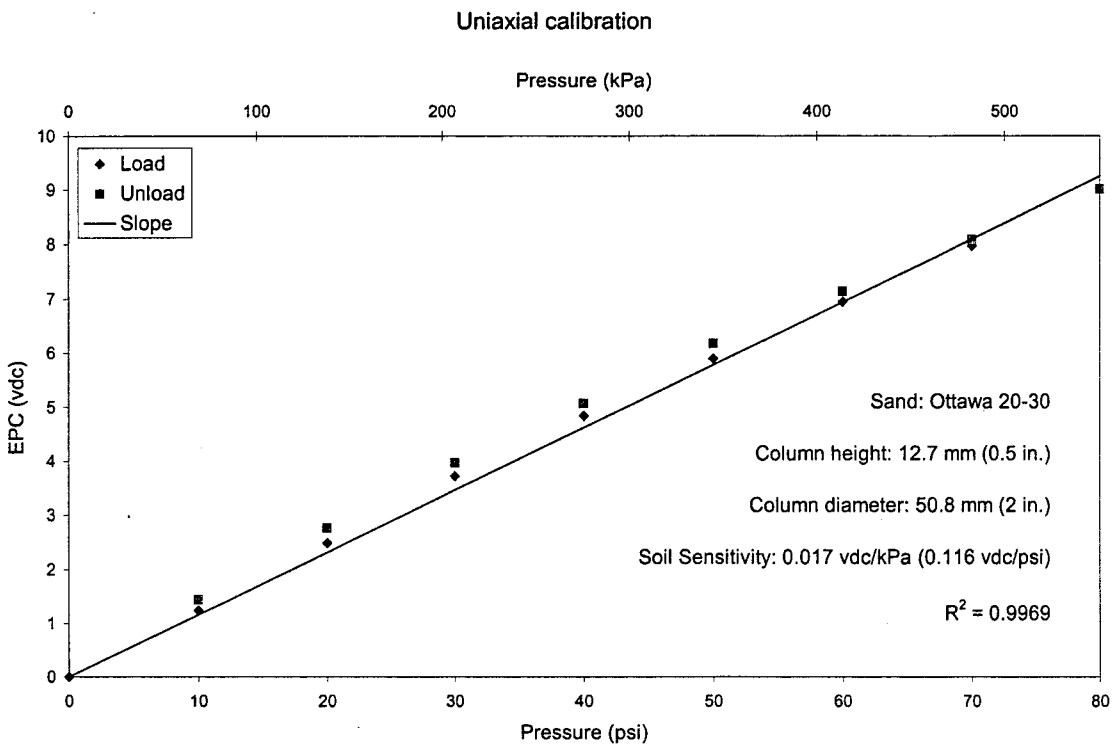

Figure A6. Test 3, cycle 1.

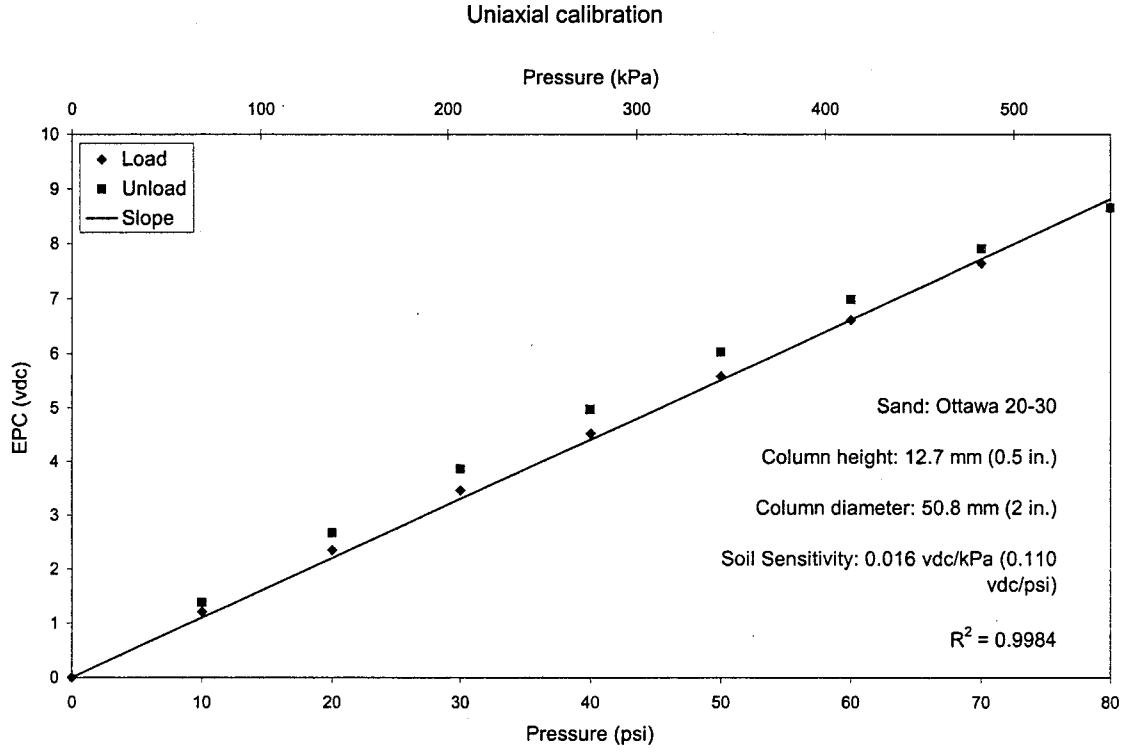

Figure A7. Test 3, cycle 2.

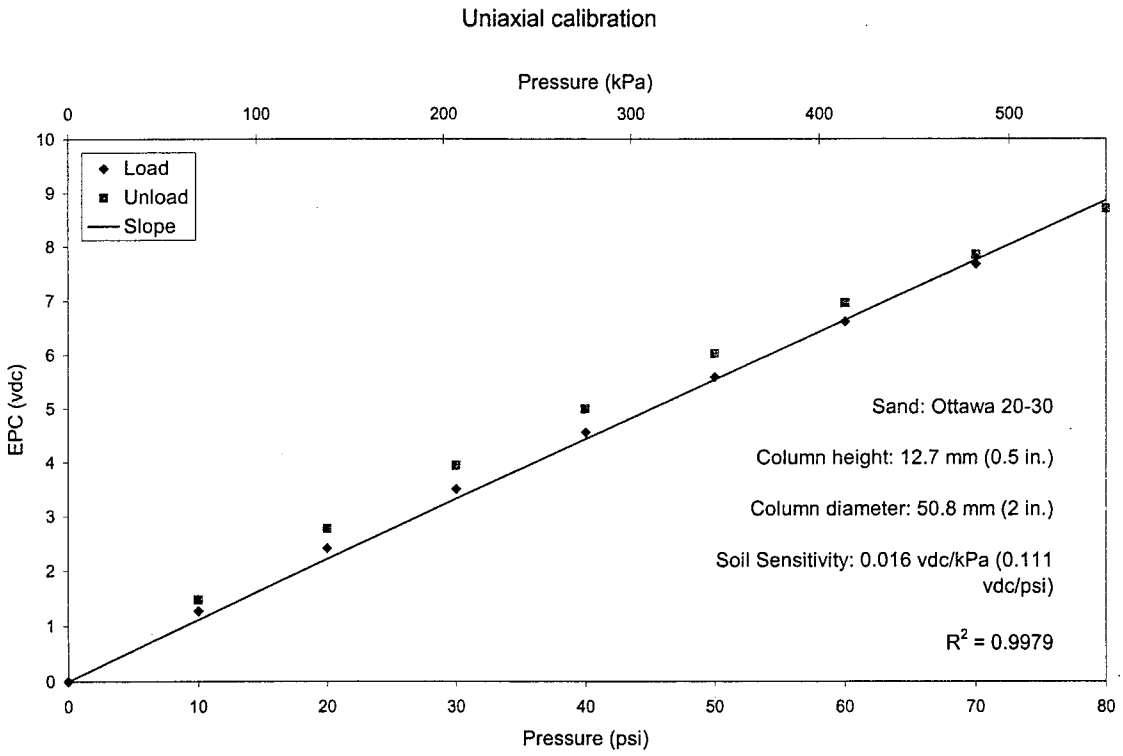

Figure A8. Test 3, cycle 3.

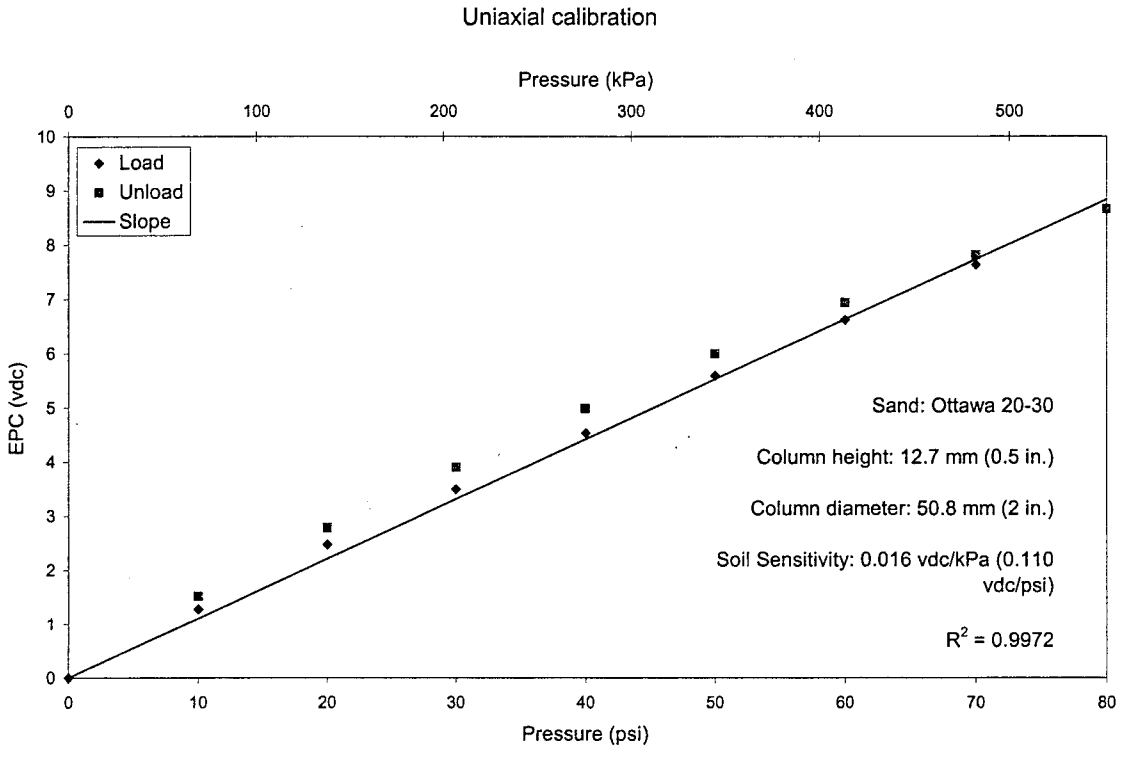

Figure A9. Test 3, cycle 4.

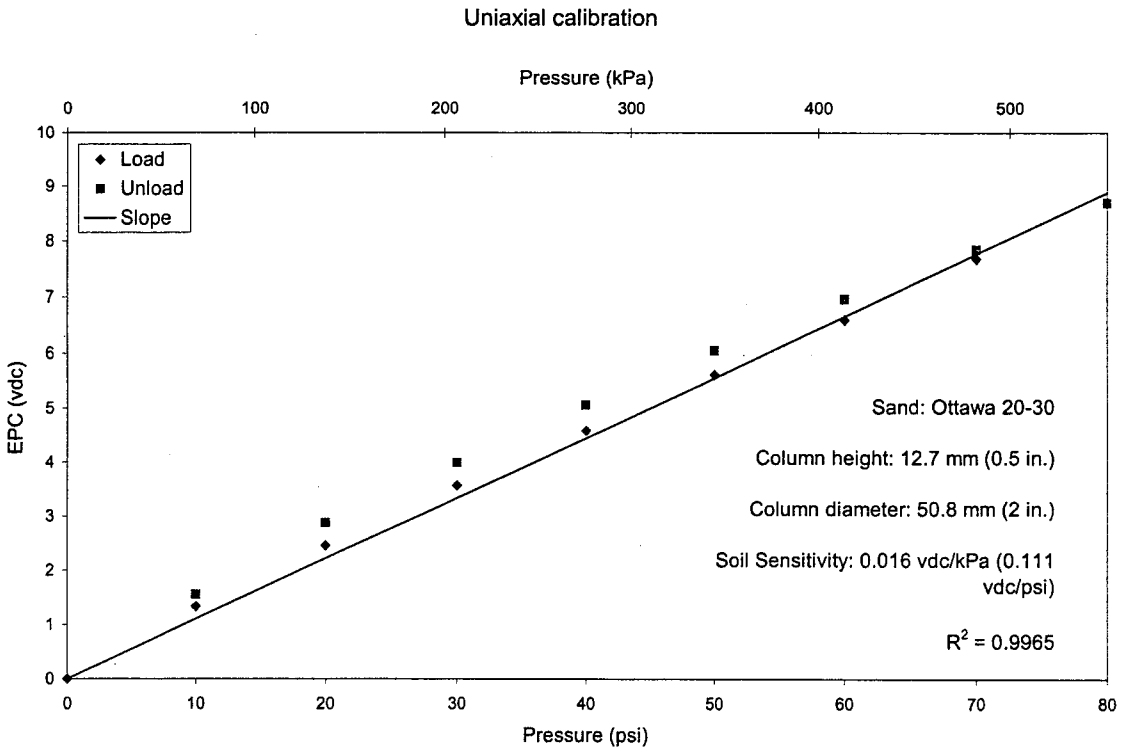

Figure A10. Test 3, cycle 5.

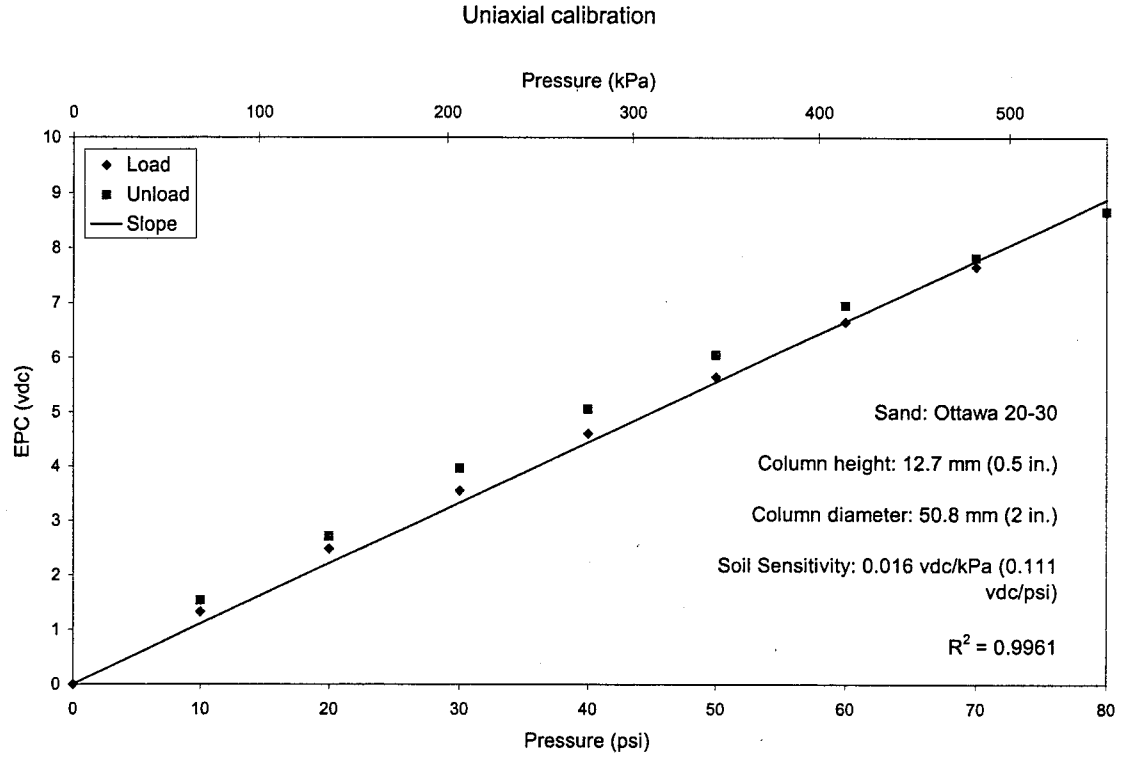

Figure A11. Test 3, cycle 6.

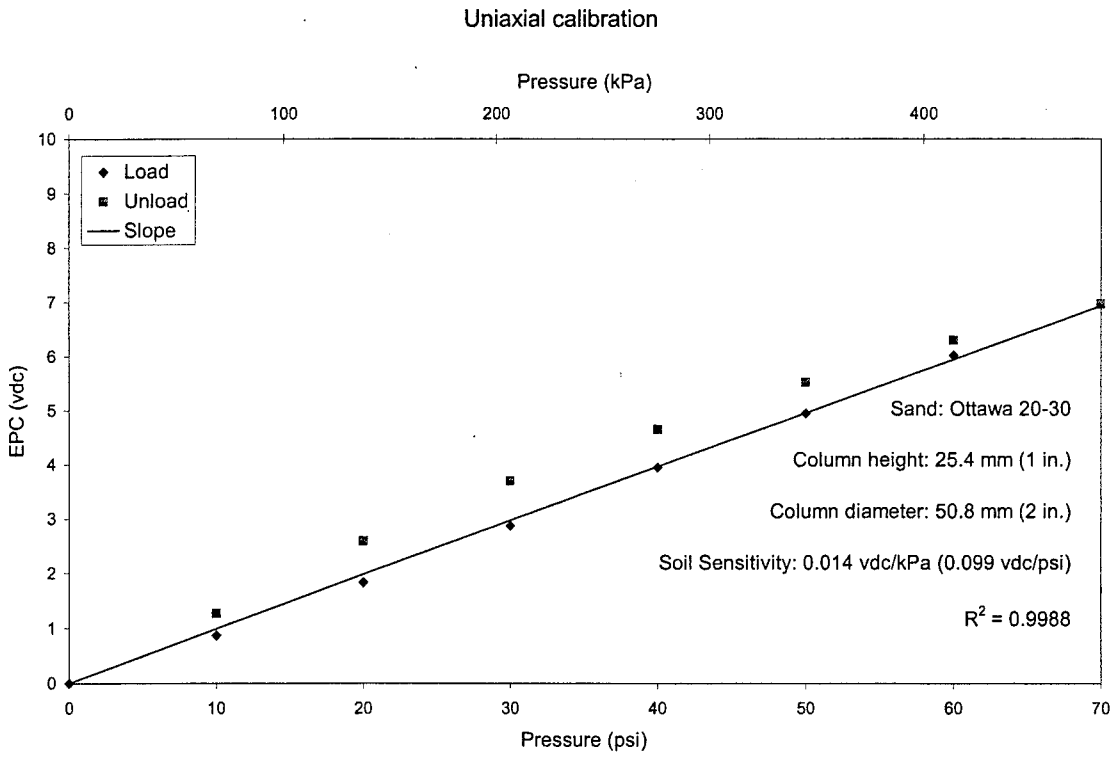

Figure A12. Test 4, cycle 1.

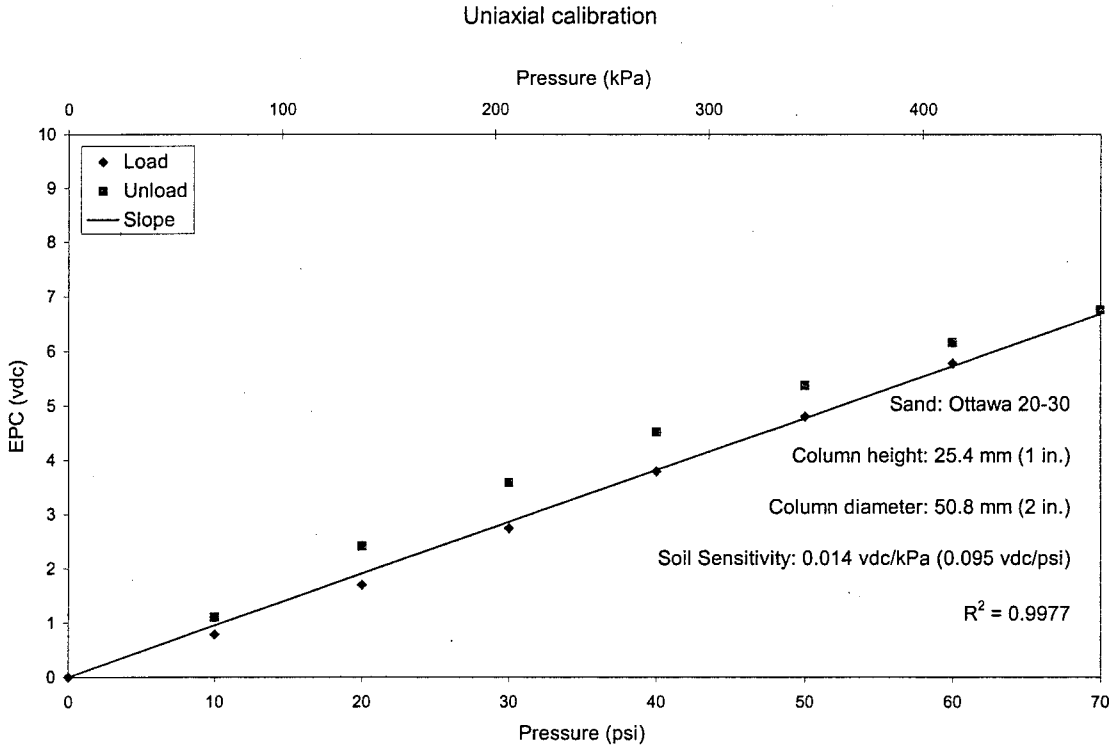

Figure A12. Test 4, cycle 2.

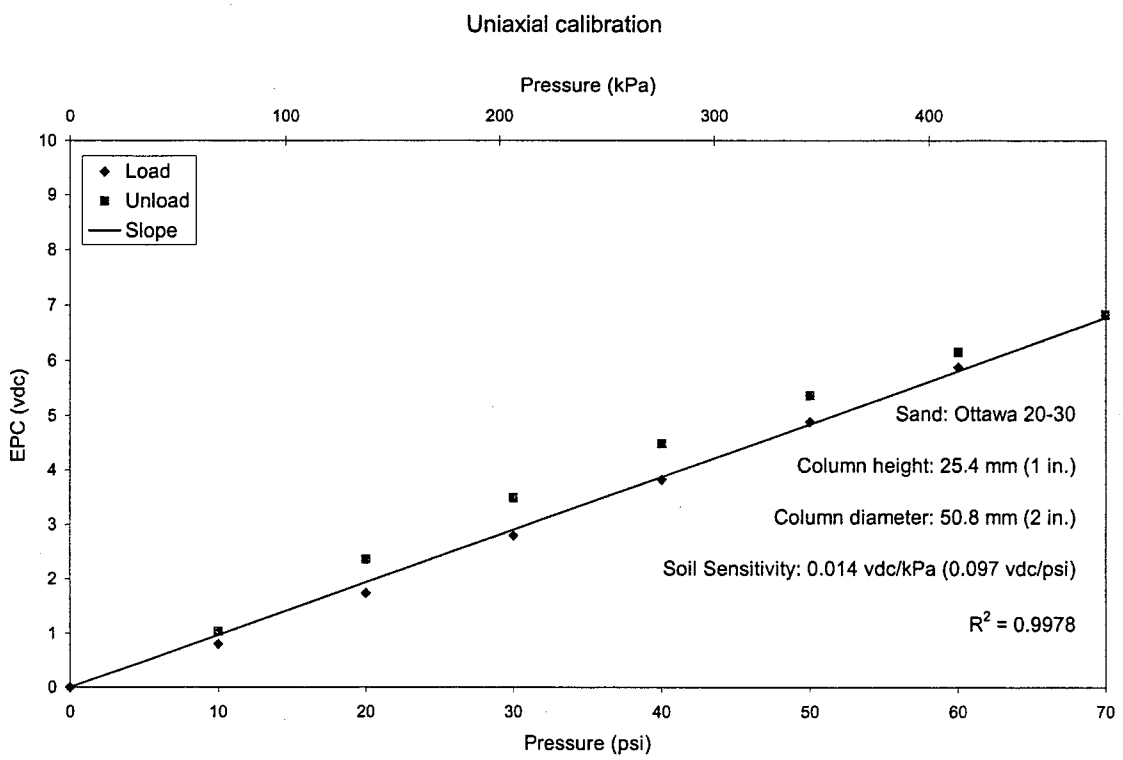

Figure A14. Test 4, cycle 3.

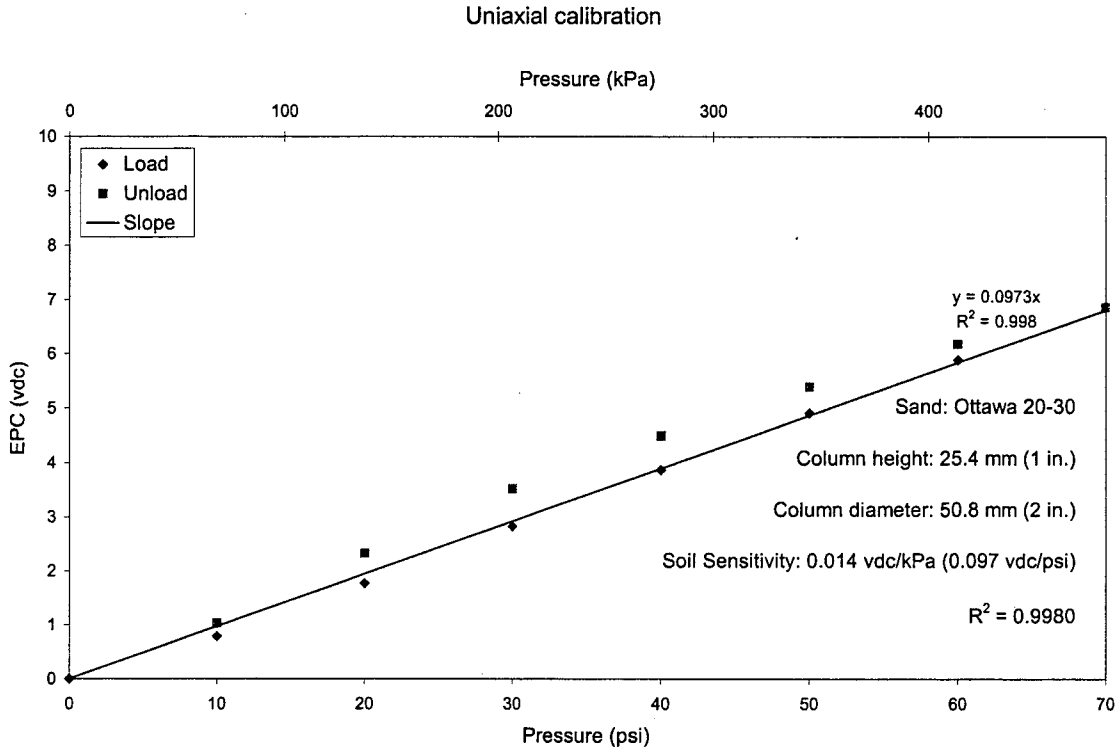

Figure A15. Test 4, cycle 4.

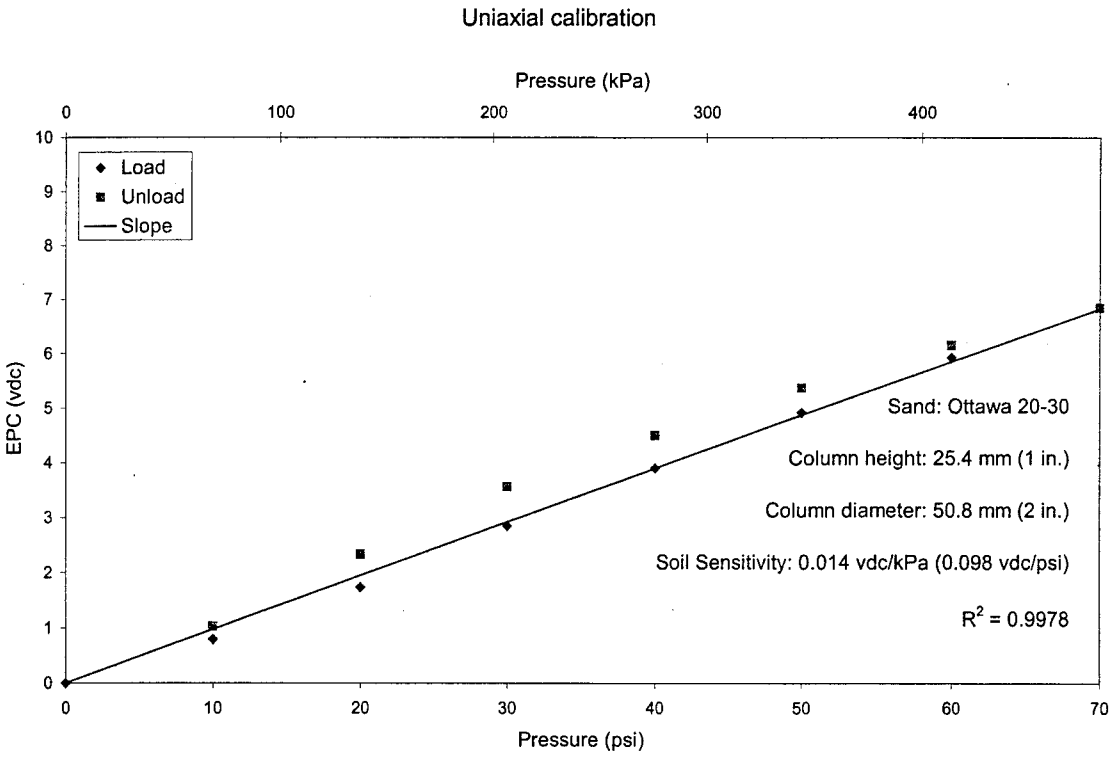

Figure A16. Test 4, cycle 5.

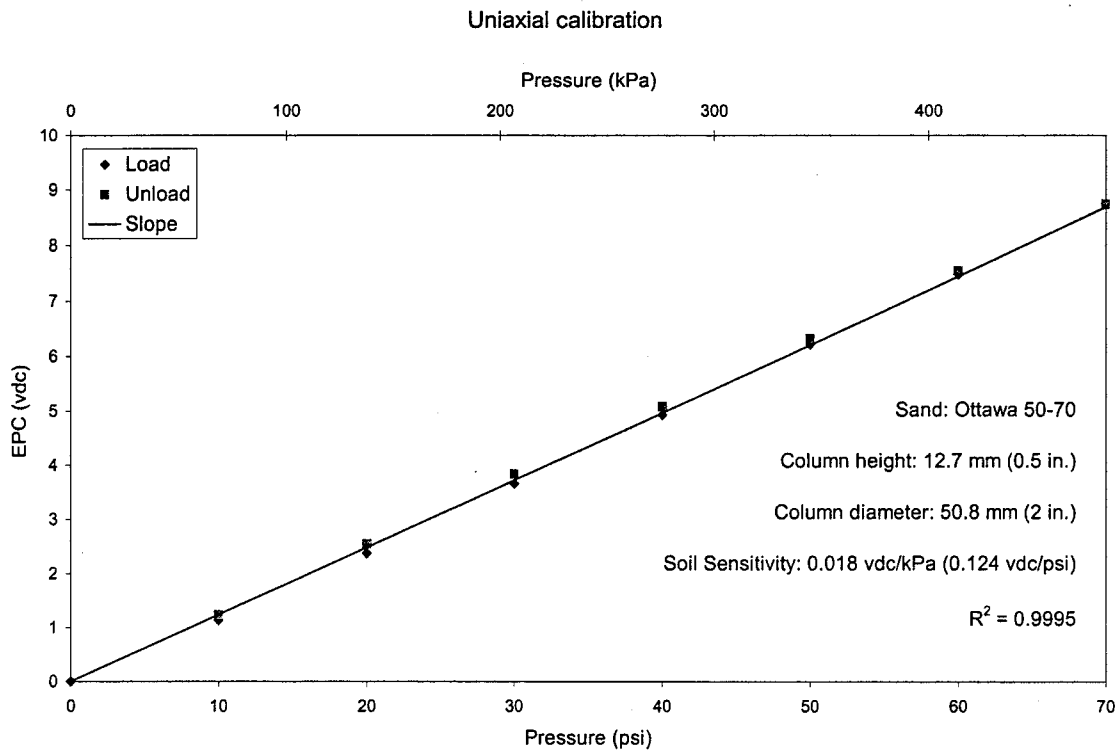

Figure A17. Test 5, cycle 1.

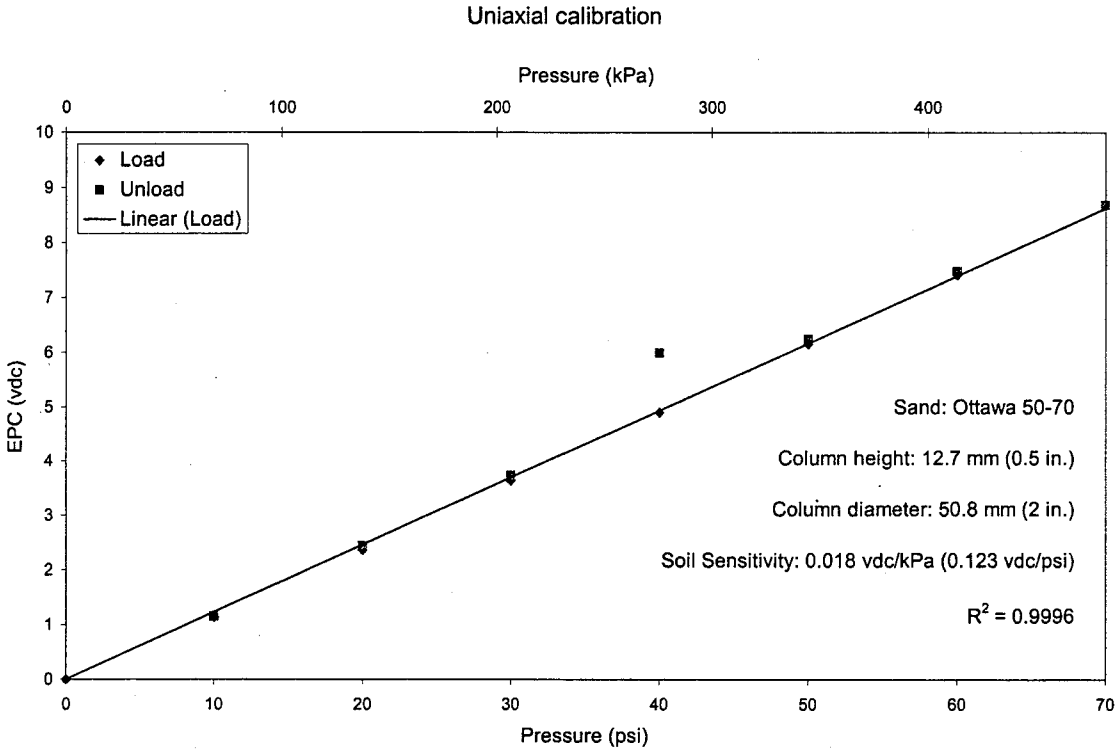

Figure A18. Test 5, cycle 2.

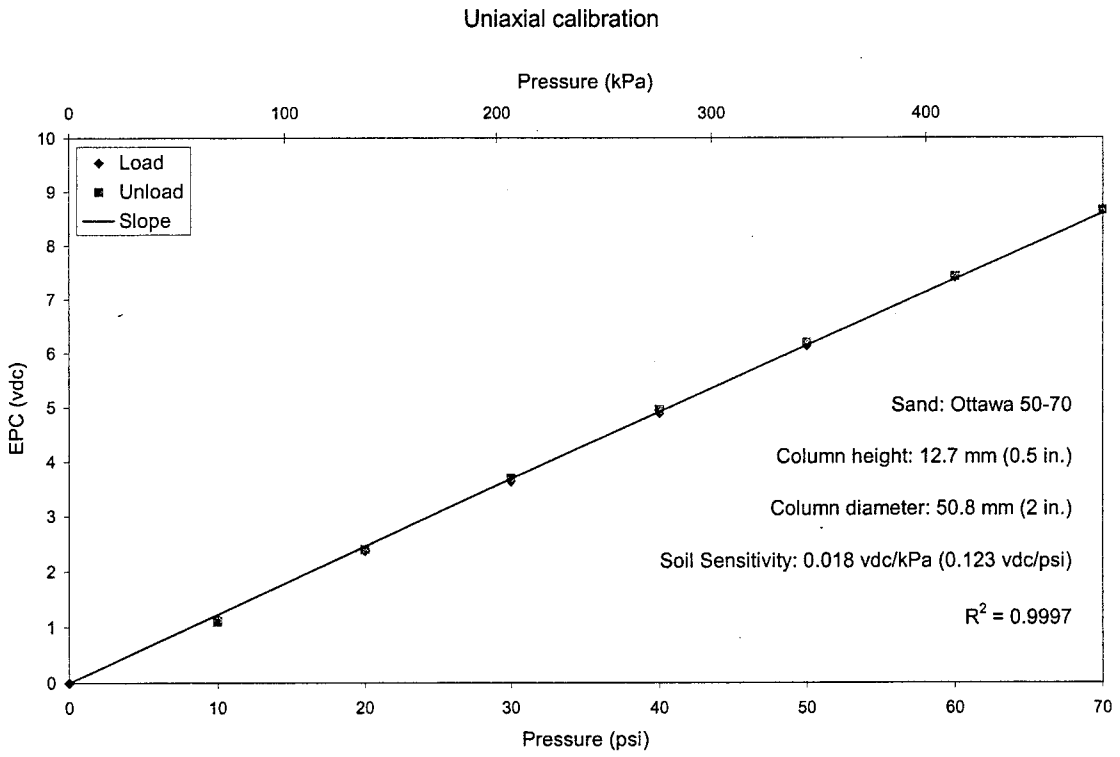

Figure A19. Test 5, cycle 3.

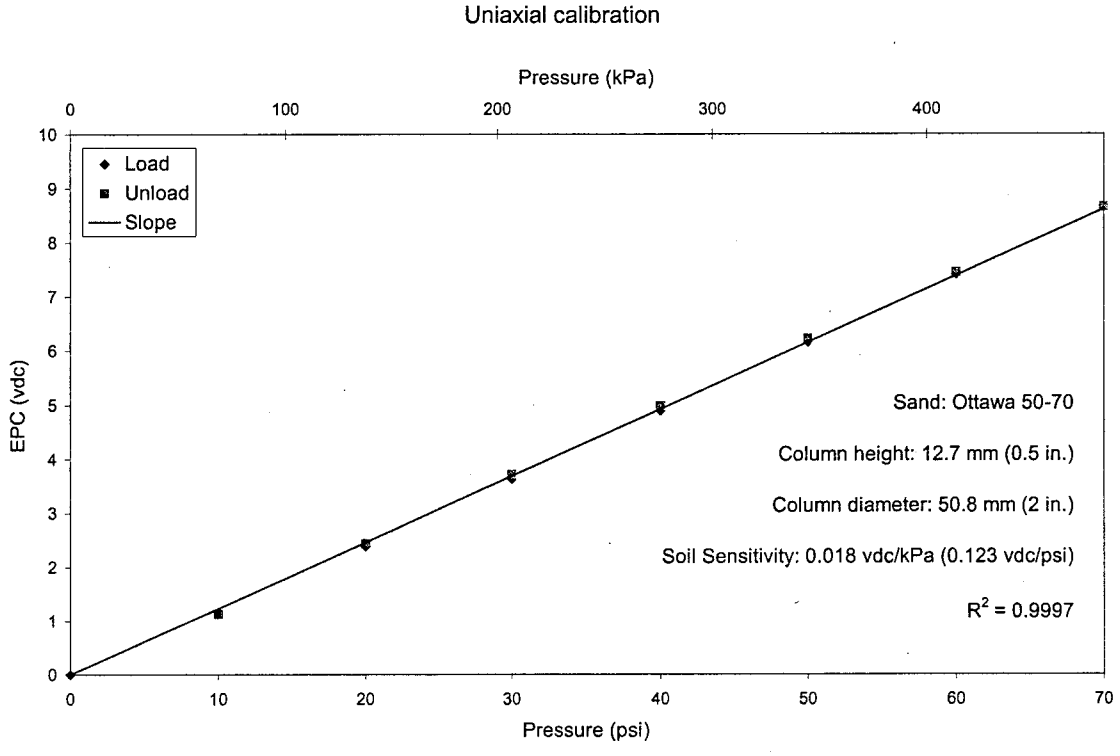

Figure A20. Test 5, cycle 4.

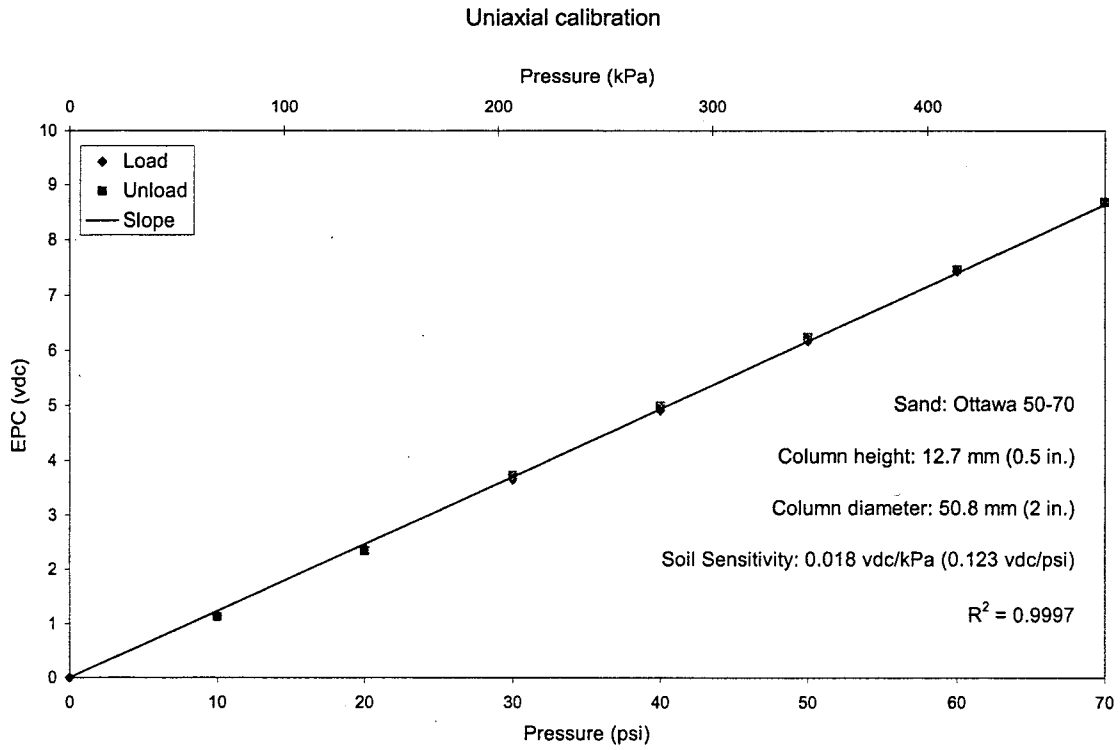

Figure A21. Test 5, cycle 5.

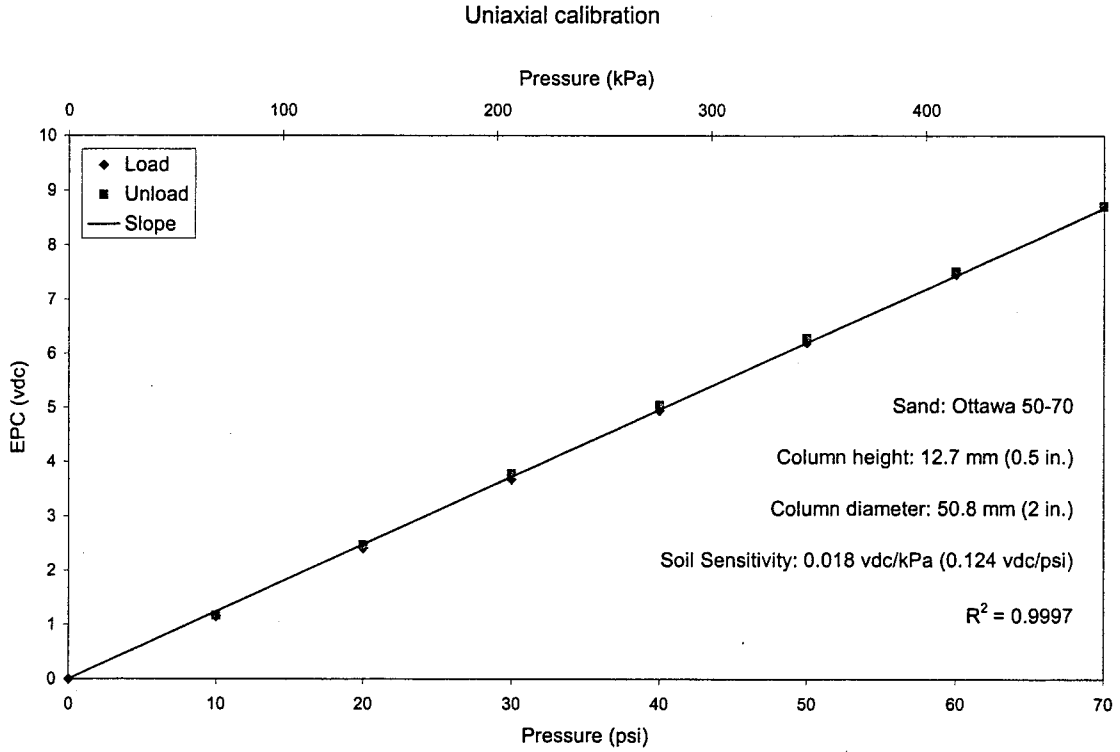

Figure A22. Test 5, cycle 6.

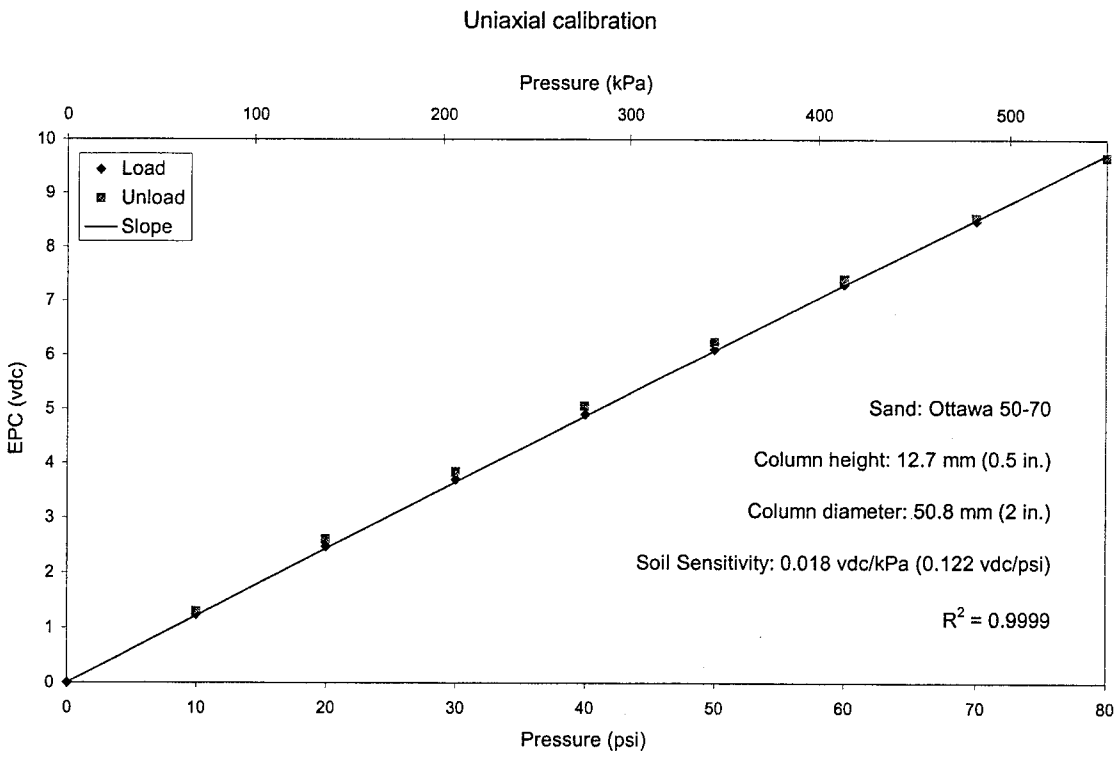

Figure A23. Test 6, cycle 1.

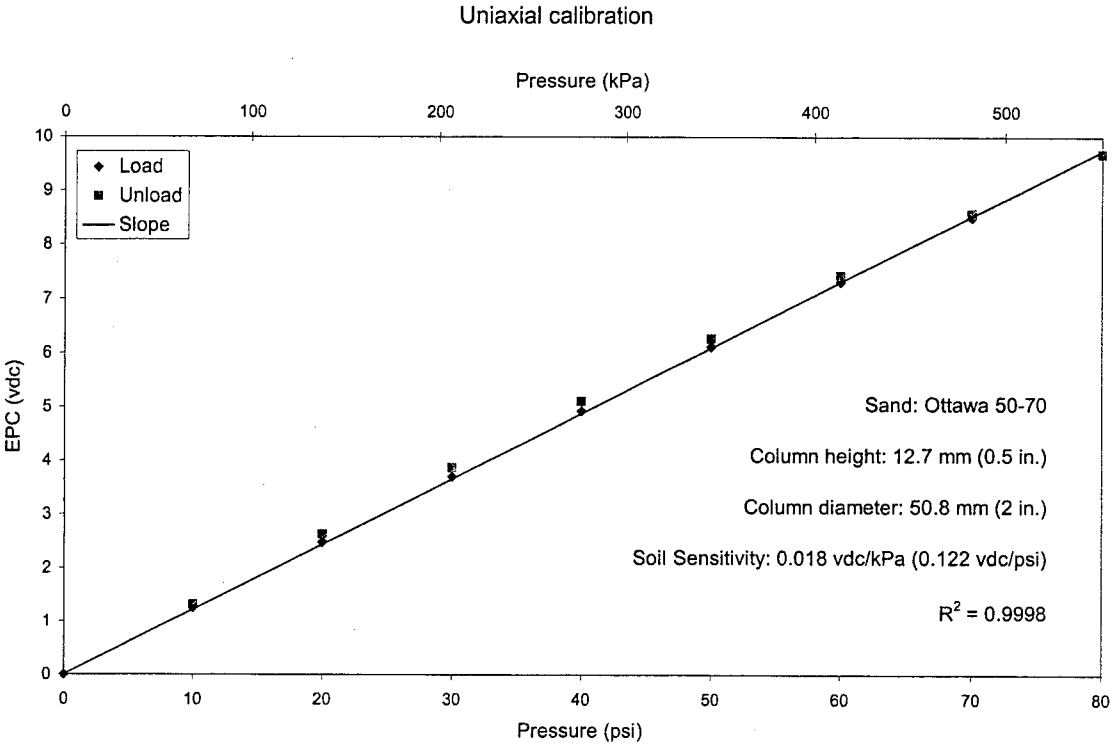

Figure A24. Test 6, cycle 2.

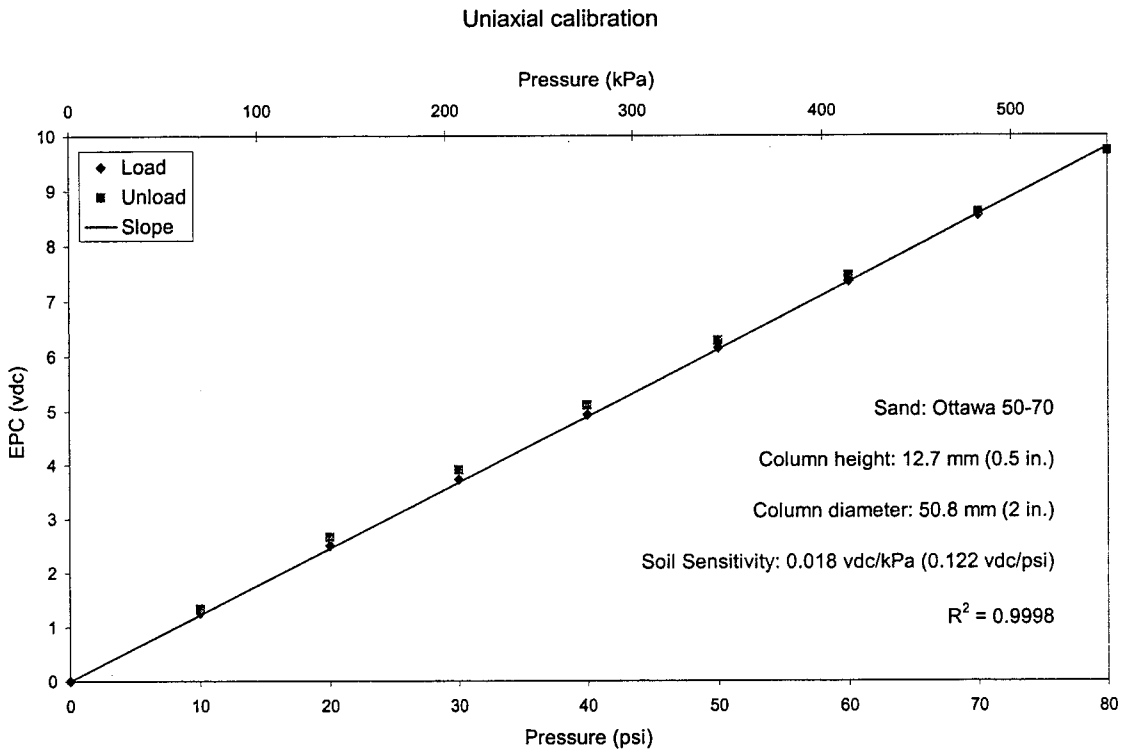

Figure A25. Test 6, cycle 3.

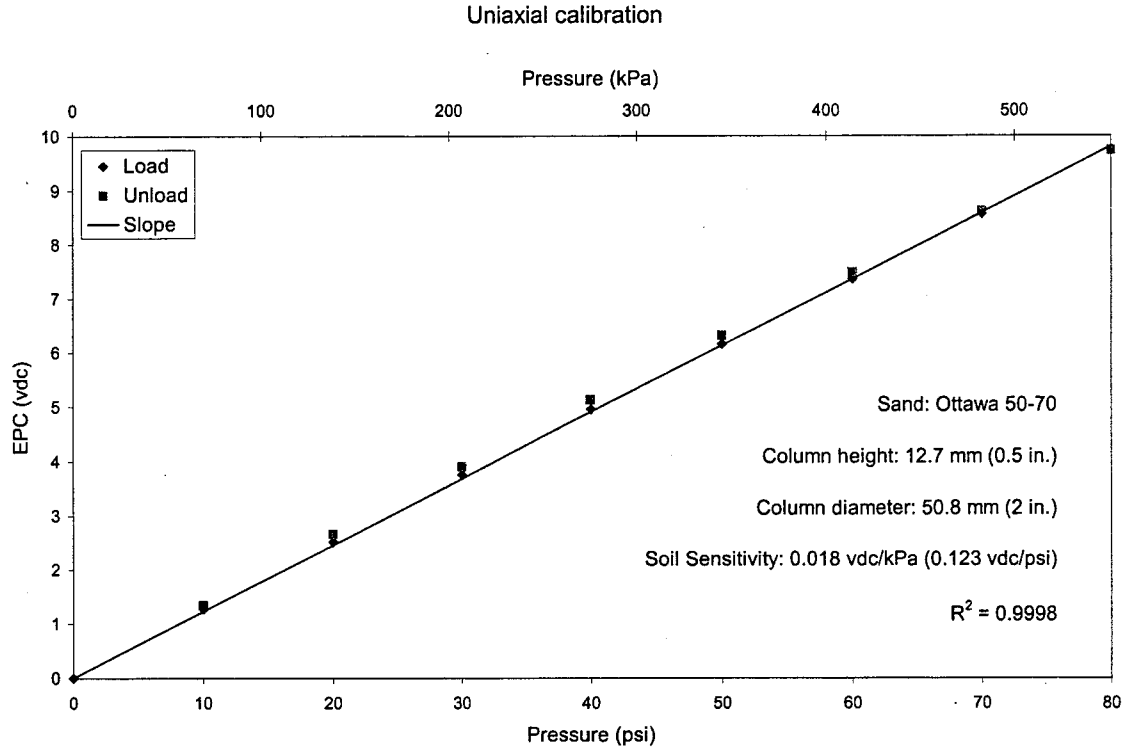

Figure A26. Test 6, cycle 4.

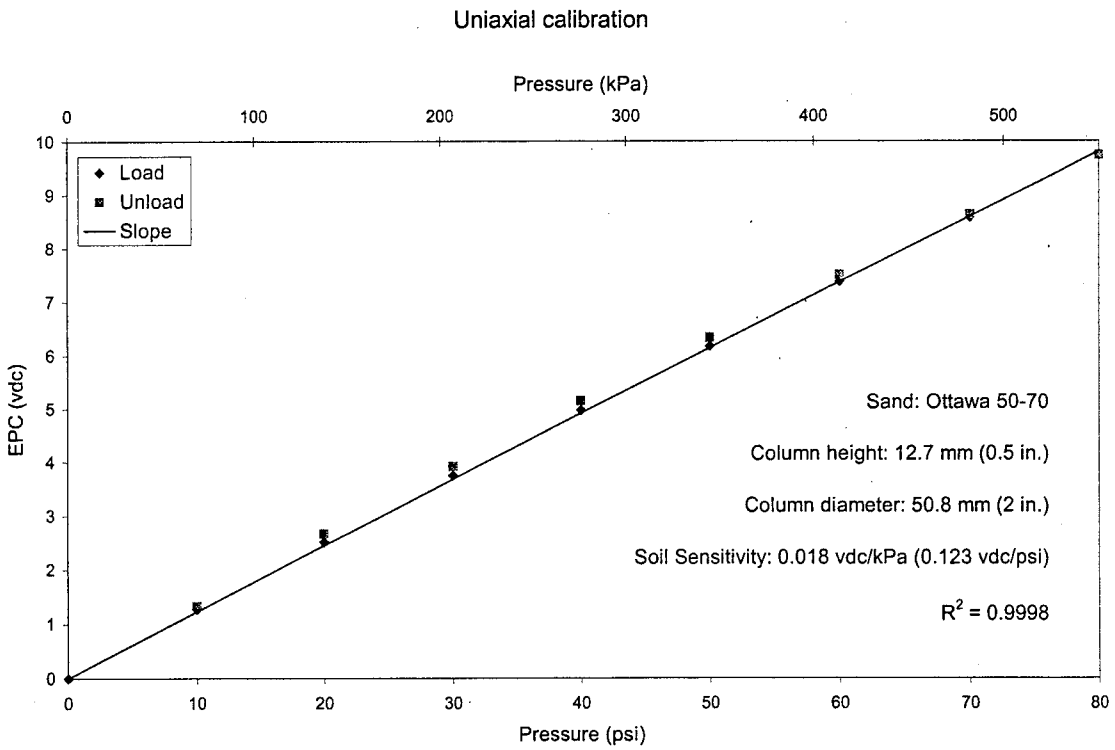

Figure A27. Test 6, cycle 5.

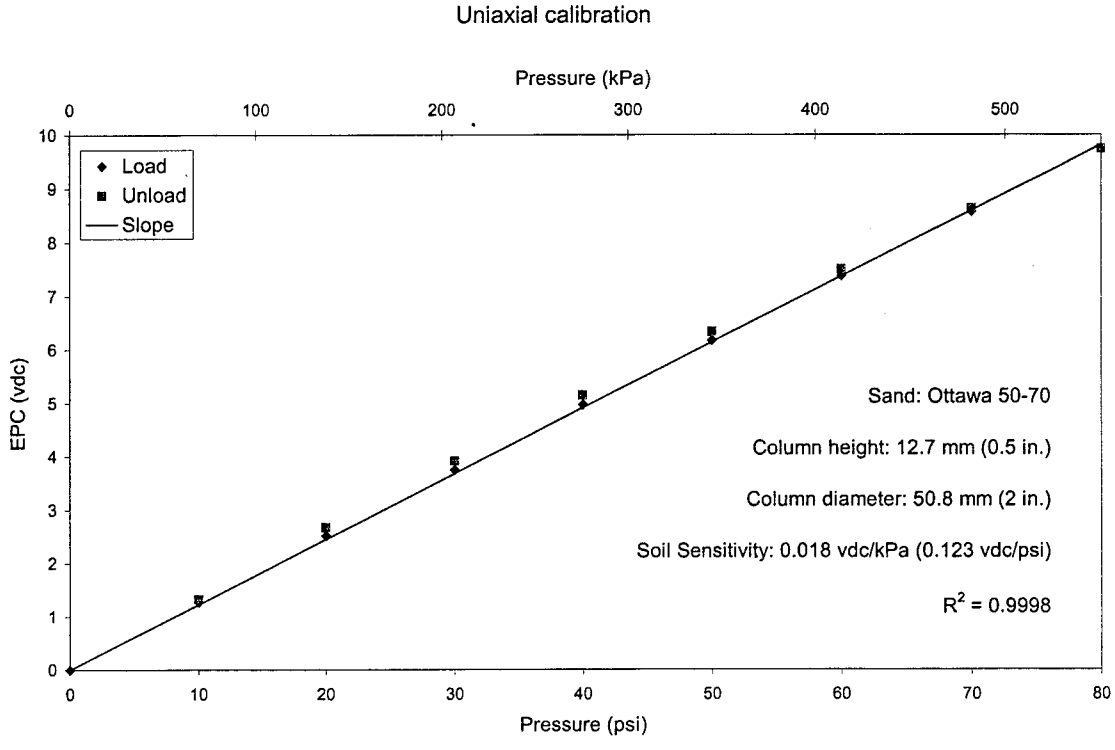

Figure A28. Test 6, cycle 6.

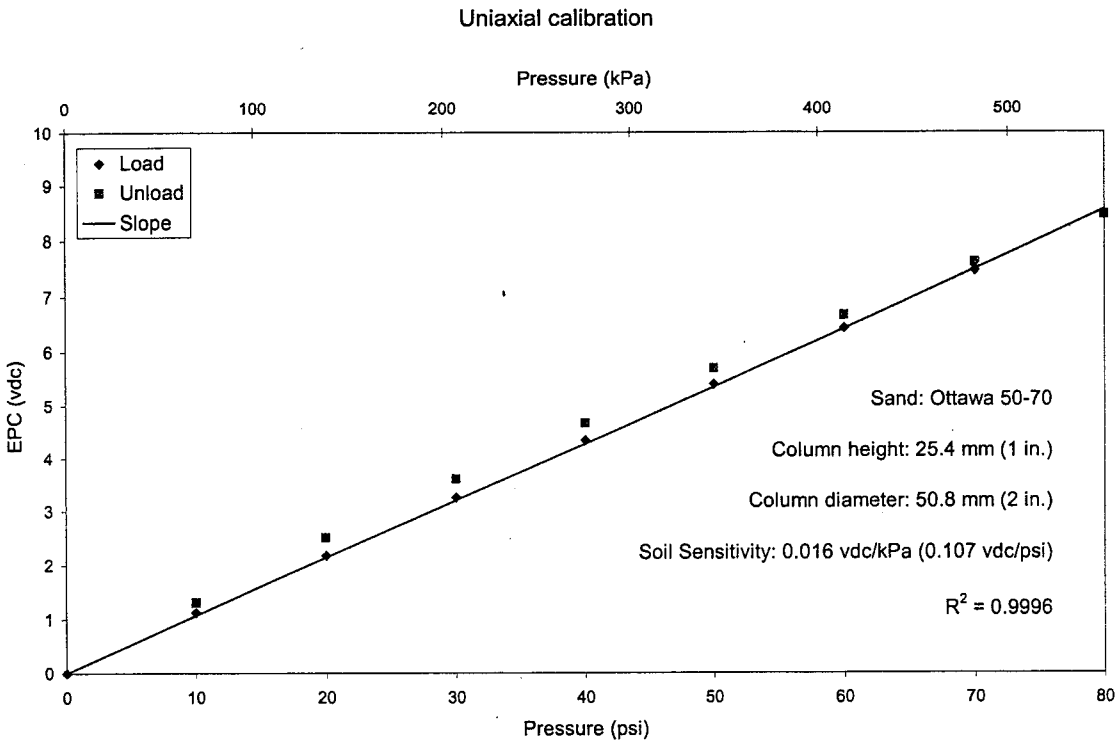

Figure A29. Test 7, cycle 1.

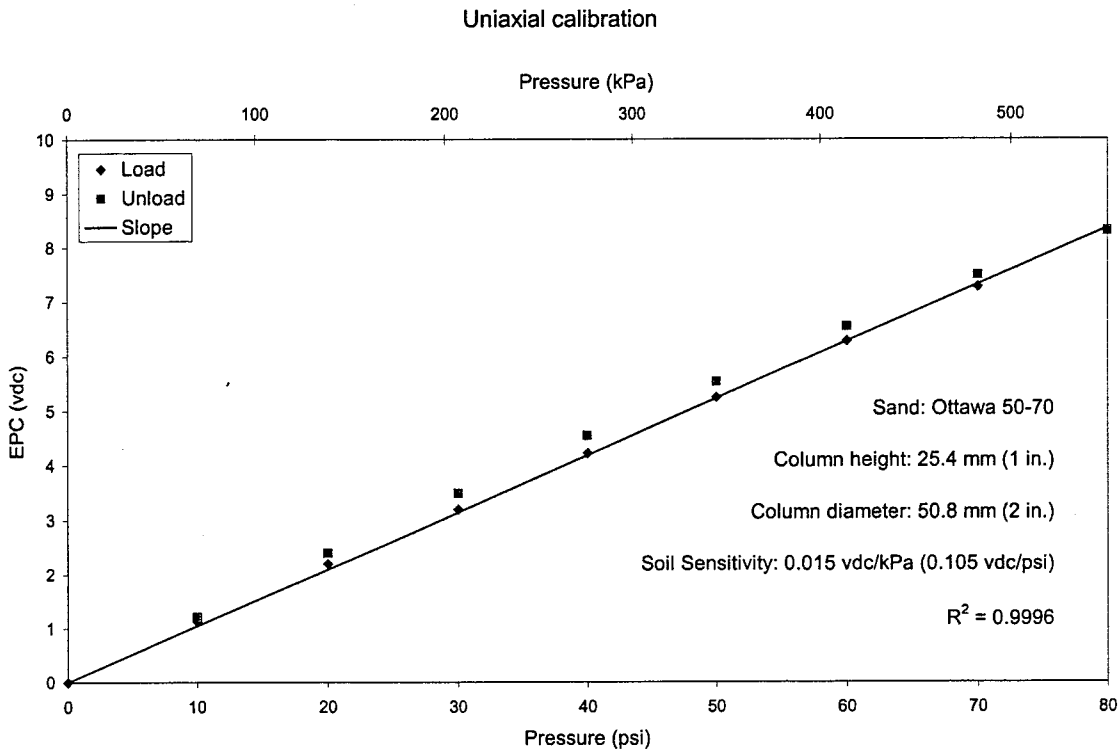

Figure A30. Test 7, cycle 2.

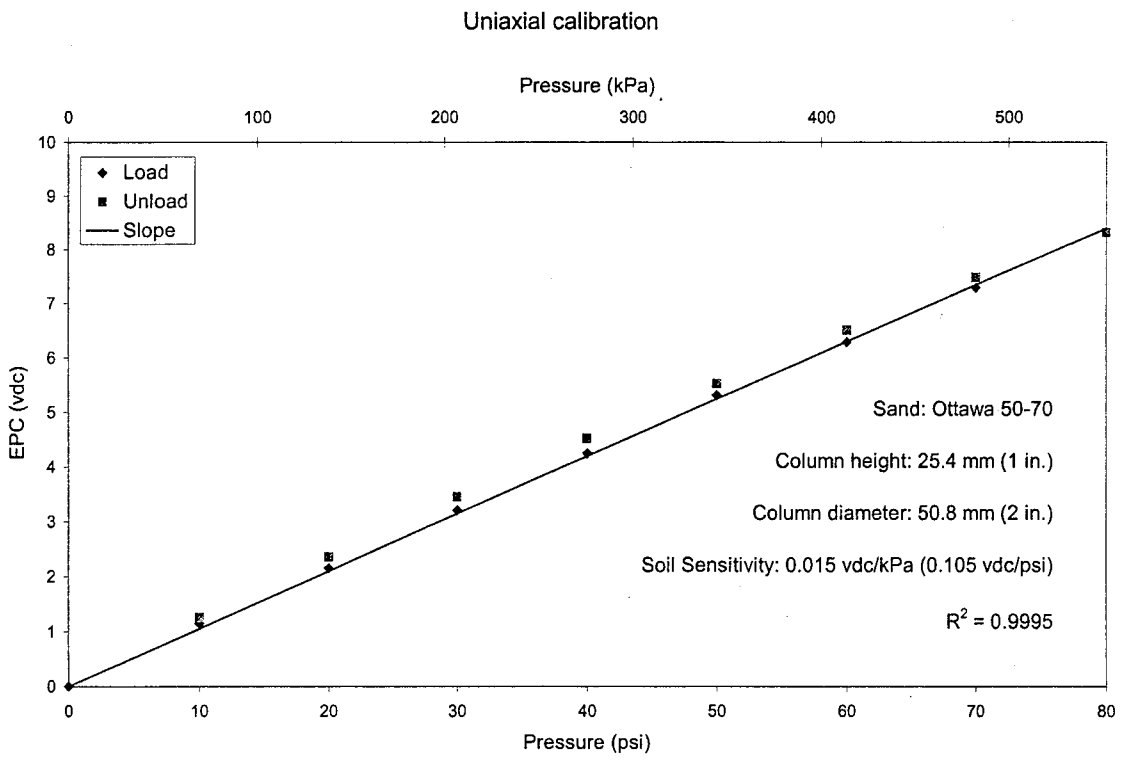

Figure A31. Test 7, cycle 3.

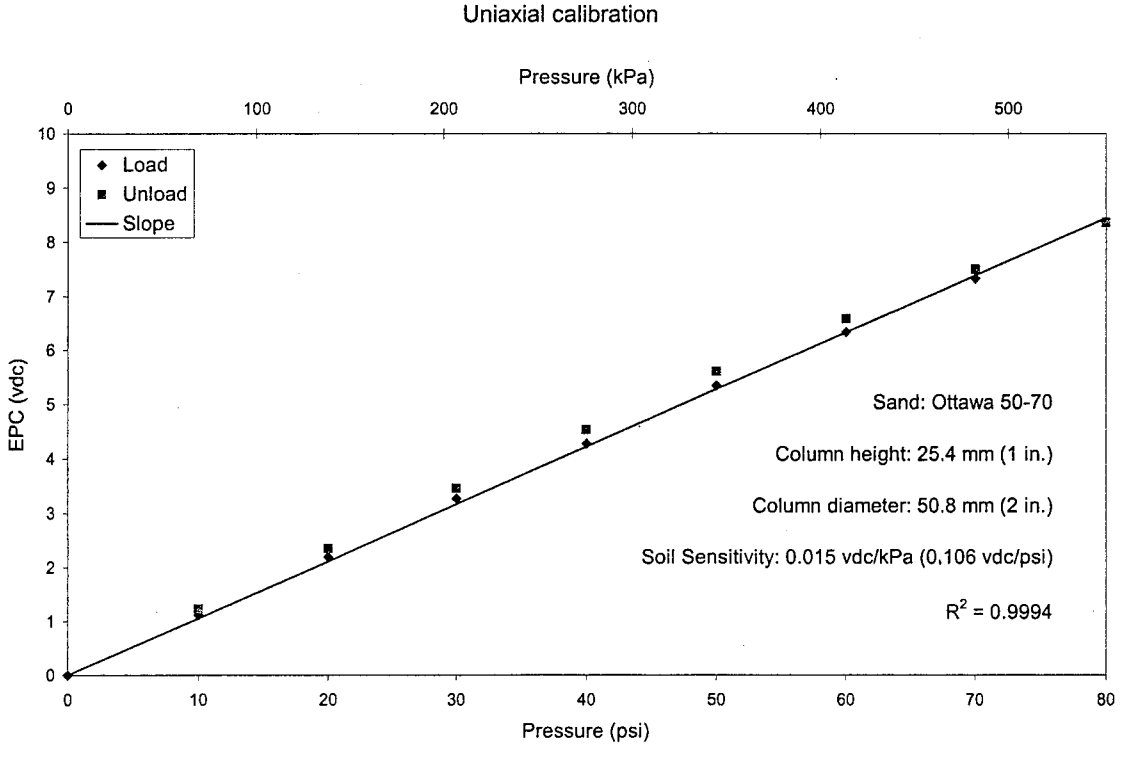

Figure A32. Test 7, cycle 4.

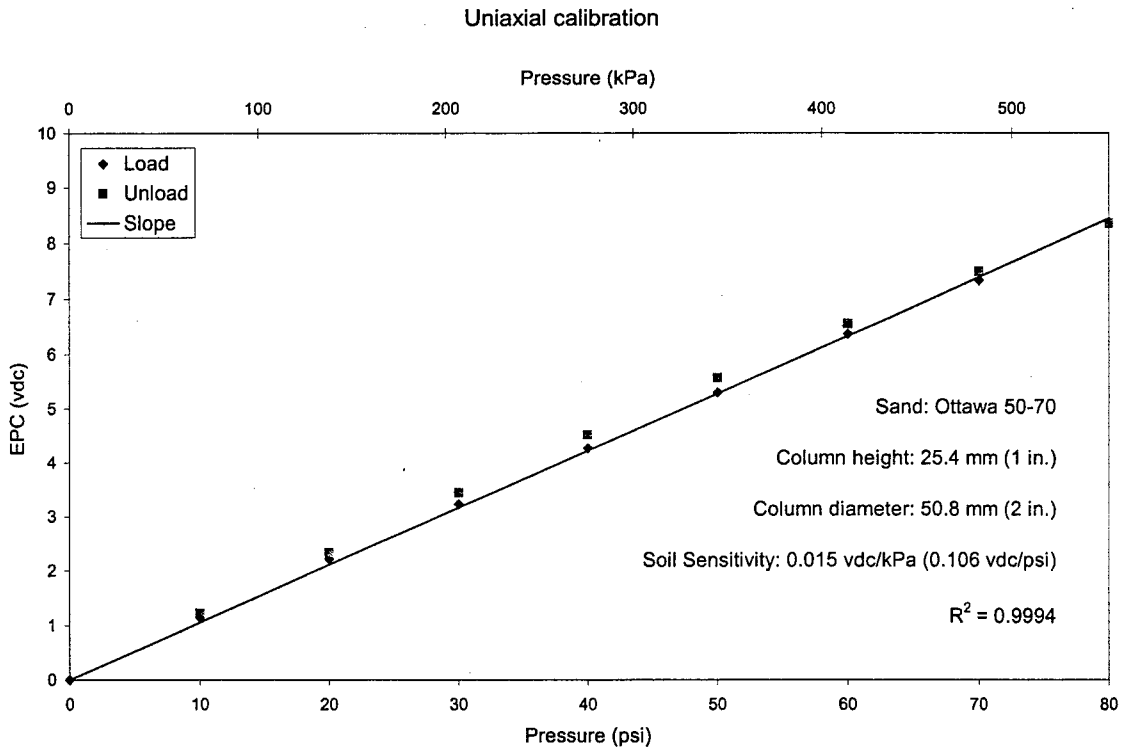

Figure A33. Test 7, cycle 5.

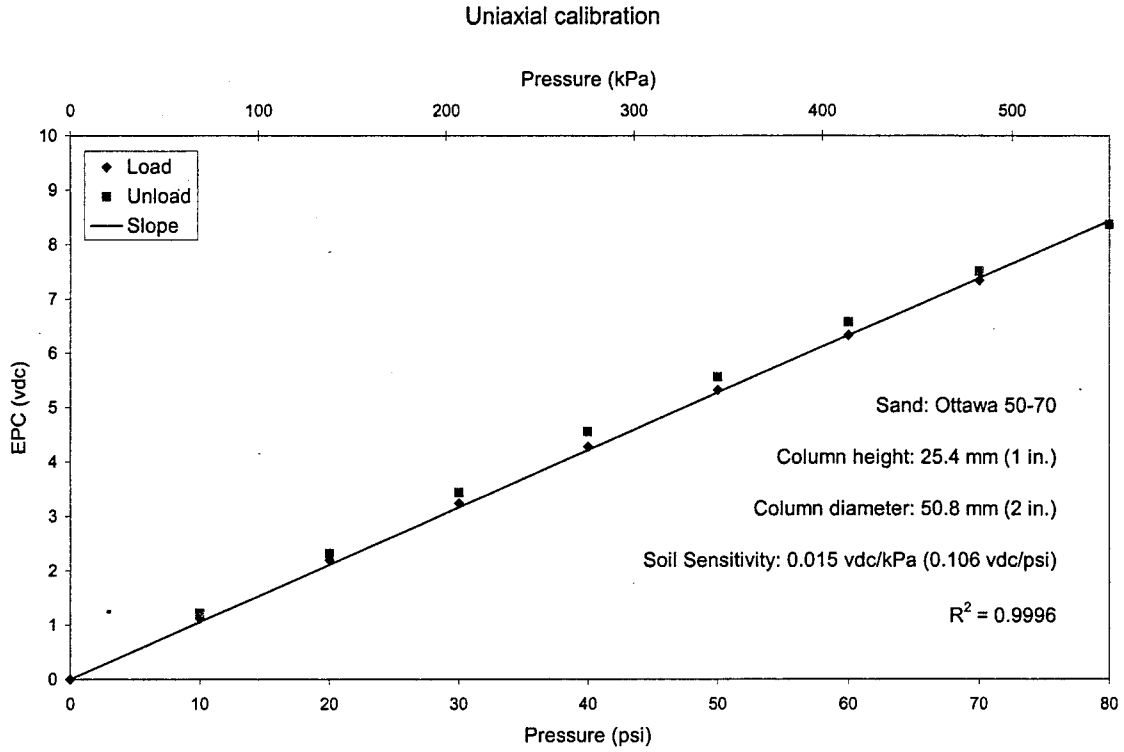

Figure A34. Test 7, cycle 6.

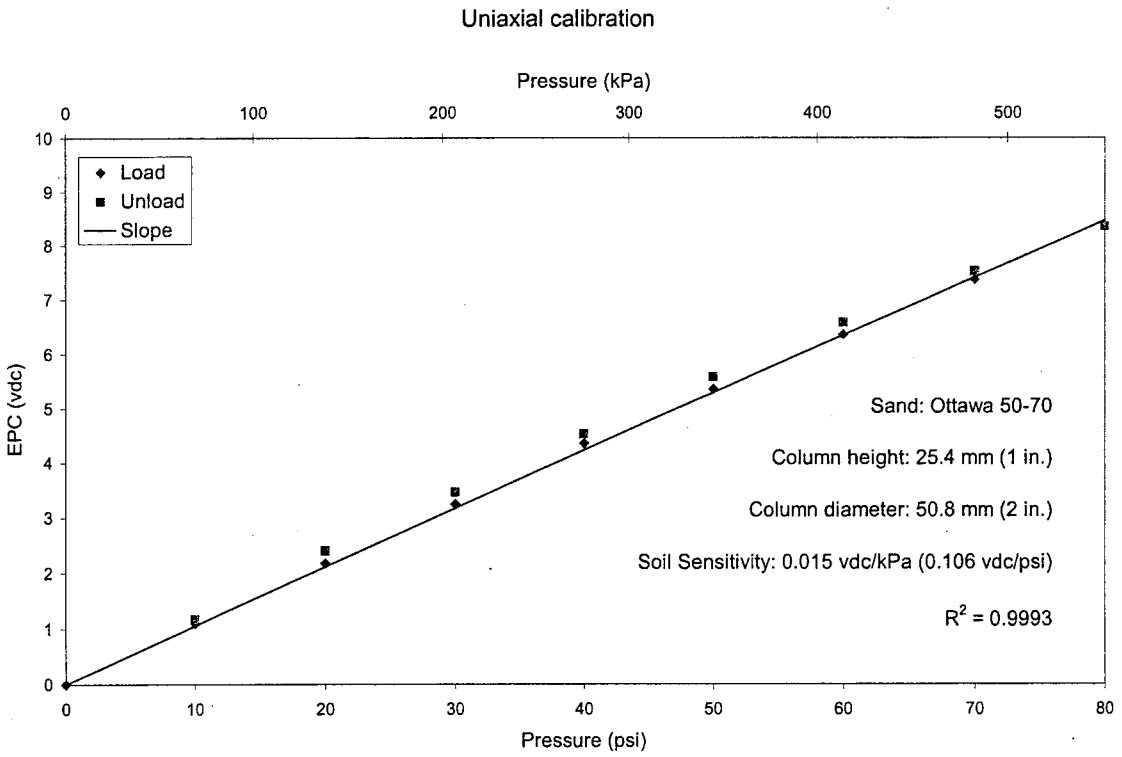

Figure A35. Test 7, cycle 7.

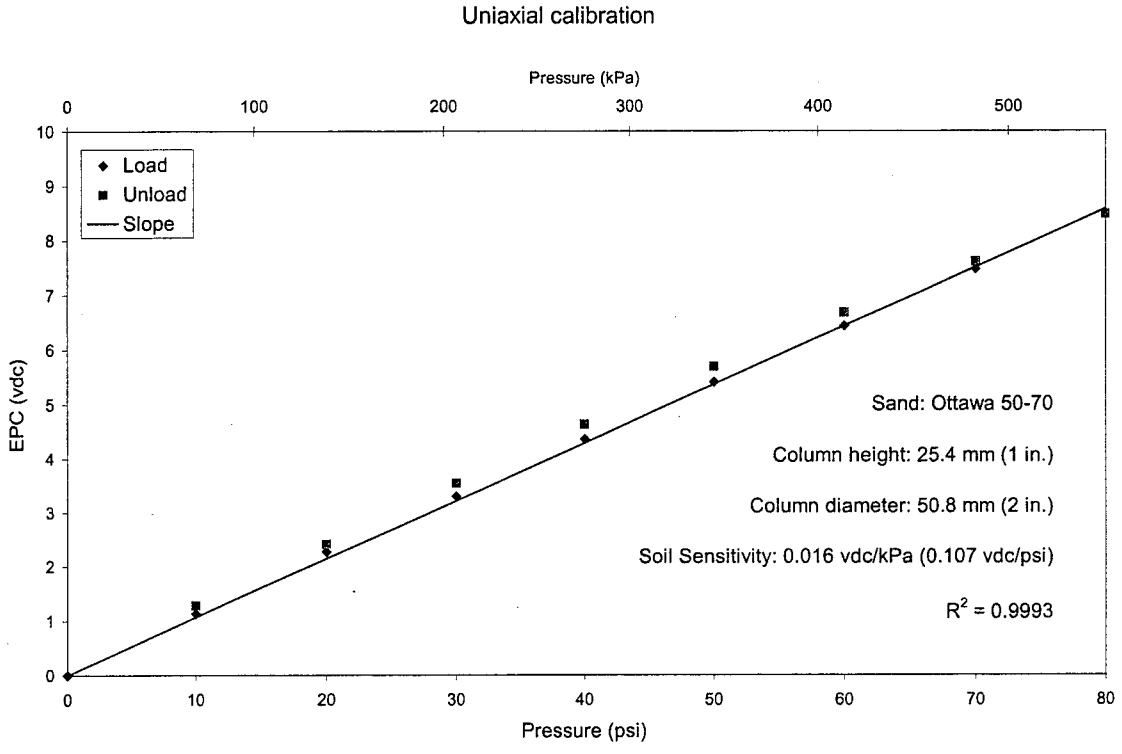

Figure A36. Test 7, cycle 8.

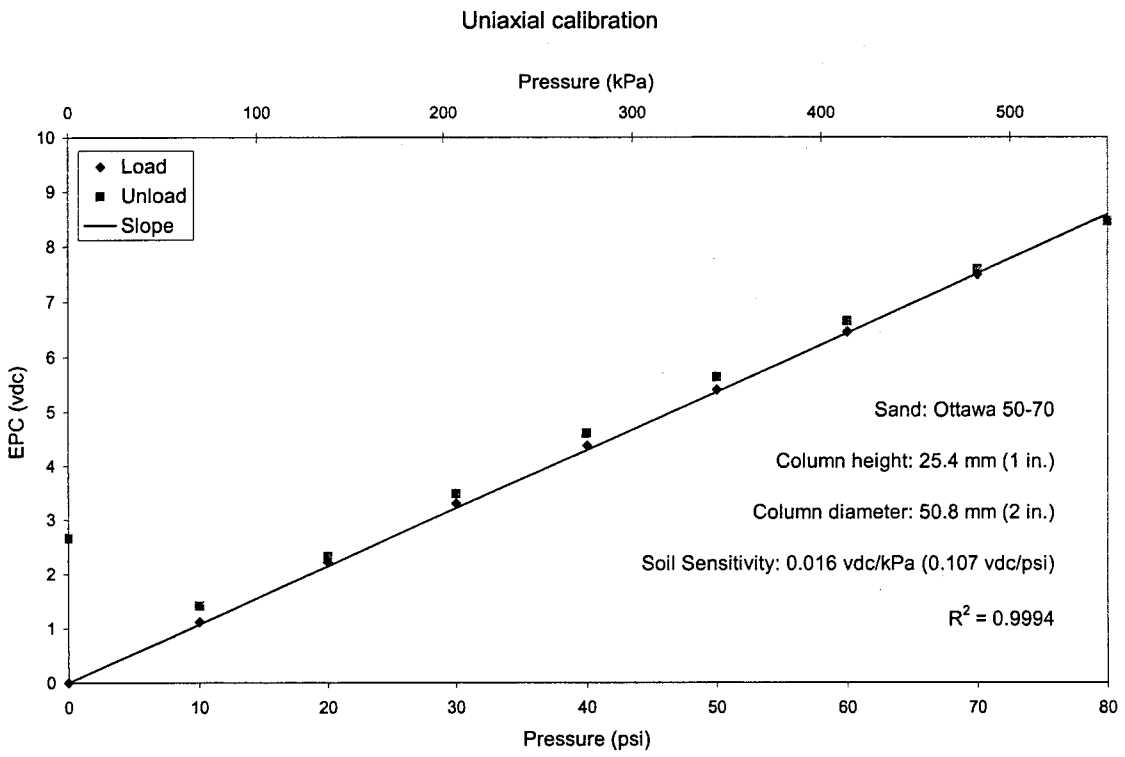

Figure A37. Test 7, cycle 9.

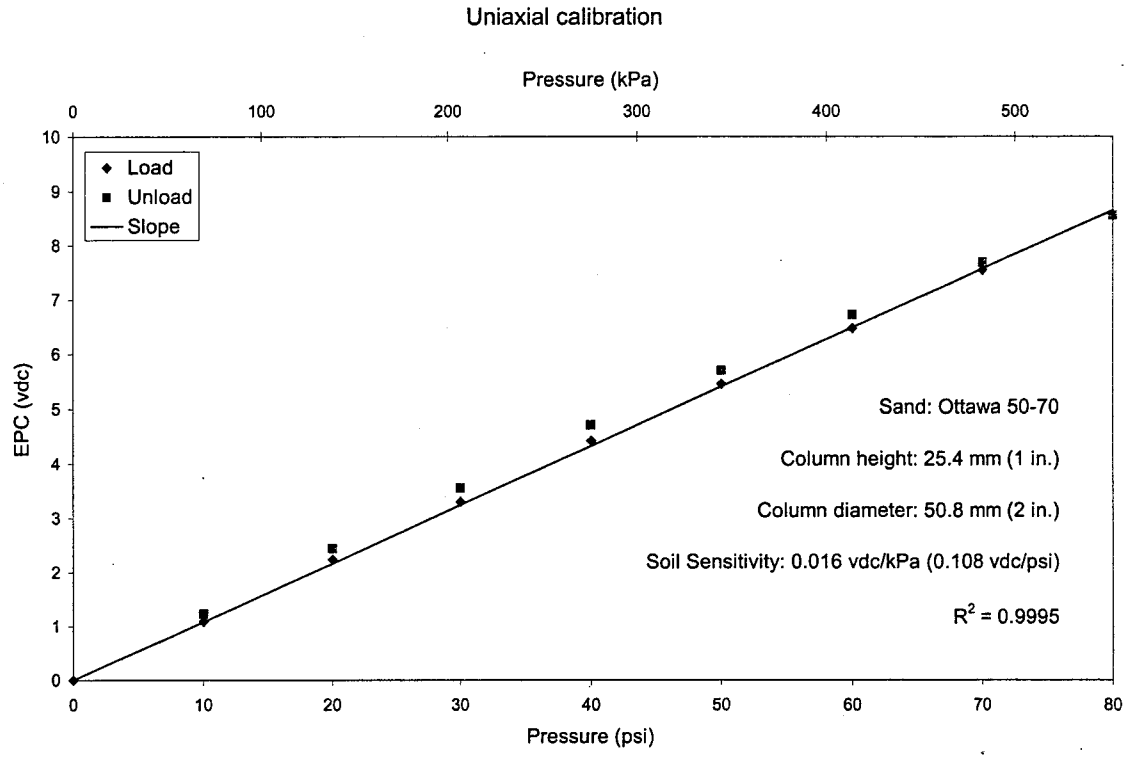

Figure A38. Test 7, cycle 10.

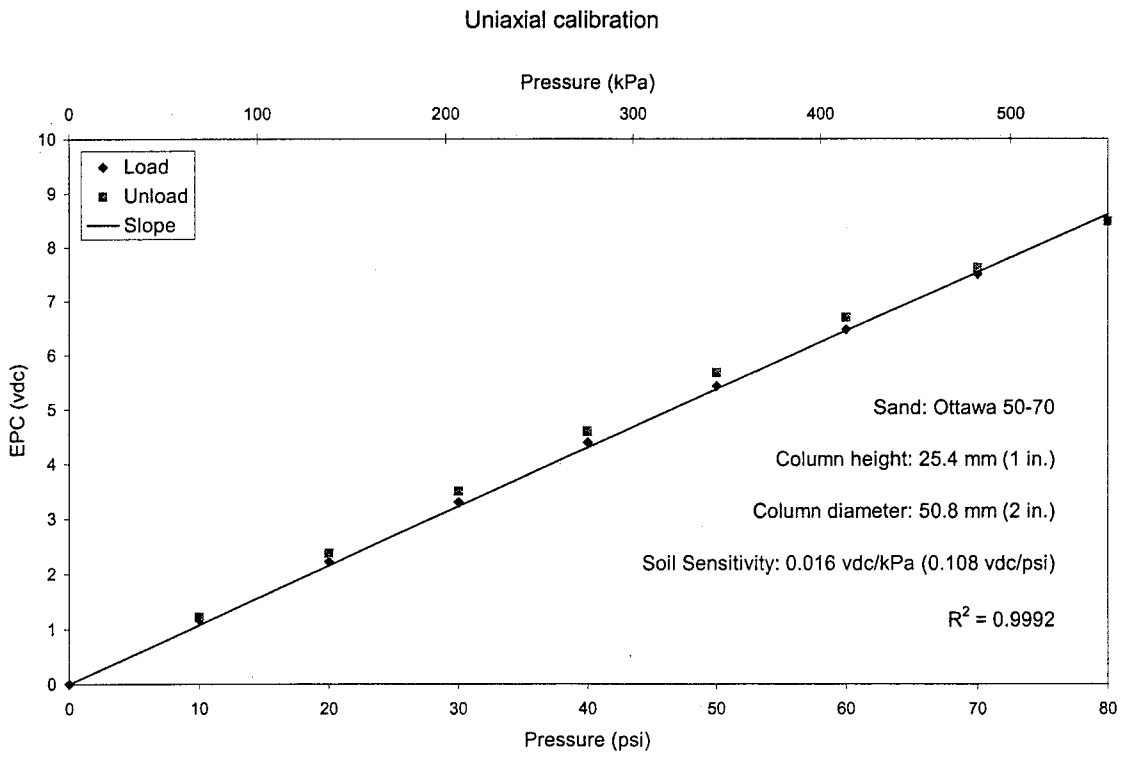

Figure A39. Test 7, cycle 11.

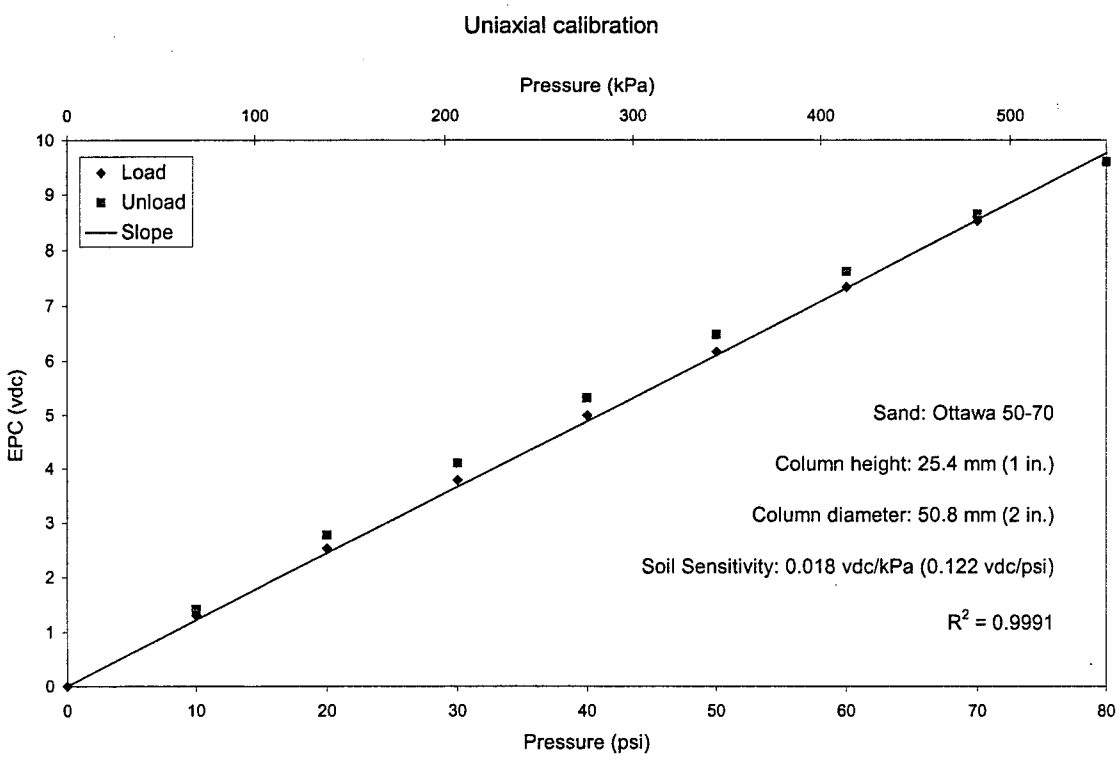

Figure A40. Test 8, cycle 1.

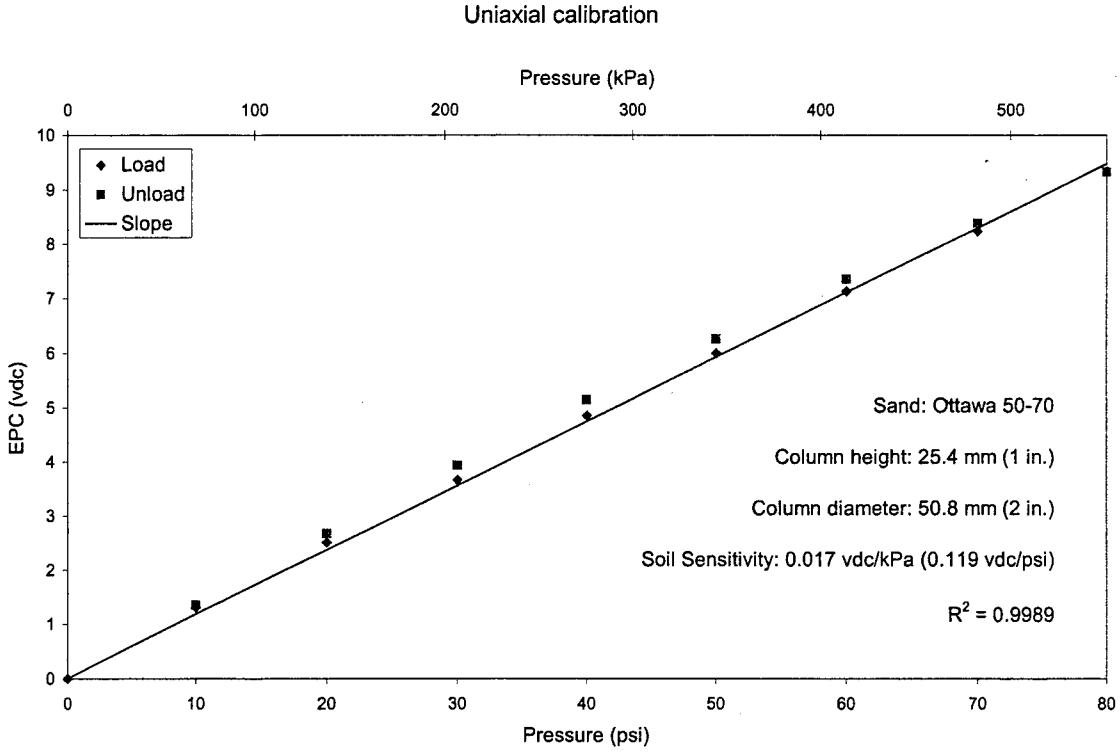

Figure A41. Test 8, cycle 2.

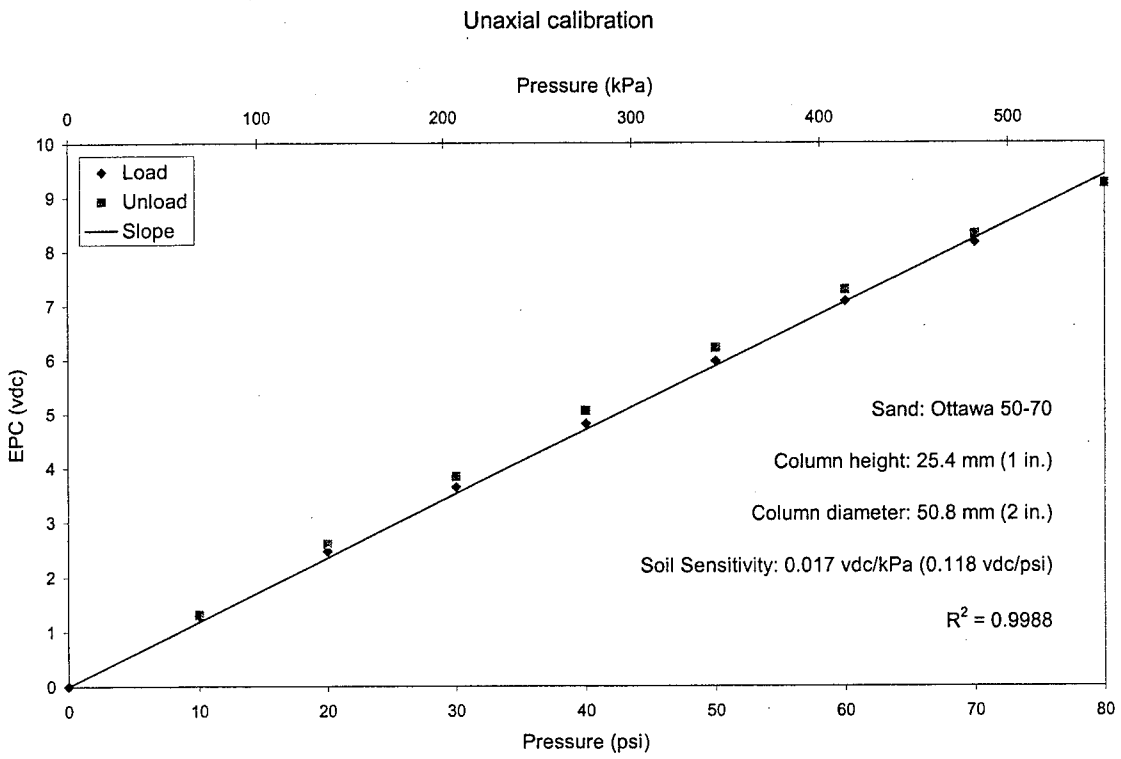

Figure A42. Test 8, cycle 3.

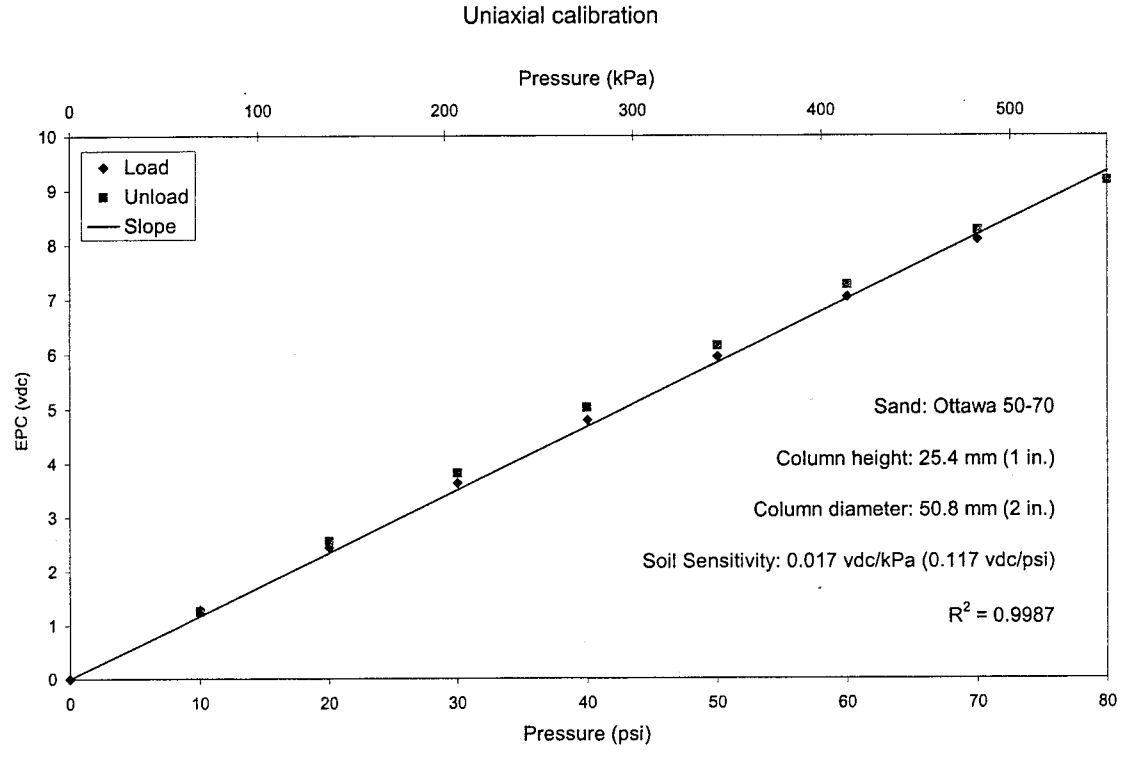

Figure A43. Test 8, cycle 4.

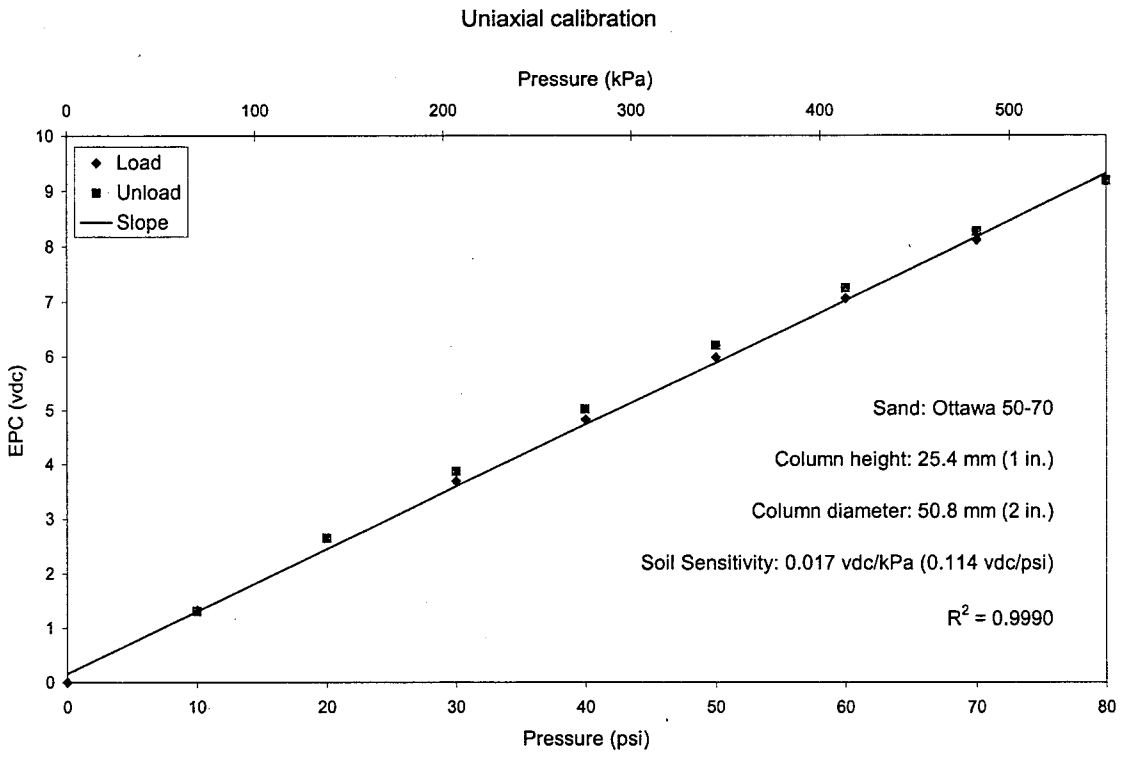

Figure A44. Test 8, cycle 5.

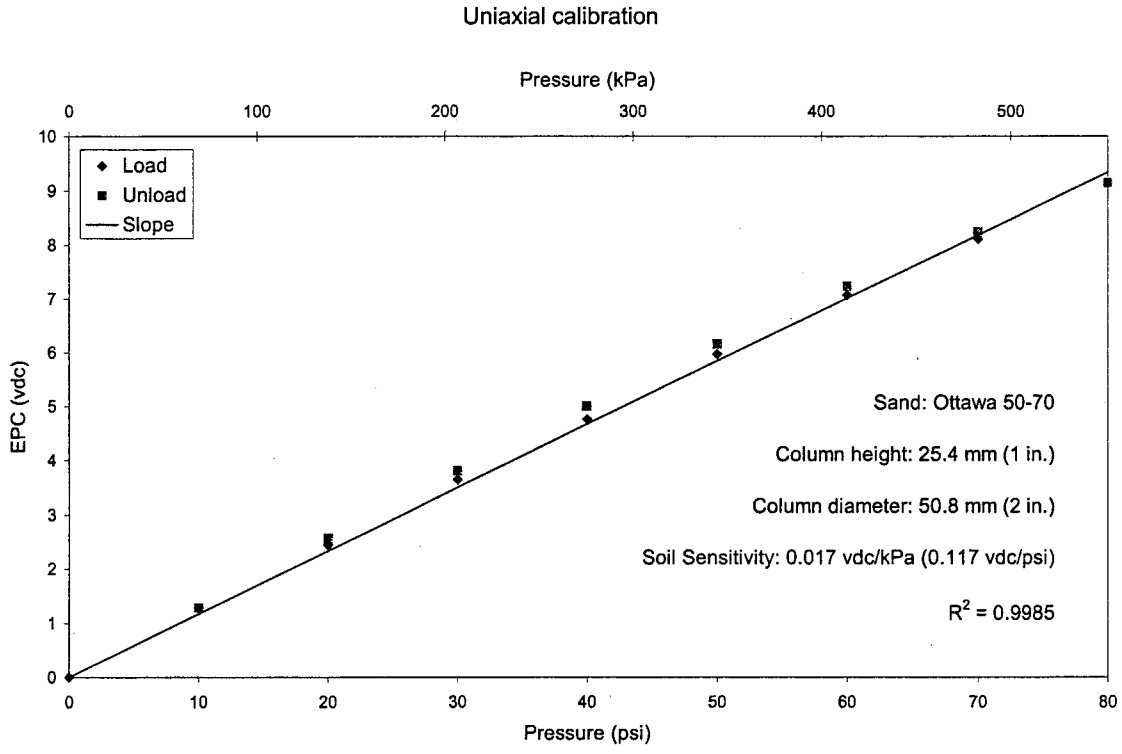

Figure A45. Test 8, cycle 6.

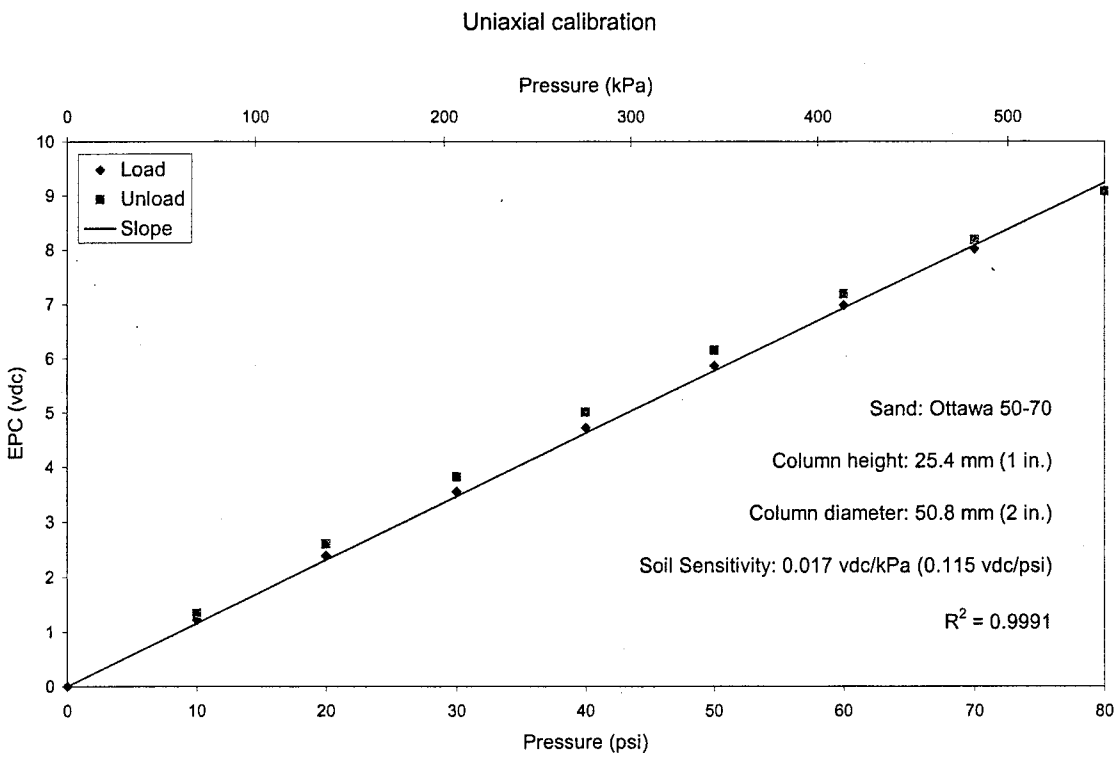

Figure A46. Test 8, cycle 7.

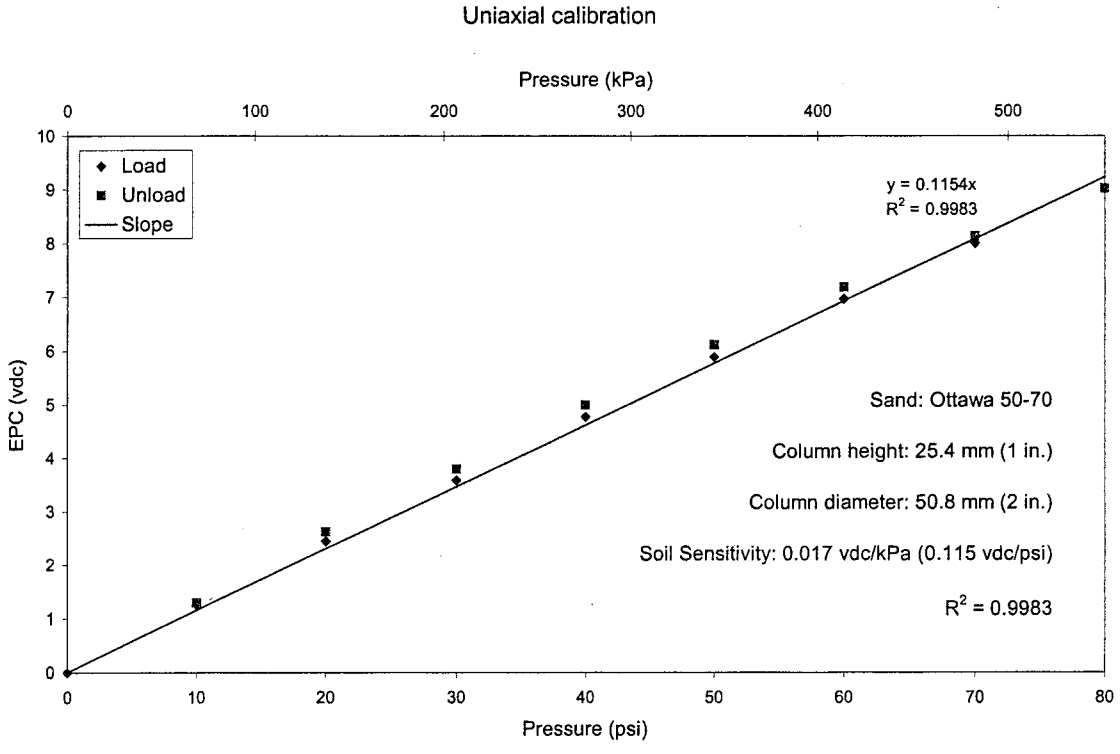

Figure A47. Test 8, cycle 8.

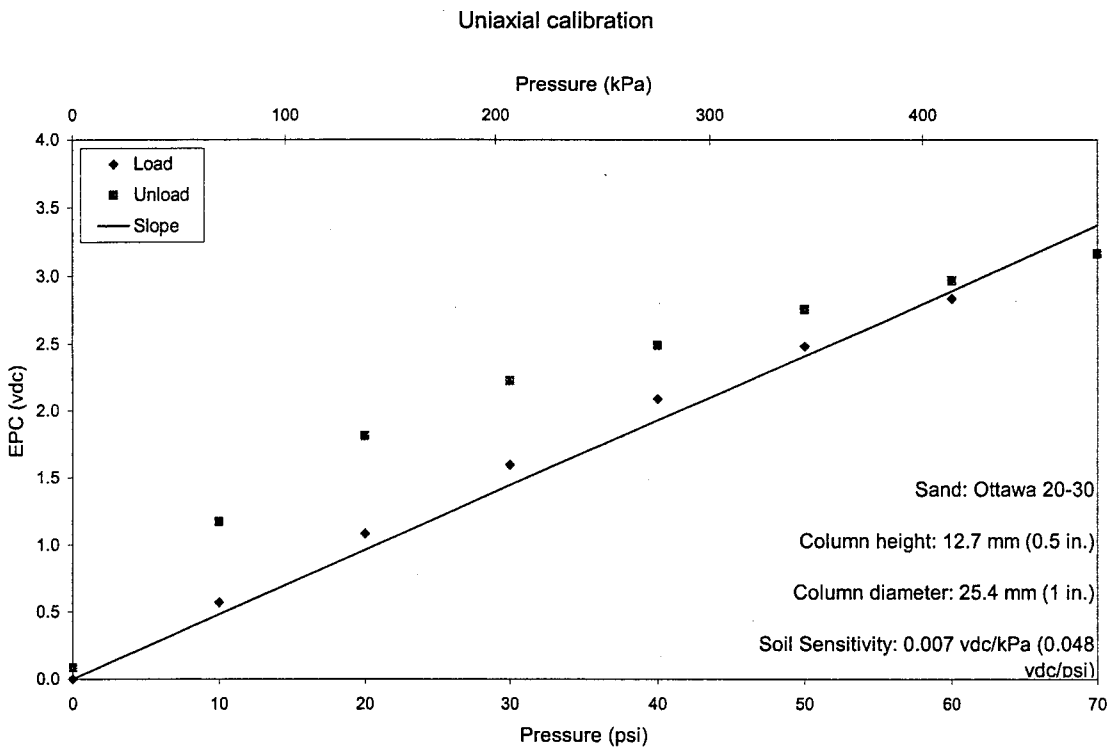

Figure A48. Test 9, cycle 1.

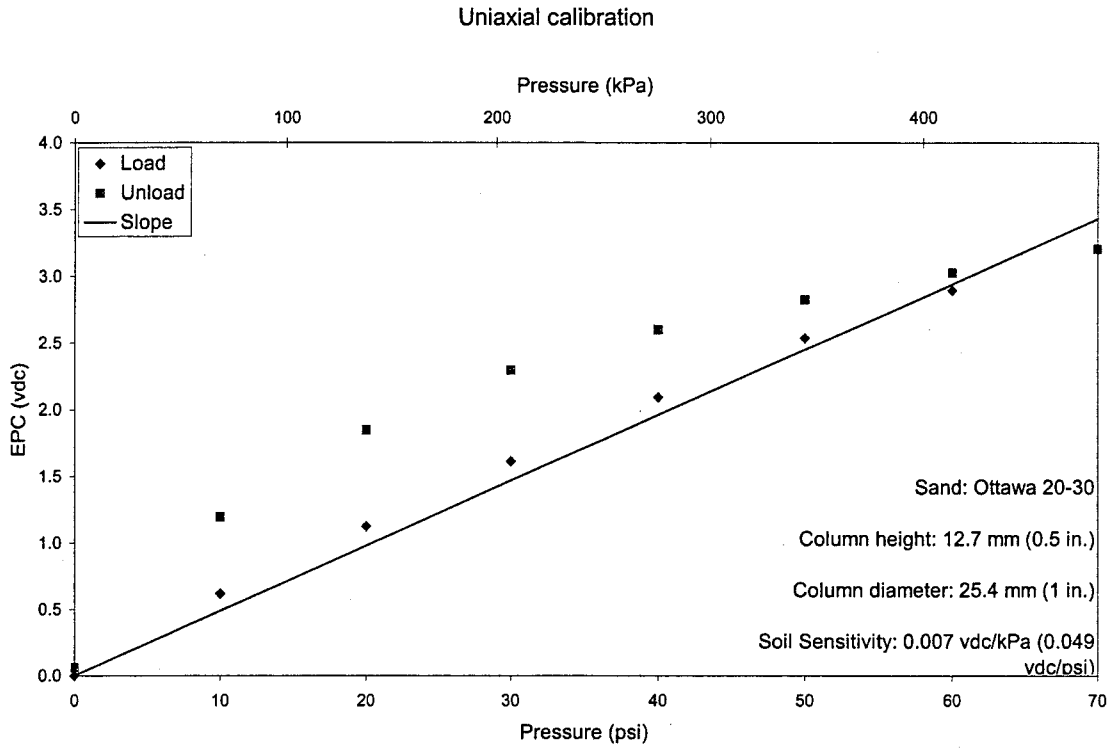

Figure A49. Test 9, cycle 2.

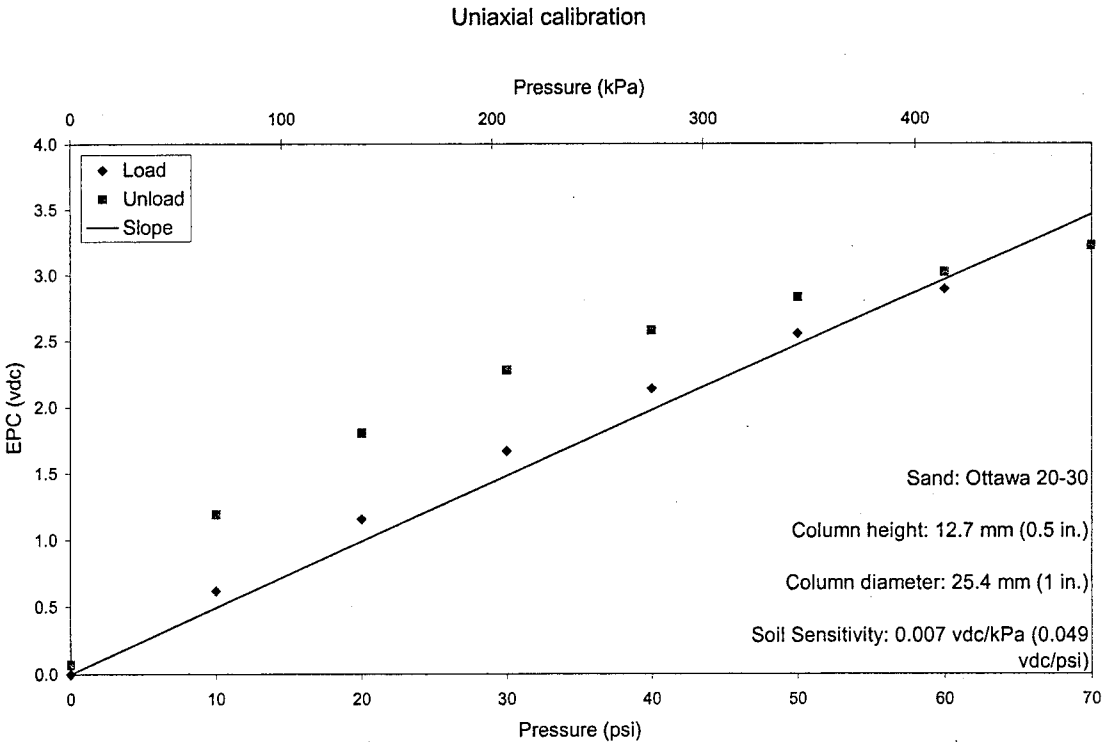

Figure A50. Test 9, cycle 3.

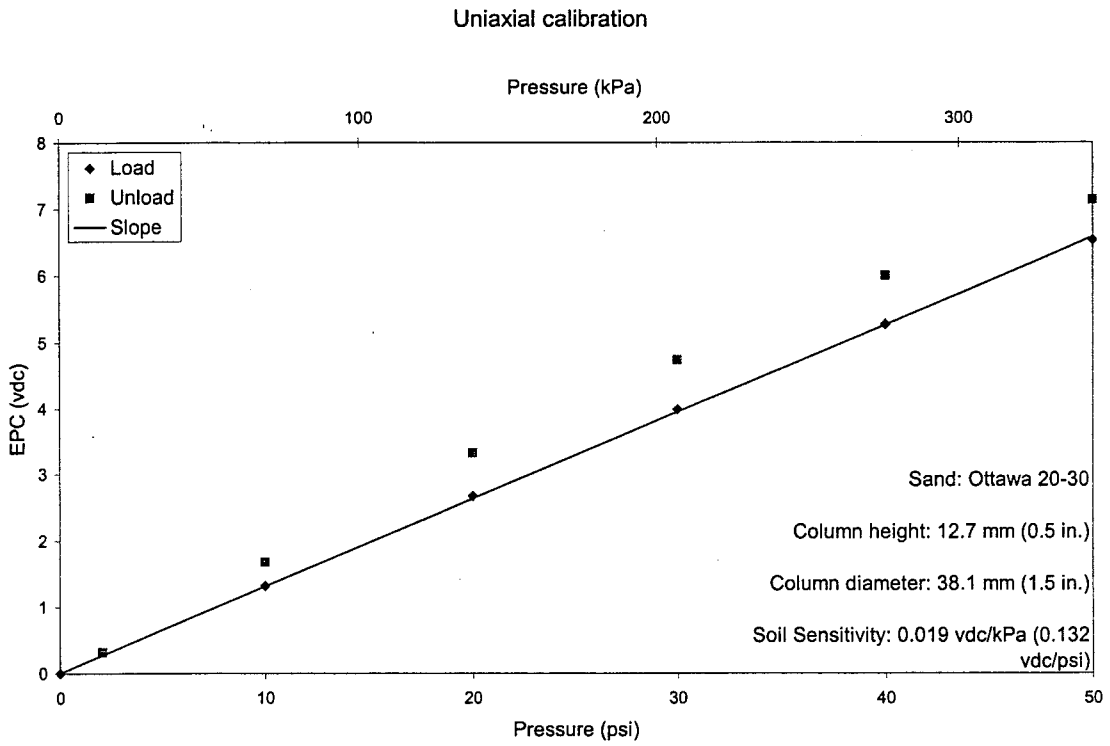

Figure A51. Test 10, cycle 1.

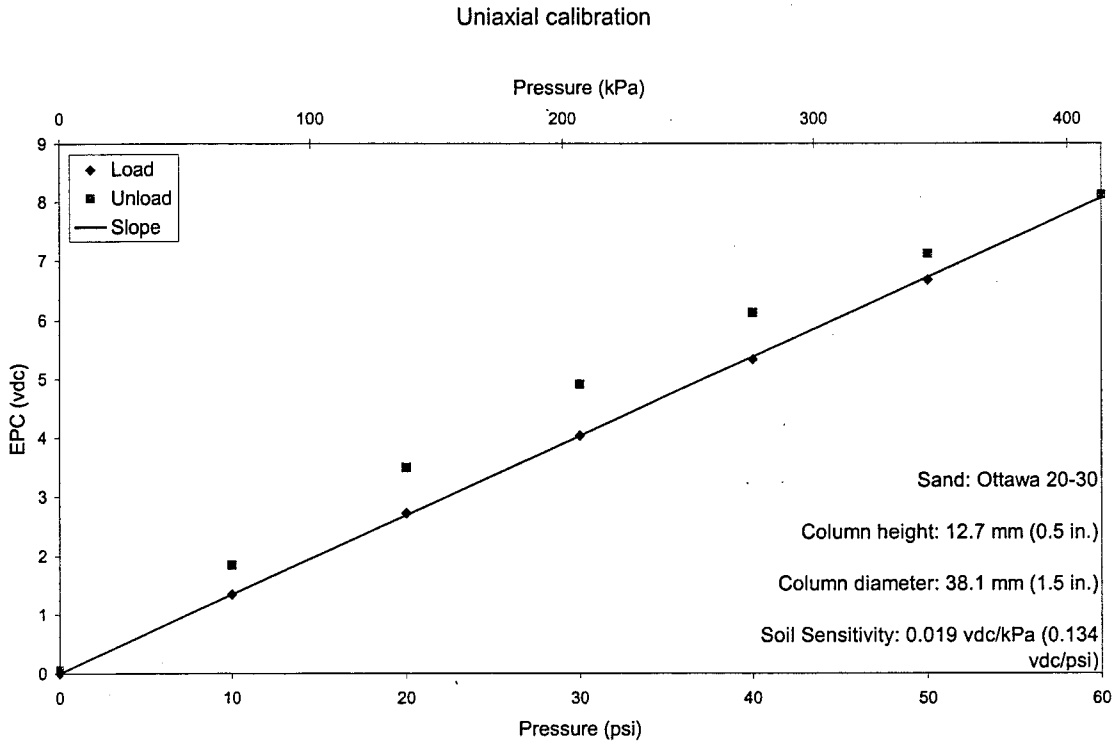

Figure A52. Test 10, cycle 2.